Why do ABCC5 KO mice show a lean phenotype?



Eleanor McKay
Lincoln College
University of Oxford

Submitted in fulfilment of the requirements for the degree of Master of Science by Research in Physiology, Anatomy & Genetics

Trinity Term 2018

Declaration

I, Eleanor McKay, declare as follows:

1. That the work described in this thesis has not been submitted to the University of Oxford, or any other tertiary institution, for purposes of obtaining and academic qualification, whether by myself or any other party.
2. That I performed the entirety of the laboratory work presented as results in this thesis.
3. That the thesis I am submitting is entirely my own work except where otherwise indicated.



Eleanor McKay Date: 30 November 2018

Why do ABCC5 mice show a lean phenotype?

Eleanor McKay

Lincoln College

Master of Science by Research in Physiology, Anatomy & Genetics

Trinity Term 2018

Abstract

ABCC5 is an ATP-dependent membrane transporter that has been shown to transport glutamate conjugates in mammalian systems. Global loss of ABCC5 from mice causes a lean phenotype with enhanced enteroendocrine GLP-1 secretion. Here we develop a protocol for the live imaging of GLP-1 secretion in vitro using a model L-cell line. ABCC5 KO gut histology analysis shows no difference in gut villi length or surface area between WT and KO mice. Despite numerous studies showing enhanced brown adipose tissue (BAT) and white adipose tissue (WAT) thermogenic capacity in the presence of elevated GLP-1 levels, data presented here do not show increased non-shivering thermogenesis occurring in our KO animals. Analysis of fat pads from ABCC5 KO mice show that both their BAT and epididymal WAT depots have significantly lower mass than WT depots. Western blot and H&E histological analysis suggests that inguinal WAT depots of ABCC5 KO mice may show a lack of browning. We theorise that the adipose physiology described is due to changes in glutamatergic signalling in the sympathetic nervous system innervating BAT and WAT. Finally, we conclude that the lean phenotype of ABCC5 KO mice cannot be attributed to an increased thermogenic capacity of BAT and WAT.

Acknowledgements

I would like to thank Prof Heidi de Wet for her supervision and invaluable guidance throughout my MSc by Research. The other members of the de Wet group - Gosia Cyranka, Swathi Lingam, and Anna Veprik - have all been generous in sharing their technical expertise and advice throughout this year. I would also like to thank the Cantley group for their continual assistance, in particular Rula Bany Bakar for her tireless help with my western blots. Finally, I am extremely grateful to Dr Pamela Lear for sharing her expertise in brown, beige and white fat metabolism and training me in accurate mouse fat pad dissection.

Contents

Abstract iii

Acknowledgements iv

List of Figures vii

List of Tables viii

Abbreviations ix

1 Introduction 1

1.1 Obesity and its current treatments 1

1.2 Enteroendocrine cells 2

1.3 Profiling of gut identifies expression of ABCC5 in hormone secreting cells 4

1.4 ABCC5 is a membrane transporter 6

1.5 ABCC5 as a T2D susceptibility gene 10

1.6 Work leading up to this study: 10
1.6.1 ABCC5 plays a role in GLP-1 secretion in a model L-cell line 10
1.6.2 ABCC5 KO mouse have a lean phenotype 11
1.6.3 RESEARCH HYPOTHESIS 16

1.7 ABCC5 tissue expression 17

1.8 Fat browning 19

2 Materials & Methods 27

2.1 Animals 27

2.2 Tissue processing and analysis 27
2.2.1 Protein extraction 27
2.2.2 Protein quantification 28
2.2.3 SDS-PAGE 28
2.2.4 Coomassie stain 28

2.3 Western Blot 29
2.3.1 Antibodies used for Western Blot 30
2.3.2 Quantification of Western Blot 30

2.4 Histology 30
2.4.1 Analysis of H&E WAT sections 31
2.4.2 Immunofluoresence of wax embedded tissue sections 32
2.4.3 Antibodies used for wax embedded tissue immunofluorescence 33

2.5 Plasmid extraction **33**

2.6 Plasmid sequencing **34**

2.7 Cell Culture **34**
2.7.1 Cell transfection 34
2.7.2 Cell fixing 35
2.7.3 Fixed cell immunofluorescence 35
2.7.4 Antibodies used for fixed cell immunofluorescence 36

2.8 Live cell imaging **36**

2.9 Statistical Analysis **36**

3 Results: Live Cell Imaging **37**

3.1 Introduction: The use of tPA as a marker of GLP-1 vesicles **37**

3.2 Results **39**

3.3 Discussion **41**

4 Results: Gut morphology **43**

4.1 Intestinal villi length **43**

4.2 Methods **45**

4.3 Results **46**

4.4 Discussion **47**

5 Results: Adipose Tissue Physiology **50**

5.1 Introduction **50**

5.2 Methods **52**

5.3 Results **52**
5.3.1 Cohort 1 52
5.3.2 Cohort 2 54

5.4 Discussion **56**
5.4.1 Technical challenges from this study 66

6 General Discussion and Conclusion **70**

References **75**

Appendix **88**

List of Figures

Figure	Title	Page No.
Figure 1.1	A summary of gastrointestinal hormone secretion and their effects.	2
Figure 1.2	The predicted structure of ABCC5.	7
Figure 1.3	GLP-1 exocytosis from GLUTag cells is dependent of ABCC5 protein levels.	11
Figure 1.4	GLP-1 secretion in ABCC5 KO mice	12
Figure 1.5	Mass and body composition of Abcc5 KO mice and WT litter mate controls	13
Figure 1.6	ABCC5 KO mice show increased insulin sensitivity	15
Figure 1.7	Metabolic profiling of ABCC5 KO mice.	16
Figure 1.8	The types of different adipocyte cells.	19
Figure 1.9	White, brown, and beige fat depots in mice and humans.	20
Figure 2.1	AdipoCount software processing.	31
Figure 2.2	Calibration of AdipoCount software arbritrary unit values to true um values.	32
Figure 3.1	Fixed cell imaging of GLUTag cells transfected with tPA-dendra 2.	39
Figure 3.2	Fixed cell imaging of immunolabelled GLUTag cells transfected with tPA-dendra 2.	40
Figure 3.3	Live cell imaging snapshots	41
Figure 4.1	Morphometric analysis of ABCC5 KO intestinal villi in a preliminary cohort	45
Figure 4.2	Representative images of ABCC5 KO and WT gut villi.	46
Figure 4.3	Measurements of villi length and surface area.	47
Figure 5.1	Cohort 1: Western blots of iWAT tissue lysate.	53
Figure 5.2	Cohort 1: H&E histology of iWAT fat depots.	55
Figure 5.3	Cohort 2: Male iBAT and eWAT depots.	56

Figure 5.4	Cohort 2: Female BAT and eWAT depots.	57
Figure 5.5	Cohort 2: Western blots of male BAT, eWAT and iWAT fat depots for UCP1 expression.	58
Figure 5.6	Cohort 2: Western blots of female BAT, eWAT and iWAT fat depots for UCP1 expression.	59
Figure 5.7	Cartoon of the neural pathways of the core thermoregulatory network innervating BAT and WAT.	62
Figure 5.8	An example of an extensively browned section of iWAT processed by AdipoCount.	67
Figure 5.9	Immunofluorescent staining of iWAT and BAT for UCP1	68

List of Tables

Table	Title	Page No.
Table 1.1	Abcc5 is expressed in the endocrine cells of the gut and is enriched in enteroendocrine cells vs enterocytes.	5
Table 1.2	Clinical chemistry data	25

Abbreviations

12,13-diHOME	12,13-dihydroxy-9Z-octadecenoic acid
ABCC5	ATP-binding cassette subfamily C member 5
BAT	Brown adipose tissue
BMI	Body mass index
COX-4	Cytochrome c oxidase subunit 4
DMEM	Dulbecco's Modified Eagle Medium
DMH	Dorsomedial hypothalamus
eWAT; epiWAT	Epididymal WAT
FACS	Fluorescence-activated cell sorting
FGF21	Fibroblast growth factor 21
GLP-1	Glucagon-like peptide 1
GLP-1R	Glucagon-like peptide 1 receptor
GLP-2	Glucagon-like peptide 2
GWAS	Genome-wide association study
H&E	Haemotoxylin and Eosin
HFD	High-fat diet
iBAT	Interscapular BAT
ICV	Intracerebroventricular
iWAT; ingWAT	Inguinal WAT
KO	Knock out
NBD	Nucleotide binding domain
PBS	Phosphate buffered saline
PRDM16	PR domain zinc finger protein 16

SNA	Sympathetic nerve activity
SDS-PAGE	Sodium dodecyl sulfate - polyacrylamide gel electrophoresis
SNS	Sympathetic nervous system
T2D	Type-2 diabetes
TMD	Transmembrane domain
tPA	Tissue-type plasminogen activator
UCP1	Uncoupling protein 1
VMH	Hypothalamic ventromedial nucleus
WAT	White adipose tissue
WT	Wild type

1 Introduction

1.1 Obesity and its current treatments

More than 1.9 billion adults were overweight in 2016, with 650 million of these individuals classed as obese.[6] The increased adiposity and body mass index (BMI) which is seen in overweight and obese patients is strongly positively correlated with a number of noncommunicable diseases including cardiovascular diseases, Type-2 diabetes (TD2) and some cancers.[6]

While lifestyle changes remain the first line treatment for overweight and obesity[7], these have only achieved moderate success, particularly in more severe cases of obesity, and often are not effective over the long term.[8] In highly obese individuals by far the most effective long term solution for lowering BMI is bariatric surgery, which can have dramatic improvements in health and reduced mortability.[8] Of the different bariatric surgical procedures available, Roux-en-Y gastric bypass shows the greatest decrease in BMI and highest remission rate for T2D.[9]

The mechanism by which Roux-en-Y gastric bypass causes such dramatic weight loss and reversal of T2D is not fully understood, however there is evidence that changes in gut hormone profile play a significant role[8] in addition to simple caloric restriction and malabsorption.[10] Indeed, it has been shown that L-cells, one type of enteroendocrine cell, double in number in the gut following Roux-en-Y surgery in rats.[11]

Whilst bariatric surgery is very successful in reducing morbidity and mortality, by its nature as a surgical procedure it is expensive and carries risk of surgical complications. A large portion of current pharmacotherapy for T2D aims to replicate these bariatric surgery benefits using pharmacological tools.

1.2 Enteroendocrine cells

The gut hormones that contribute to the effects of bariatric surgery are secreted from enteroendocrine cells. These hormones are thought to account for the immediate reversal of T2D seen immediately after Roux-en-Y surgery.[12] Enteroendocrine cells are a diverse range of hormone secreting cells which make up only 1 in every hundred cells in the gut, and together secrete many different gut hormones. Gastrointestinal hormones are secreted in response to detection of food in the gut lumen and have a wide range of effects, including modulating gut motility, stimulating pancreatic exocrine and endocrine secretion, causing gall bladder contraction and mediating satiety.[2] These effects are summarised in Figure 1.1. Studies in obese adults suggest that impaired gut hormone secretion is associated with obesity due to the reduced satiety signalling.[13]

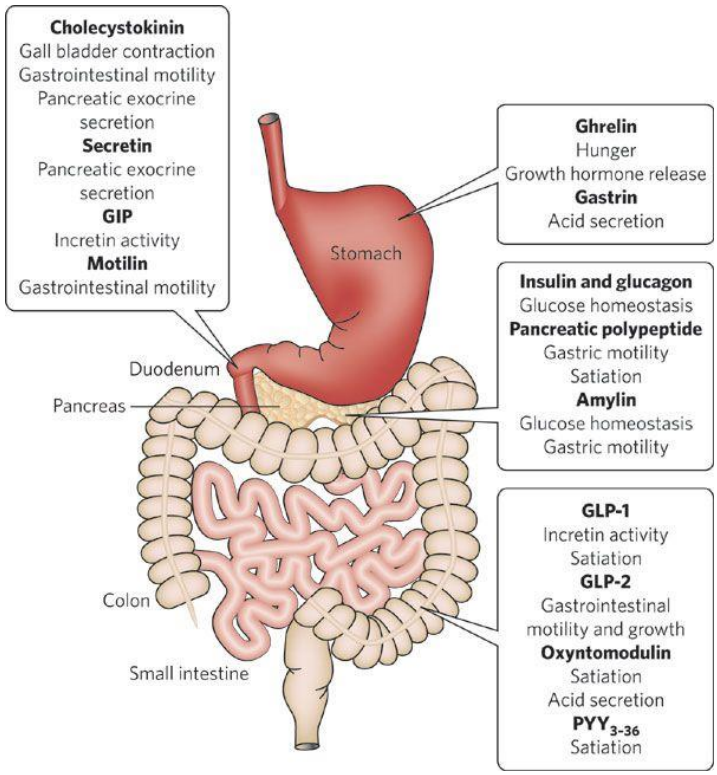


Figure 1.1. A summary of gastrointestinal hormone secretion and their effects.
Adapted from Murphy & Bloom (2006), Gut hormones and the regulation of energy homeostasis.[2] *Nature 444(7121):854-9. doi: 10.1038/nature05484*

Whilst it was originally thought that each enteroendocrine cell sub-type secreted a specific set of hormones, we now understand that the profile of hormones secreted from enteroendocrine cells is more fluid. Instead the gut hormone secretion profile in response to ingested food varies based on the location of the enteroendocrine cell along the length of the gastrointestinal tract.[14]

Of the large numbers of enteroendocrine hormones, glucagon-like peptide 1 (GLP-1) and gastric inhibitory peptide (GIP) are classed as 'incretin' hormones. The incretin hormones are responsible for mediating the incretin effect – the observation that insulin secretion after oral glucose administration is significantly greater than insulin secretion levels after intravenous glucose administration.[15] This is because the incretin hormones act to potentiate insulin secretion from the β-cells in the pancreas. Because the incretins are gut hormones, their secretion is only triggered through oral administration of glucose which activate enteroendocrine cells. In contrast, incretin secretion will not occur after intravenous glucose delivery, and insulin release from the pancreas will be driven by elevated blood glucose levels alone. Through activation of GPCR signalling pathways in pancreatic beta cells, the incretin hormones are estimated to be responsible for up to 50-70% of total post-prandial insulin secretion.[16] Indeed in individuals with T2D, an impaired incretin effect is observed.[15]

GIP is secreted from K-cells which are predominantly located in the duodenum, while GLP-1 is secreted from L-cells which increase in number towards the distal portion of the intestine.[17] GLP-1 is secreted by L-cells in proportion to ingested calories, and as well as potentiating insulin secretion from pancreatic β-cells, has effects on many tissues such as

acting on the brain to inhibit appetite, and acting on the stomach to slow gastric emptying.[17]

Incretin mimetics are a recent drug class for treatment of T2D. Endogenous GLP-1 has a very short circulating half-life of one-two minutes due to degradation by DPP-4, a peptidase enzyme.[18] This severely limits any therapeutic benefits of endogenous GLP-1 infusion. Instead, DPP-4 inhibitors such as sitagliptin, saxagliptin and linagliptin have been developed to raise circulating endogenous GLP-1 levels.[18] In addition to this, DPP-4-resistant GLP-1R agonists such as exenatide and liraglutide are becoming a popular second- or third-line treatment for T2D because of their insulinotropic action [18]. However, these incretin mimetic drugs have several side-effects including nausea and are not nearly as effective as bariatric surgery.[19]

1.3 Profiling of gut identifies expression of ABCC5 in hormone secreting cells

RNA sequencing of gut cells was performed as previously described in the Gribble and Reimann laboratory, Cambridge.[20] Cells were obtained from the gut of NeuroD1-CrexRosa26EYFP or GLU-Venus mice. NeuroD1-CrexRosa26EYFP express yellow fluorescent protein (YFP) in all enteroendocrine cells while GLU-Venus mice express yellow fluorescent protein (YFP) in only proglucagon-expressing cells (L-cells). Gut was collected from the duodenum/jejunum (top 10 cm of the small intestine), the ileum (bottom 10 cm of the small intestine) and the colon. Both fluorescent and non-fluorescent cells were isolated in triplicate by FACS. Total RNA was then sequenced and aligned to the mouse genome. The enteroendocrine cell line GLUTag (a murine L-cell model cell line[21]) was also analysed by the same RNA-seq analysis.

These results show that the membrane transporter ATP-binding cassette subfamily C member 5 (ABCC5) is expressed in enteroendocrine cells and proglucagon-expressing L-cells. (Table 1.1) Furthermore when compared to non-endocrine cells from the same gut section, Abcc5 mRNA expression is enriched in the enteroendocrine cells. This effect is most notably seen in the duodenal and ileal cells. The level of Abcc5 mRNA in GLUTag cells is similar to those measured in the FACS isolated mouse enteroendocrine and L-cells. [Cyranka et al. 2018, manuscript in preparation]

Abcc5			
	FPKM positive cells	FPKM negative cells	log2FC positive / negative (padj)
duodenum_EEC	9.739	1.903	2.050 (0.001)
ileum_EEC	8.851	3.389	0.884 (0.414)
colon_EEC	3.676	2.932	0.809 (0.640)
duodenum_L-cells	7.939	3.350	1.525 (0.228)
ileum-L-cells	12.353	2.039	1.928 (0.019)
colon-L-cells	4.456	4.800	1.357 (0.116)
GLUTag cells	6.491		

Table 1.1. Abcc5 mRNA is expressed in the endocrine cells of the gut and is enriched in enteroendocrine cells vs enterocytes. EEC, enteroendocrine; FPKM, Fragments per Kilobase; log2FC, log2 of the fold change expression between the positive and the negative population; padj, the adjusted p-value indicating if the Log2FC is different from 0 using a Wald test. Data from [Cyranka et al. 2018, manuscript in preparation]

1.4 ABCC5 is a membrane transporter

ABCC5 is a member of the human ATP-binding cassette transporter superfamily. This superfamily translocate substrates across both extra- and intra-cellular membranes, using energy from the hydrolysis of bound ATP.[22] Several ABC proteins have genetic variants associated with human disease, for example ABCC7 (CFTR) mutations cause cystic fibrosis[23] and mutations in ABCC8 lead to either congenital hyperinsulinism or neonatal diabetes[24]. Some ABC proteins, in particular P-gp (ABCB1) and MRP1 (ABCC1), have also been identified as playing a role in multidrug resistance (MDR), and several members of the C subfamily (also known as the MRP family) have been implicated in MDR.[22] MDR is a phenomenon when cells or organisms develop resistance to a range of pharmacological compounds. This is caused by a range of factors, including an acquired ability to decrease drug uptake, increase drug efflux, and altered breakdown.[22].

Like several other ABCC subfamily proteins, ABCC5 (or MRP5) has two transmembrane domains (TMDs) TMD1 and TMD2, each made up of six transmembrane helices which are connected by extracellular and cytoplasmic loops (shown in Figure 1.2a). There are two nucleotide binding domains (NBDs) NBD1 and NBD2, which dimerise to form two composite intracellular ATP binding sites. The energy generated by binding and hydrolysis of ATP is used to drive the dimerization of the NBDs and the translocation of substrates across the membrane, but the exact mechanism is not yet fully understood.

The predicted 3D structure of ABCC5 is shown in Figure 1.2b. This homology structure was created in the Carpenter laboratory, Oxford, using HHpred pairwise sequence alignment from known crystal structures. MODELLER was used with the following crystal structure IDs from the protein data bank: (i) 4q9h (ABCB1 P-glycoprotein Mus

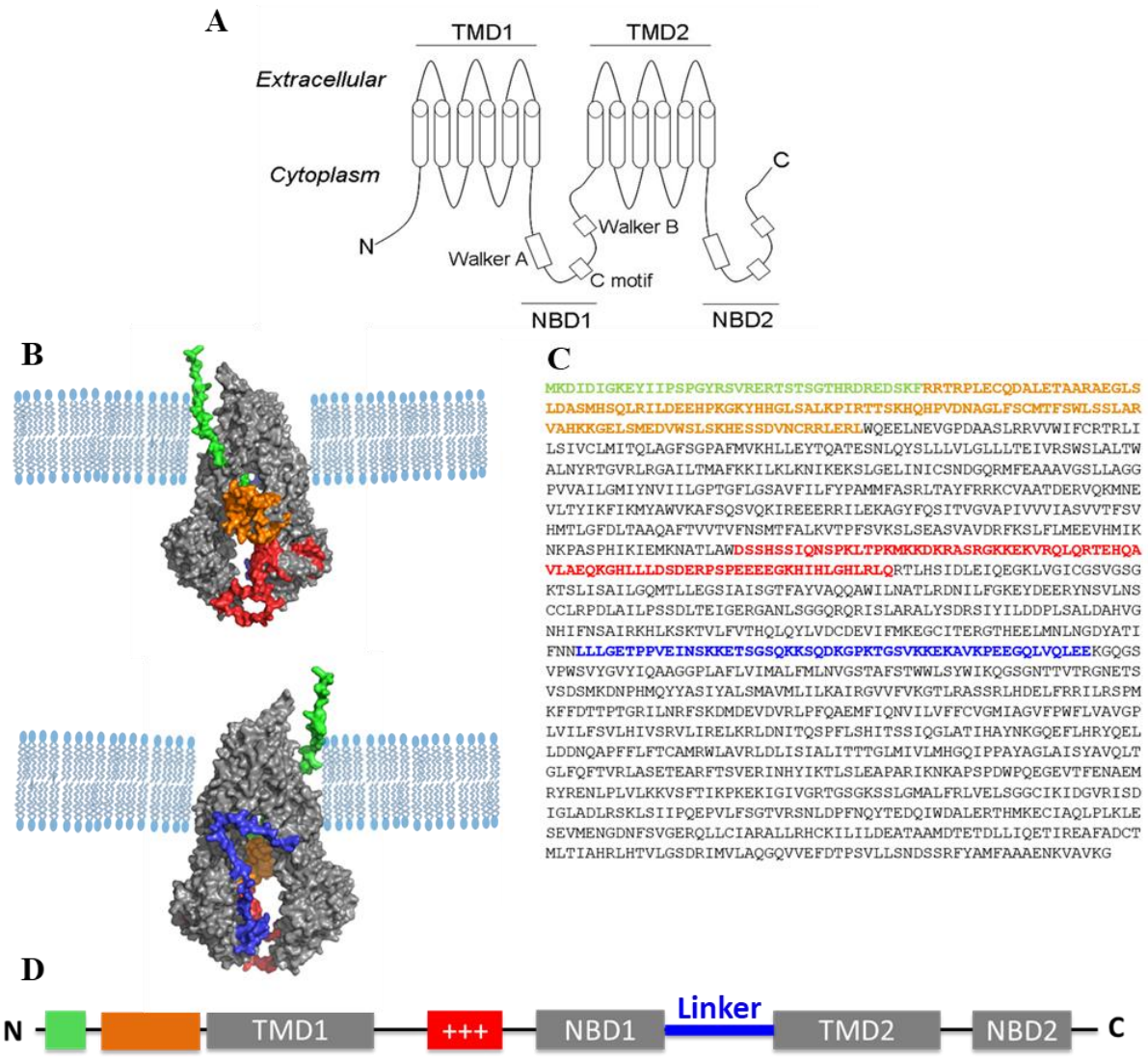


Figure 1.2. The predicted structure of ABCC5. (A) A cartoon representation of the structural organisation of ABCC5, adapted from Leprohon et al[3] Essays Biochem. 2011 Sep 7;50(1):121-44. doi: 10.1042/bse0500121. (B) A model of the structure of ABCC5. (C) The animo acid sequence of ABCC5. (D) The domain sequence of ABCC5, highlighting unique features of ABCC5 within the ABCC subfamily. **Green**, contains two possible lysosomal targeting sequences; **Orange**, models to a subdomain with known peptidase activity; **Red**, positively charged peptide sequence. Work and figures for (B), (C) & (D) done by Belinda Faust.

musculus), (ii) 4ry2_A (peptidase-containing ABC transporter PCAT1 from Ruminiclostridium thermocellum), (iii) 4q4h_A and 4q4h_B (TM287/288 from Thermotoga maritima), (iv) 3nh6_A (NBDs only ABCB6 from Homo sapiens), (v) 3gd7_A (NBDs only ABCC7 from Homo sapiens), (vi) 3b5x_A (MsbA from Vibrio cholerae) and (vii) 4c37 (NBDs only ABCC1 from Homo sapiens).

In the sequence of ABCC5, (Figure 1.2c) several regions have been identified that are unique to this particular subfamily member (Figure 1.2d). At the N-terminal end of the ABCC5 sequence, a region with no known homology to any other protein has been identified. This domain features two possible lysosomal targeting sequences (YRSV & YIIP) and is shown in green in Figure 1.2d. Adjacent to this domain is another domain that is not found in other mammalian ABC proteins, however it contains a subdomain that has been shown to have peptidase activity in another ABC protein[25] (ABCC5 C39 is proposed as the catalytic cysteine residue seen at C21 in PCAT1[25]), this is shown in orange in Figure 1.2d. Finally, a positively charged peptide sequence located between TMD1 and NBD1, unique to ABCC5, has been identified and is shown in red in Figure 1.2d.

ABCC5 has been shown to transport cyclic nucleotides[26] and folates[27] – mediating drug resistance to antifolates[27,28]. However, this work has only been performed in cell culture and the affinity of the substrates for ABCC5 is low, limiting the conclusions that can be drawn about whether cyclic nucleotides and folates are true physiological substrates of ABCC5. Studies in *C. elegans* show that RNAi knockdown of ABCC5 is lethal in embryogenesis, and that in this organism ABCC5 acts as a heme exporter.[29] In sea urchin

embryos ABCC5 has been shown to play a developmental role in hindgut invagination through transport of cAMP.[30]

More recently, Jansen and colleagues at the Netherlands Cancer Institute have used untargeted metabolomics in HEK cells overexpressing ABCC5 to identify the metabolite N-lactoyl-Phe as an ABCC5 substrate.[31] They showed that N-lactoyl-Phe was transported into inside-out vesicles by ABCC5.[31] Furthermore, this same group investigated the role of ABCC5 at a mammalian whole-organism level through generating $ABCC5^{-/-}$ mice.[32] Untargeted metabolomics was used to show an accumulation of a range of metabolites in the tissues of $ABCC5^{-/-}$ mice compared to WT controls.[32] Of the nine metabolites that were found to be upregulated in more than one tissue-type, six were identified by matching to metabolomic database standards. Five of these six metabolites were shown to contain a C-terminal glutamate residue, with the sixth metabolite's C-terminal residue identified as the chemically similar aspartate.[32] These results strongly indicate that ABCC5 may be transporting glutamate conjugates. Indeed, HEK cells overexpressing ABCC5 were then used to confirm that these identified glutamate conjugates were effluxed from the cells to a significantly greater extent than those not overexpressing ABCC5.[32] Finally, vesicular transport assays showed that the glutamate conjugates *N*-acetylaspartate (NAA), *N*-acetylaspartylglutamate (NAAG), *N*-acetylaspartyl-glutamyl-glutamate ($NAAG_2$), and phosphoribosylaminoimidazolesuccinocarboxamide (SAICAr) were transported into inside-out vesicles in a manner that was both ABCC5- and ATP-dependent.[32]

The disparate range of studies described implicates ABCC5 in a myriad of diverse functions and physiological roles in different organisms. While in vitro, ABCC5 is clearly

capable of transporting a range of different substrates, the physiological relevance of this data is limited. In mammals, however, the physiological role of ABCC5 would appear to be the transport of glutamate analogues.[32]

1.5 ABCC5 as a T2D susceptibility gene

A genome-wide association study (GWAS) by Direk *et al.* identified ABCC5 as a novel T2D susceptibility gene. Human subjects with high expression of ABCC5 in subcutaneous adipose tissue were three times more likely to have T2D than those with low ABCC5 expression.[33] Additionally, even in individuals without T2D, elevated ABCC5 expression in adipose tissue was shown to be associated with reduced insulin sensitivity and increased visceral fat accumulation. The link to T2D was confirmed in three different populations, suggesting that ABCC5 is a universal risk factor, independent of ancestry.[33]

1.6 Work leading up to this study:

1.6.1 ABCC5 plays a role in GLP-1 secretion in a model L-cell line

Previous work performed in our laboratory has shown that ABCC5 plays a role in GLP-1 secretion in GLUTag cells, an L-cell model cell line[21]. siRNA knockdown of ABCC5 in GLUTag cells resulted in 60% increased secretion of GLP-1, while plasmid overexpression of ABCC5 decreased the GLP-1 secretion to below the secretion levels observed in the absence of nutrients (Figure 1.3). ABCC5 protein expression levels are therefore inversely related to GLP-1 secretion levels. [Cyranka et al. 2018, manuscript in preparation]

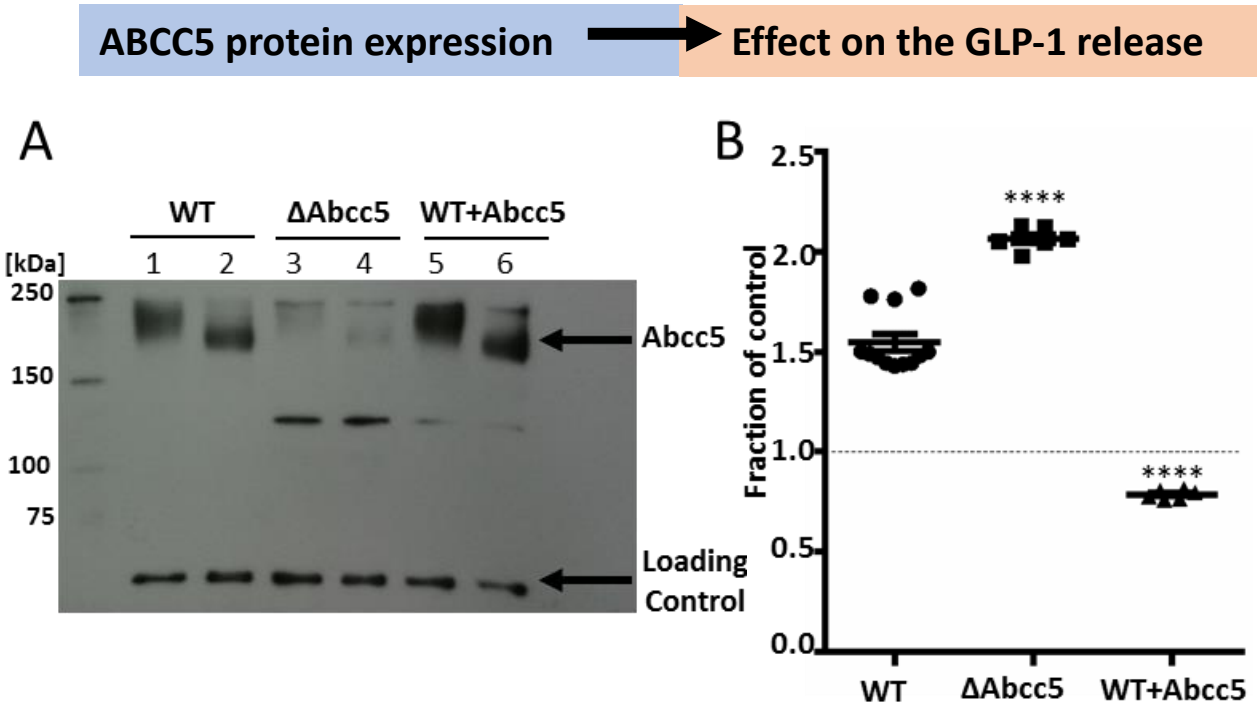


Figure 1.3. GLP-1 exocytosis from GLUTag cells is dependent of ABCC5 protein levels. (A) Western Blot analysis of WT GLUTag cells (lanes 1,2), GLUTag cells with attenuated ABCC5 expression (lanes 3,4) and overexpressed ABCC5 (lanes 5,6). Lanes 1,3,5: unheated samples; lanes 2,4,6: heated samples. (B) GLP-1 exocytosis following a 2 hour incubation in 5.6mM glucose (n=4) as determined by ELISA (Cisbio); exocytosis levels observed at rest (no glucose, dashed line,). *****P≤0.0001; unpaired, two tailed t-test*.

1.6.2 ABCC5 KO mouse have a lean phenotype

The negative correlation between ABCC5 protein expression levels and GLP-1 secretion was confirmed in primary gut organoid cultures grown from ABCC5 KO and WT mice. ABCC5 KO primary cultures secrete more GLP-1 that WT primary cultures. This result was shown in both the fed and fasted state (Figure 1.4a).

This result is further confirmed from *in vivo* measurements. Due to limitations of the GLP-1 assay, we have been consistently unable to detect GLP-1 from tail bleeds. However, terminal heart punctures have allowed successful measurements of circulating GLP-1 levels. Terminal bleeds were collected 5 minutes after an oral glucose gavage

administered following overnight fast. Analysis of these samples show that the circulating levels of GLP-1 in ABCC5 KO mice are significantly higher than WT controls 5 minutes after oral gavage of glucose (Figure 1.4b).

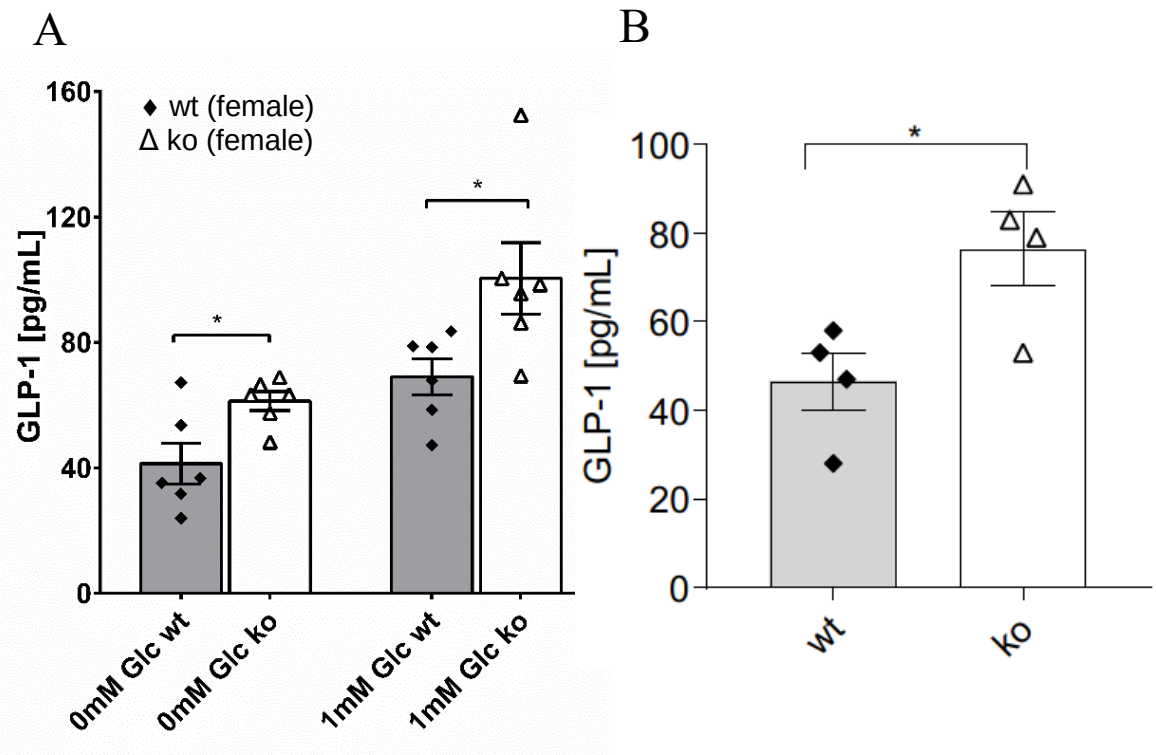


Figure 1.4 GLP-1 secretion in ABCC5 KO mice (A) from gut primary cell cultures. Gut organoids grown from ABCC5 KO mice (n=6) secrete more GLP-1 than WT littermate (n=6) control organoids. This difference is seen in both the fasted (0mM Glucose) and fed (1mM Glucose) states. (B) from terminal heart bleeds. Blood samples collected from terminal bleeds 5 minutes after an oral glucose gavage administered following overnight fast (n=4 of each). Data shown as mean±SEM, unpaired, two tailed t-test, *P≤0.05

In obese subjects, reduced GLP-1 secretion after meals is often observed and has been proposed as contributing to the pathophysiology of obesity.[34] Therefore higher circulating levels of GLP-1 would be predicted to provide resistance to obesity or even contribute to a lean phenotype. This is widely seen through the weight loss caused by GLP-1 mimetics in clinical treatment of T2D.[35]

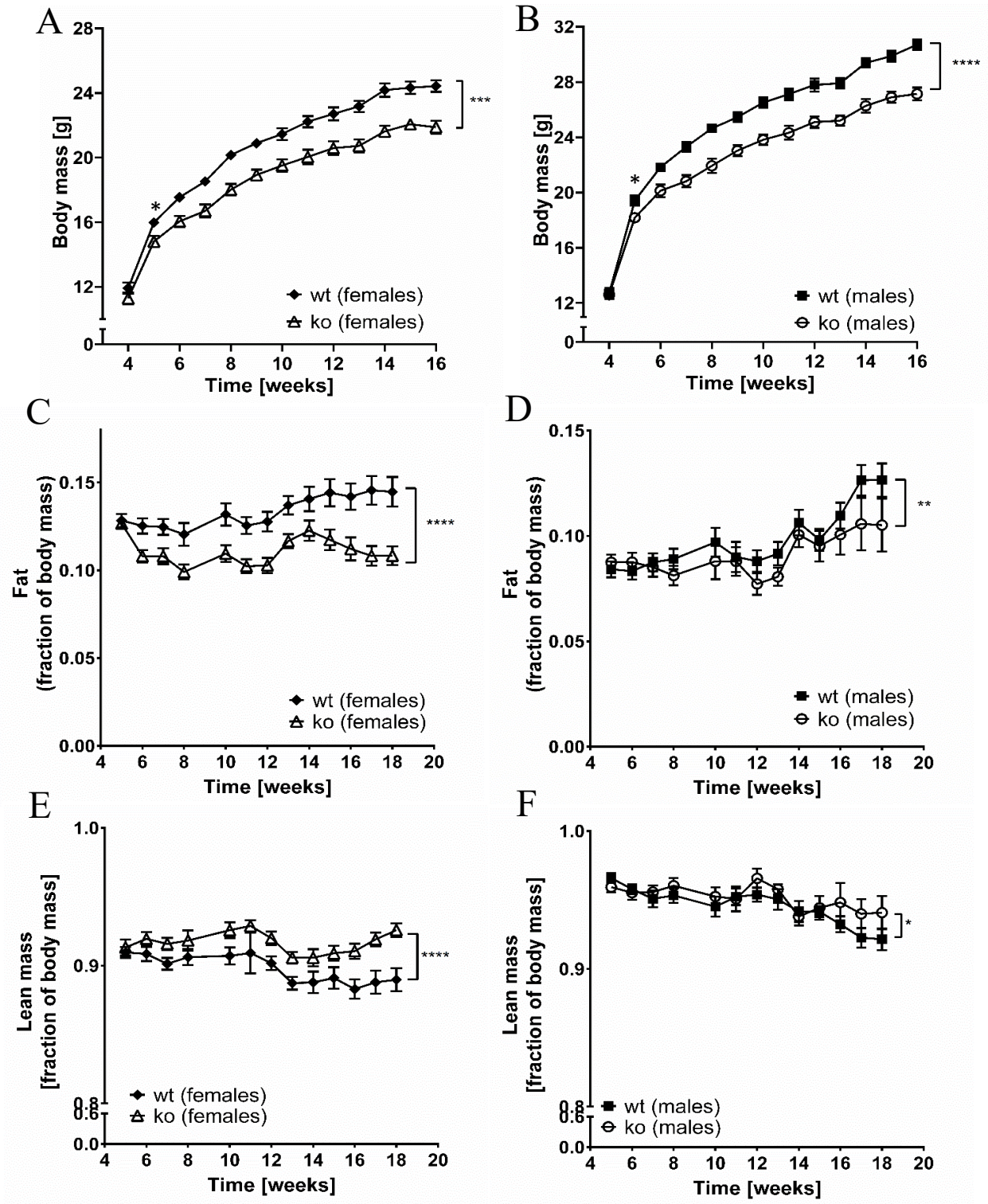


Figure 1.5. Mass and body composition of Abcc5 knock-out (ko) mice and wild-type (wt) litter mate controls. Weekly body mass (A,B), lean mass (C,D) and fat mass (E,F) were recorded by EcoMRI for male:female:wt:ΔAbcc5 = 15:15:15:14 from weaning over a period of 12 weeks. Each data point represents mean±SEM of n=9-15 for males and n=13-15 for females for each genotype. Data were analysed by Two-way Anova, Bonferroni ad-hoc test. *P≤0.05, **P≤0.01, ***P≤0.001; ****P≤0.0001. Body mass (A,B) at week 5 for both female and male mice were analysed by unpaired, two-tailed *t*-test, *P<0.05. Data for C-F is presented as a fraction of whole body mass measured at the same time point.

Indeed as reasonably predicted, ABCC5 KO mice show a lean phenotype (Figure 1.5) with less body mass (Figure 1.5a,b), less fat (Figure 1.5c,d) and more lean mass (Figure 1.5e,f), determined by EchoMRI™. There were no observed changes in water or food consumption between KO and WT animals.

In-vivo glucose tolerance tests and insulin tolerance tests showed that ABCC5 KO mice have increased insulin sensitivity when compared to WT littermates (Figure 1.6). [Cyranka et al. 2018, manuscript in preparation]

Indirect calorimetry was performed on the ABCC5 KO mice and WT littermate controls. The data obtained show that female KO mice have increased oxygen consumption (VO_2), enhanced carbon dioxide release (VCO_2) and increased energy expenditure (EE) in both dark and light cycles (Figure 1.7a-c). [Cyranka et al. 2018, manuscript in preparation] The KO males show a similar trend although it does not reach statistical significance (Figure 1.7d-f). Since respiratory exchange ratio (RER) is calculated by VCO_2/VO_2 and these two values follow the same trends, there were no changes in RER for either genders (data not shown). Both female and male KO mice are more active in both dark and light cycles, therefore showing increased total activity, XT (the sum of ambulatory movement and fine movement) (Figure 1.7g and h). [Cyranka et al. 2018, manuscript in preparation]

In the female mice, the increase in locomotive activity can explain the increased total energy expenditure in ABCC5 KO mice. The increased locomotive activity is also observed in male KO mice, but unlike the females their energy expenditure does not change significantly compared to WT controls. As the KO males also show a lean phenotype this led us to conclude that there may be another contributing factor(s), which

remains to be identified, most likely thermogenesis, that is modulating energy expenditure in the ABCC5 KO mice.

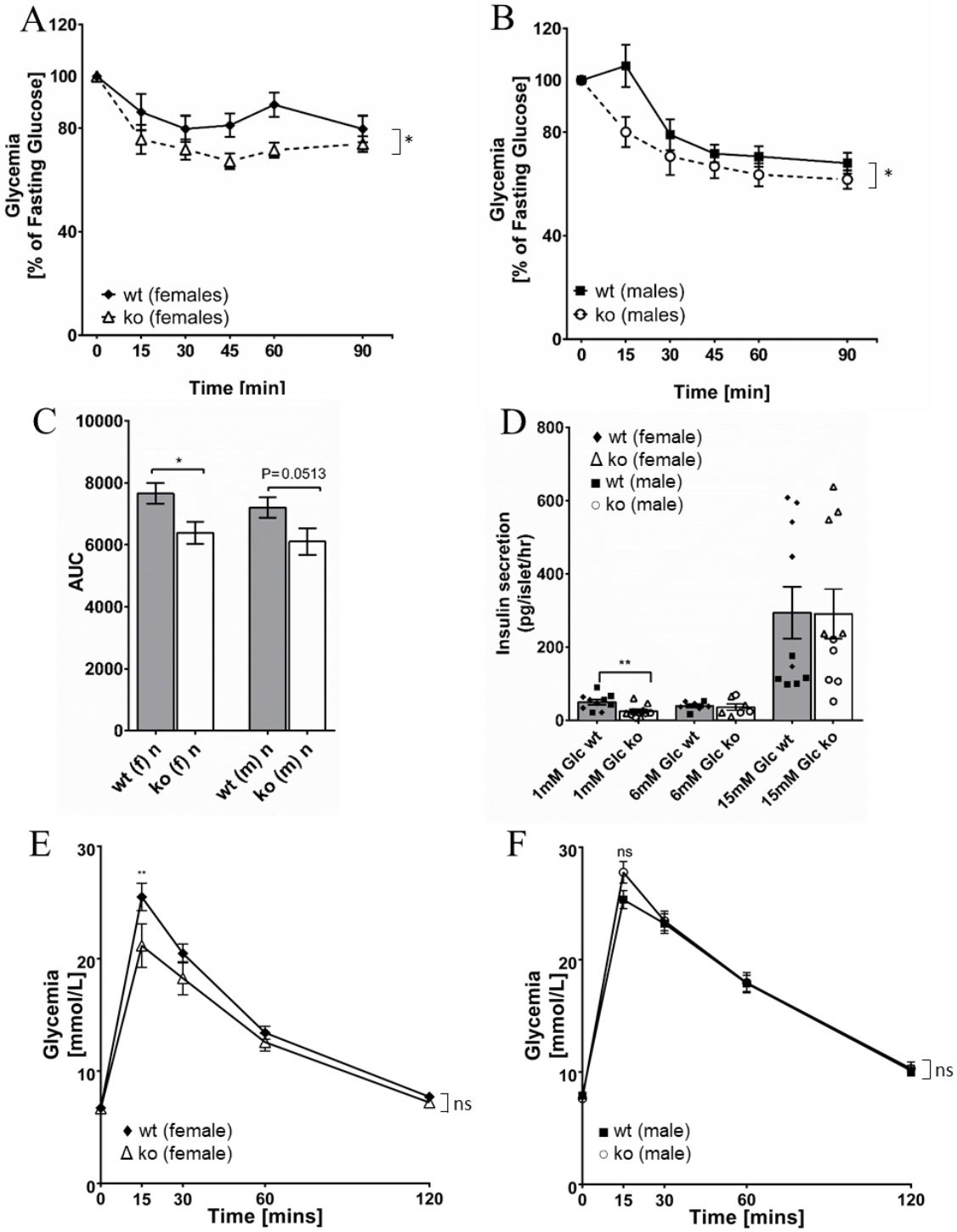


Figure 1.6. ABCC5 KO mice show increased insulin sensitivity. (A) Intraperitoneal Insulin Sensitivity Tolerance Test (IPIST) for female and (B) male mice. (C) Calculated area under the curve (AUC). IPIST was performed on mice aged 14 weeks, male:female:wt:ΔAbcc5 = 15:15:15:14. Data shown as mean± SEM, and were analysed by two-way ANOVA, Bonferroni ad-hoc test. *P<0.05, **P<0.01. Area under the curve results were analysed by unpaired, two-tailed *t*-test. *P<0.05. (D) Total insulin secretion was measured from isolated islets in parallel from Abcc5 ko mice and wt litter mate controls (male:female:wt: ΔAbcc5=5:5:5:5) Data shown as mean± SEM, and were analysed by two-way ANOVA. *P<0.05, **P<0.01. (E) intraperitoneal glucose tolerance tests (IPGTT) on 13 week old female and (F) male mice (male:female:wt:ΔAbcc5 = 15:15:15:14). Data shown as mean± SEM and were analysed by multiple comparison two-way ANOVA with a Bonferroni ad-hoc test.

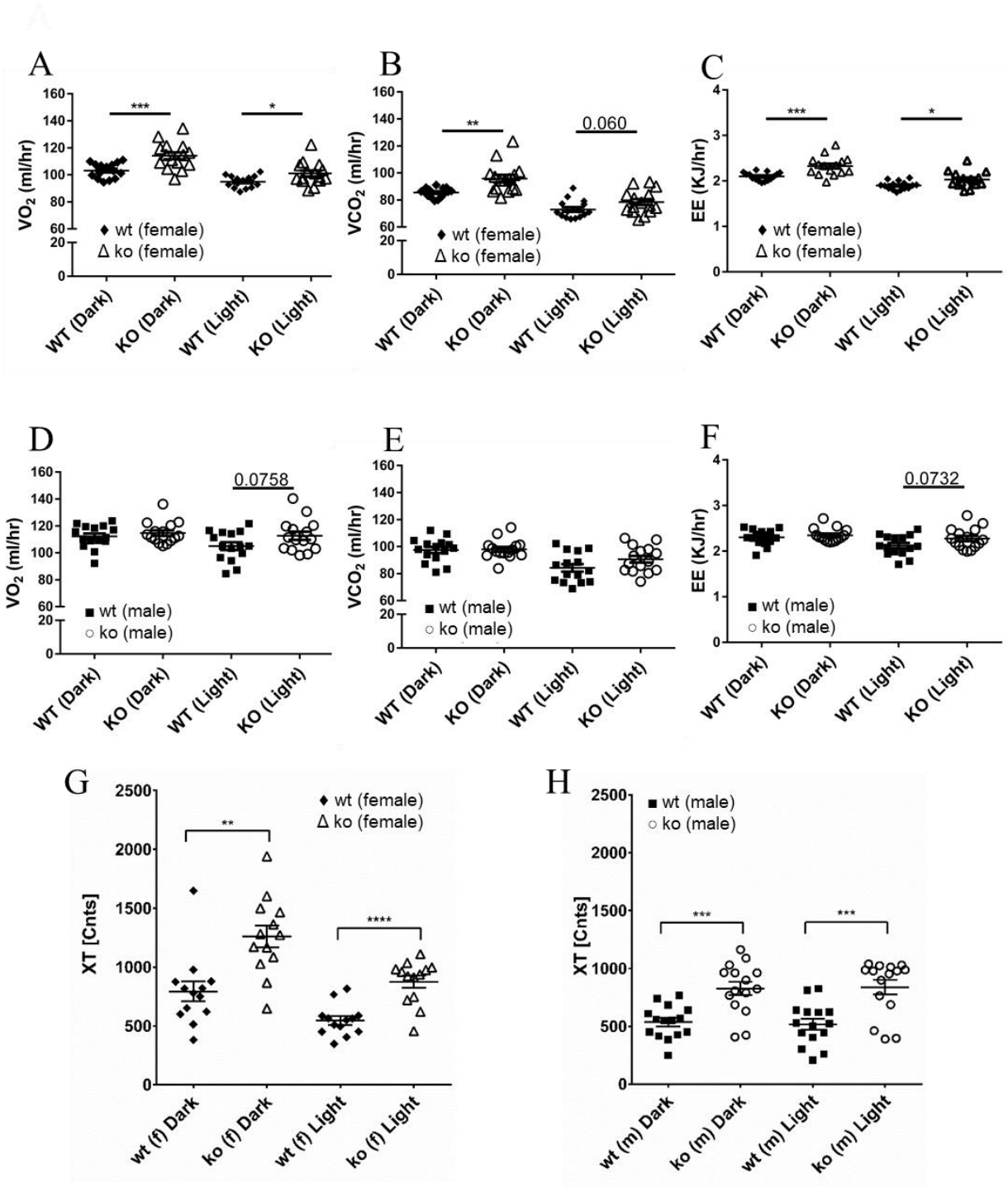


Figure 1.7. Metabolic profiling of ABCC5 KO mice. (A) Female oxygen consumption VO2 (B) female carbon dioxide release VCO2, (C) female energy expenditure and (D) male oxygen consumption VO2 (E) male carbon dioxide release VCO2 and (F) male energy expenditure. All data was ANCOVA adjusted for lean mass. Total activity (XT) is shown in (G) for females and (H) males. Abcc5 ko mice and wt littermates controls (male:female:wt:ΔAbcc5 =15:11:15:15) were individually housed in PhenoMaster cages fitted with photo beam-based activity monitoring systems at 12 weeks of age. The data shown in G and H is the average XT activity per hour plotted separately for light/dark cycle for each mouse; Error bars: mean±SEM; unpaired, two-tailed *t*-test,*P<0.05, **P<0.01, ***P<0.001.

1.6.3 RESEARCH HYPOTHESIS

Because of the discrepancy in energy expenditure and locomotive activity data in male KO mice we hypothesise that the additional factor(s) modulating energy expenditure in the ABCC5 KO mice may be thermogenic activity of adipose tissue. We therefore propose that the ABCC5 KO mice show a difference in brown adipose tissue (BAT) thermogenic activity and/or white adipose tissue (WAT) browning when compared to WT littermate controls.

Furthermore, ABCC5 KO animals show increased GLP-1 levels, which has been shown to increase the thermogenic activity of BAT[36-41] and WAT[41] (discussed further in section 1.8). Increased BAT activity as a result of GLP-1R agonism has been shown to accelerate clearance of triglycerides from the circulation into BAT for use as thermogenic fuel.[37]

The blood chemistry of ABCC5 KO mice also supports this theory. Analysis of blood samples collected from terminal heart puncture of mice aged 18 weeks show that ABCC5 KO mice have lowered circulating cholesterol, LDL, HDL, and triglycerides compared to WT controls. These samples were collected 5 minutes after oral glucose gavage following overnight fast [TABLE 1.2]. The reduced circulating triglyceride levels in females further suggest increased thermogenic activity of BAT and/or WAT.

1.7 ABCC5 tissue expression

ABCC5tm1b/+ (TM1b LacZ) reporter mice were generated to show the expression pattern of ABCC5. However, the LacZ reporter mice show no expression of LacZ in adipose tissue.

The GWAS data from the Direk *et al.* paper[33] correlates expression of ABCC5, specifically in adipose tissue, to T2D. However this is based solely on mRNA data, not

confirming ABCC5 protein expression. It is important to note that association studies do not differentiate between cause and effect. Hence the observed increase in ABCC5 expression in adipose tissue of diabetics could be induced by lipid toxicity for example, as opposed to ABCC5 expression driving lipid deposition and contributing to a T2D phenotype.

ABCC5 protein detection has been hampered by the fact that many antibodies against ABCC5 are non-specific, and protein expression data generated from immunohistochemistry is therefore thought to have variable reliability. For example 'The Human Protein Atlas' shows a large variability between ABCC5 RNA expression and protein expression in nearly all tissues.[42] Indeed this is discussed by Nies *et al.* who also observe discordant expression of ABCC5 mRNA and protein levels and confirm the difficulty of detecting ABCC5 protein levels[43]. Scheffer and colleagues also described difficulty detecting ABCC5 protein despite robust mRNA expression, and suggest that this may be due to inefficient translation of ABCC5 mRNA.[44] In agreement with this proposal, 'The Human Protein Atlas' reports RNA expression of ABCC5 in adipose tissue with no correlated protein expression.[42] Furthermore, Protein databanks do not report any data on ABCC5 mRNA or protein expression in adipose tissue in mice.

Data from the Allen brain atlas shows that ABCC5 is highly expressed in the hippocampus, but not in any other mouse brain regions. In a study of ABCC proteins in the human brain, Nies *et al.* used qPCR and immunohistochemistry to show that ABCC5 is expressed in the capillary endothelial cells of the luminal blood-brain barrier, in astrocytes of subcortical white matter, and in pyramidal neurons in the human brain.[43]

Finally, as discussed in Section 1.3, ABCC5 mRNA is detected in enteroendocrine cells in the gut where ABCC5 is observed to be upregulated in comparison to surrounding enterocytes. [Cyranka et al. 2018, manuscript in preparation]

1.8 Fat browning

Adipose tissue has historically been viewed as an inactive storage tissue. However in more recent years it has been shown to be a dynamic organ with multiple physiological roles, including hormone secretion and thermogenesis – making it an exciting target for obesity treatment.[45] There are two distinct types of adipose tissue in mammals: white adipose tissue (WAT) and brown adipose tissue (BAT). WAT functions primarily as a large energy store in the form of triglycerides in lipid droplets. In contrast BAT is a primarily thermogenic tissue that generates heat via oxidation of triglycerides. WAT cells are unilocular (a single lipid droplet) with few mitochondria whilst BAT cells are multilocular (several smaller lipid droplets) with a much higher number of mitochondria (Figure 1.8) which causes their brown appearance.[46]

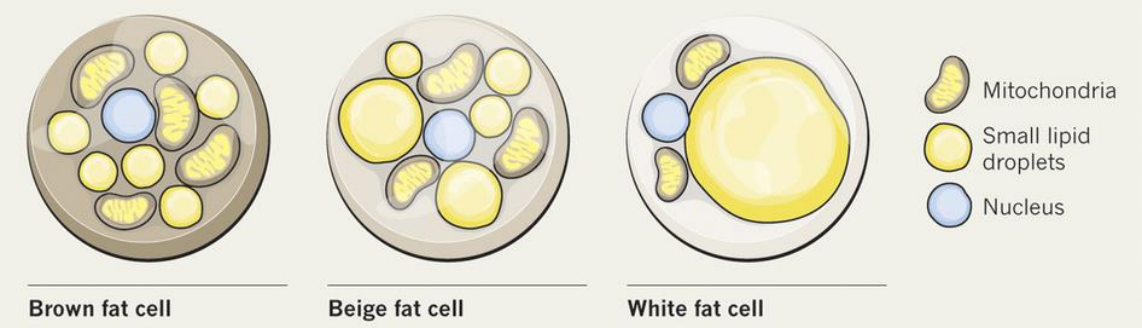


Figure 1.8. The types of different adipocyte cells.
Adapted from Owens (2014) Nature 508, S52–S53 (17 April 2014) doi:10.1038/508S52a [5]

BAT tissue generates heat through expression of uncoupling protein 1 (UCP1) in mitochondria. UCP1 allows protons to leak back into the mitochondrial matrix, thereby

dissipating the proton gradient and uncoupling the electron transport chain from ATP synthesis; this generates heat through futile cycling.[47]

There are two types of WAT: visceral WAT and subcutaneous WAT. Increased levels of visceral WAT are associated with T2D and cardiovascular disease.[48] In contrast, subcutaneous WAT is associated with a lowered risk of T2D and improved insulin sensitivity.[48] After bariatric surgery, the distribution of fat changes – subcutaneous WAT storage is favoured over visceral WAT, likely contributing to the metabolic benefits of the surgery.[49] WAT is widely spread throughout the body in a large number of different depots in both mice and humans. BAT is located in a small number of discrete depots – in mice these are intrascapular and axillary (Figure 1.9a). In humans BAT depots are found deep in the neck, close to muscle tissue (Figure 1.9b).

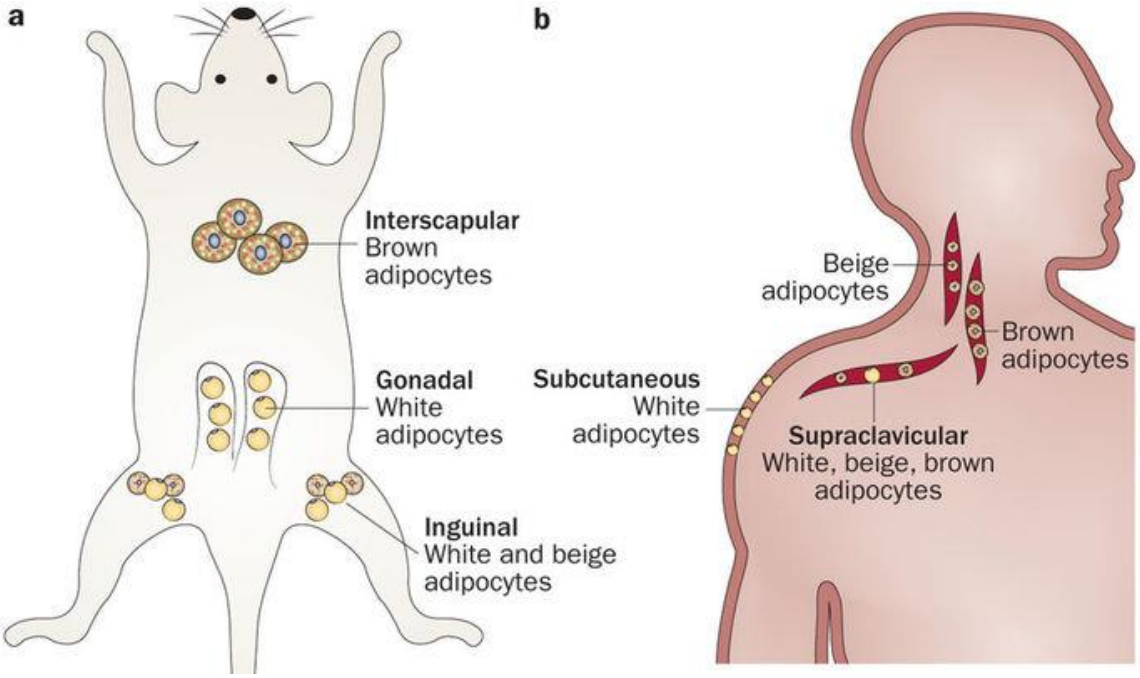


Figure 1.9. White, brown, and beige fat depots in mice (a) and humans (b). Adapted from Bartelt et al. Nature Reviews Endocrinology volume 10, pages 24–36 (2014) doi:10.1038/nrendo.2013.204 [4]

The discovery that brown-like adipocytes are found outside of classical BAT depots has been a significant one.[50] These cells are described as beige or brite (brown-in-white) adipocytes and are generally thought of as adipocytes within WAT depots that have brown-like features such as multilocular lipid droplets and increased number of mitochondria and UCP1 expression (Figure 1.8). The accumulation of beige adipocytes in WAT depots is known as 'browning' and this is an inducible and reversible process.[4]

Different WAT depots have different levels of susceptibility to browning. This has been studied in mice where it has been shown that inguinal WAT (iWAT)(labelled in Figure 1.9) is highly susceptible to browning.[51] In contrast, male epididymal WAT (eWAT) is much more resistant to browning.[51]

BAT and WAT have distinct embryonic lineages. BAT cells are derived from the same lineage as skeletal muscle cells and are Myf5-positive.[48] In contrast, it was thought that all WAT cells are Myf5-negative, making Myf5 a simple marker for distinguishing the two cell types.[52] However, more recently the developmental origins of BAT and WAT have been shown to be much more highly complex, with a subset of WAT cells being Myf5-positive.[52] Nonetheless, beige and BAT cells are still distinct populations of cells, for example beige adipocytes are Tbx1-positive while BAT is not.[51] The full picture of WAT, beige, and BAT cell lineages is complicated and not fully understood and will not be discussed in detail for the purpose of this thesis.

An increase in obesity in humans is marked by both an increase in adipocyte size (hypertrophy) and adipocyte number (hyperplasia). Since mature adipocytes are post-mitotic and terminally differentiated cells, they cannot cause adipocyte hyperplasia. Through analysing the levels of ^{14}C in genomic DNA from individuals exposed to nuclear

bomb tests it is possible to pinpoint the birth date of individual cells. This technique was used to show that there is an approximately 10% annual turnover of adipocytes in humans at all adult ages and BMI levels.[53] Therefore resident adipocyte precursors must be present in humans.[52] Indeed adipocyte precursors are present, although they have proved difficult to find and identify. With evidence from lineage tracing it is currently hypothesised that the BAT and WAT adipocyte precursors may reside in the vasculature,[52] however the exact identity of these precursors is not yet confirmed. In mice it has been shown that beige adipocytes arise from different precursors to classical WAT cells, and these precursors are also different to BAT precurors.[4] However there is also evidence supporting the ability of classical WAT cells to adopt beige-like characteristics, suggesting that beige adipocytes in WAT originate from both WAT transdifferentiation and beige de novo differentiation.[4]

Another consideration of both BAT and WAT tissues are their roles as secretory organs; both tissues secrete a range of so-called adipokines and 'batokines'. Among the hundreds of adipokines secreted from WAT, two of the best known are leptin and adiponectin. Because of its known primary function as a thermogenic tissue, BAT was not investigated as a secretory tissue for many years. However more recent study has shown that a variety of secretory proteins, with autocrine, paracrine, and possibly some endocrine roles are produced in BAT.[54] The complete role of these 'batokine' molecules has yet to be fully explained.

The process of browning has been widely studied and is of great interest as a therapeutic target for obesity due to the large metabolic benefits. Animals with more beige adipocytes have been observed to be protected from T2D and obesity.[49] Due to the nature of beige

fat as an inducible thermogenic tissue, cold temperature is a major inducer of browning.[4] However a range of other stimuli have also been shown to cause browning, such as β_3 receptor agonism, exercise[4,55,56], and various hormonal stimuli. Browning of eWAT (but not iWAT) is also observed after Roux-en-Y gastric bypass surgery in rats[57].

In addition to browning of WAT, the activity of BAT tissue can be modulated. BAT activity is controlled by BAT mass, its activation status, and environmental factors.[4] Similarly to WAT, cold stimulus is a major inducer of increased BAT activity, acting via increased sympathetic stimulation. Circulating endocrine factors like FGF21, BMP-9 and irisin also increase BAT activity, a result that is seen in parallel with beiging of WAT.[58] Therefore, as would physiologically be expected, a large number of the stimuli for WAT beiging also cause increased BAT activity. However, this doesn't always occur and some pathways and activators of BAT activity are not shared with inducing WAT beiging and vice versa (for example - [59,60]).

GLP-1 has been implicated in several studies as an inducer of fat thermogenesis. The first to report this phenomenon were Lockie *et al.*, who showed that intracerebroventricular (ICV) infusion of GLP-1 led to an increase in BAT temperature and increased electrophysiological activity of the interscapular BAT (iBAT) sympathetic nerves.[40] Beiroa and colleagues subsequently showed that ICV injection of liraglutide, a commercially used GLP-1 analogue, causes both increased BAT thermogenesis and increased expression of UCP1 in epididymal WAT (eWAT).[41] It was then shown that the thermogenesis stimulated in BAT and WAT by liraglutide was dependent on signalling of AMPK in the hypothalamic ventromedial nucleus (VMH).[41] Similarly, Wei *et al.* treated HFD-mice intraperitoneally with another commercially available GLP-1

analogue, exendin-4, and showed increased markers of BAT activity.[39] Heppner and colleagues used indirect calorimetry of HFD-fed Glp-1r-KO mice to provide more evidence that GLP-1R signalling contributes to BAT thermogenesis.[38] However this study also showed that BAT thermogenesis did not play a significant role in lowering body-weight in liraglutide treated diet-induced obese mice.[38] Repeating the Wei *et al.* study but with ICV injection, Kooijman *et al.* also showed that exendin-4 treatment activates BAT and also shows beiging of the subcutaneous WAT.[37] Lee *et al.* also confirm that GLP-1 activates BAT after injection into the dorsomedial hypothalamus (DMH), and furthermore that knockdown of Glp-1r in the DMH causes reduced BAT temperature and UCP1 expression.[36]

The process of thermogenesis in BAT requires large amounts of energy and this is fuelled primarily by glucose and fatty acids. The fatty acids are sourced from de novo lipogenesis, the lipid droplets within BAT cells, and from uptake of circulating fatty acids.[61] Lee *et al.* demonstrated that injection of GLP-1 into the DMH increased triglyceride mobilisation from the liver, in tandem with the increased BAT activity observed.[36] This increased triglyceride mobilisation is proposed to be the fuel source for the increased BAT activity. However, in a longer-term model used in the same paper, in which GLP-1Rs were knocked down for 4 weeks, impaired BAT activity was seen alongside increased circulating triglyceride levels and fat accumulation in the liver. In this case the authors suggest that this is because the impaired BAT is unable to use the triglyceride.[36] In another long-term model of GLP-1R agonism, Wei *et al.* treated HFD mice with exendin-4 for 14 weeks and observed lowered circulating triglyceride levels compared to saline control; this was observed alongside markers of increased BAT activity.[39] In our ABCC5 KO mouse model, we observe lowered circulating levels of triglycerides in blood collected

from terminal heart puncture at 18 weeks in the female mice (see Table 1.2). Perhaps this might indicate a difference in BAT metabolism.

		t-Test results					
Parameter	**Units**	**Female**			**Male**		
		WT (n=15)	KO (n=14)	P-value	WT (n=15)	KO (n=15)	P-value
Total Cholesterol	(mmol/l)	1.69 ± 0.07	1.43 ± 0.05	**	1.94 ± 0.06	1.79 ± 0.04	*
HDL	(mmol/l)	1.19 ± 0.05	1.01 ± 0.05	**	1.45 ± 0.05	1.36 ± 0.03	ns
LDL	(mmol/l)	0.46 ± 0.02	0.39 ± 0.02	**	0.50 ± 0.01	0.46 ± 0.01	*
Triglycerides	(mmol/l)	0.78 ± 0.03	0.63 ± 0.03	***	0.82 ± 0.04	0.72 ± 0.03	ns

Table 1.2 Clinical chemistry data. Blood samples collected from terminal heart puncture of 18 week old mice. Samples collected 5 minutes after oral glucose gavage following overnight fast. mean±SEM; unpaired, two-tailed *t*-test,*P<0.05, **P<0.01, ***P<0.001. Data from [Cyranka et al. 2018, manuscript in preparation]

In its primary function as a thermogenic tissue, BAT contributes to the whole-organism energy balance and is a critical tissue for thermogenesis in response to a cold challenge.[62] As such, BAT thermogenic activity is controlled by the central nervous system via the activity of the sympathetic nerves innervating the BAT.[63] The hypothalamus acts as a site of integration for cutaneous temperature signals, endocrine signals, and a plethora of other factors that subsequently modulate BAT activity via hypothalamic regulation.[63] Indeed, the studies previously discussed by Lee *et al*. and Beiroa *et al.* demonstrate the critical role of dorsomedial hypothalamic signalling for BAT thermogenesis, particularly for mediating GLP-1-induced thermogenesis.[36,41]

While the complete neuronal signalling pathway (mostly described for BAT, see Morrison *et al.* 2014[62]) is not as completely known for WAT, there are numerous studies that also show that activity and regulation of beige fat depots is controlled through central

nervous system regulation, with the hypothalamus again playing a critical role.[62,64-67] This is unsurprising considering that changes in BAT and beige fat activity often occur in parallel.

We see our protein of interest, ABCC5, expressed in the brain and in enteroendocrine cells, and propose that the lean phenotype seen in ABCC5 KO mice may be as a result of a difference in fat metabolism, perhaps due to altered central thermogenic signalling pathways.

2 Materials & Methods

2.1 Animals

ABCC5 knockout mice were generated at MRC Harwell using CRISPR/Cas9 to create a 372nt deletion of Exon ENSMUSE00001236135 in murine embryos with a C57BL/6NTac background strain. Homozygous wild type (WT) and knockout (KO) mice were generated from heterozygous breeding pairs, enabling comparison of littermate controls, and pups were weaned at 4 weeks of age. Animals were housed on a 12-hour light-dark cycle (light 7 a.m. to 7 p.m., dark 7 p.m. to 7 a.m.) with controlled temperature (21 ± 2°C) and humidity (55 ± 10%), and with ad libitum access to water (10 ppm chlorine) and standard laboratory chow [RM3; Special Diet Services, Essex, United Kingdom]. Animals were sacrificed by cervical dislocation at the ages of 18 - 20 weeks and tissues were collected as described below. All procedures and animal studies were carried out in accordance with the Animals (Scientific Procedures) Act 1986, UK, Amendment Regulations 2012 (SI 4 2012/3039).

2.2 Tissue processing and analysis

After collection the entire eWAT and iBAT tissues were immediately weighed. All tissues were then placed into cryovials and immediately snap-frozen in liquid nitrogen after which they were stored at -80°C until processing.

2.2.1 Protein extraction

Total protein from WAT and BAT tissues was extracted by mechanical homogenisation using a pestle and mortar. The pestle and mortar were pre-chilled in liquid nitrogen. Each tissue sample was homogenised with 1mL ice-cold lysis buffer containing 50mM Tris-HCl (pH 7.5) [Sigma Aldrich], 1mM EGTA (pH 8) [Alfa Aesar], 1mM EDTA (pH 8) [Alfa Aesar], 1% Triton X-100 [Sigma Aldrich], 1mM Sodium Orthovanadate [Sigma

Aldrich], 50mM Sodium Fluoride [Sigma Aldrich], 5mM Sodium Pyrophosphate [Sigma Aldrich], 0.27M Sucrose [Sigma Aldrich], 1mM PMSF [Thermo Fisher Scientific] and Complete protease inhibitor cocktail (1 tablet/50 mL) [Roche Diagnostics]. Samples were then centrifuged at 21,000 x g for 25 min at +4°C. Supernatants were isolated (thus excluding the pellet and top layer of fat) and then stored at -80°C until quantification and subsequent SDS-PAGE.

2.2.2 Protein quantification

Total protein concentration for each sample was quantified by the Bicinchoninic Acid Assay (BCA) [Thermo Fisher Scientific] according to the manufacturer's instructions.

2.2.3 SDS-PAGE

16ug of protein extract mixed with LDS sample buffer [Thermo Fisher Scientific] and DTT [Sigma Aldrich] was loaded to each well of a hand-cast 12% polyacrylamide gel, with 5% stacking gel. Gels were run for 1h 30 at 110V. Gels were run in duplicate to enable one gel to be used for protein quantification and one to be used for immunoblotting.[68]

2.2.4 Coomassie stain

The duplicate gel run as a loading control was stained with Coomassie Brilliant Blue R-250 staining solution [BioRad] for 1 hour with gentle agitation. The gel was destained overnight with Coomassie Brilliant Blue R-250 destaining solution [BioRad] also with gentle agitation. Gel images were captured using the AlphaImager 3400 [Alpha Innotec] with transillumination and reflective white light.

2.3 Western Blot

A wet tank transfer was performed. PVDF membrane [BioRad] was primed in 100% methanol [Sigma Aldrich], then washed in ddH_2O and equilibrated in transfer buffer. The gel was primed for 10 mins in transfer buffer. The transfer sandwich was assembled, and transfer was performed on ice for 2h 30 at 300mA.

After transfer, the membrane was washed 3x 5 mins in TBS-T with agitation. Membrane blocking was performed in 5% milk TBS-T for 1 hour at room temperature. Next, the membrane was incubated with primary antibody diluted in 5% milk TBS-T overnight at +4°C. Unbound antibodies were washed off through 3x 5 min agitation with TBS-T before incubation with HRP-conjugated secondary antibody diluted in 5% milk TBS-T for 1 hour at room temperature. A final washing step of 3x 5 mins agitation with TBS-T was performed to remove unbound secondary antibodies.

Detection of proteins was performed using the Lumiglo Chemiluminescent Substrate System [KPL] according to the manufacturer's instructions. Membranes were imaged using the ImageQuant LAS4000 [GE Healthcare].

2.3.1 Antibodies used for Western Blot

	Target	Manufacturer & Catalogue Number	Species Raised in; Monoclonal or Polyclonal	Dilution Used
Primary antibodies	UCP1	Abcam; ab10983	Rabbit polyclonal	1:500
	α-tubulin	Abcam; ab4074	Rabbit polyclonal	1:700
	PRDM16	Abcam; ab106410	Rabbit polyclonal	1:500
Secondary antibodies	Rabbit IgG	AbD Serotec (BioRad); STAR124P	Goat polyclonal	1:5000

2.3.2 Quantification of Western Blot

To quantify the density of bands detected using the ImageQuant LAS4000, Image J software was used. The density of the band of interest was normalised to its loading control band (α-tubulin); the density of band of interest was divided by the density of loading control band.

2.4 Histology

Collected animal tissues (BAT, WAT, & gut) were placed in histological cassettes into individual 10% neutral buffered formalin pre-filled specimen jars [Leica Biosystems]. After 24 hours the tissues were removed from the neutral buffered formalin and stored in 70% ethanol [Sigma Aldrich] until processing. Tissues were wax embedded and sectioned by the Kennedy Institute, University of Oxford. The Kennedy Institute also performed hematoxylin and eosin (H&E) staining sections of all collected tissues.

2.4.1 Analysis of H&E WAT sections

For each animal, 5 representative images of the H&E stained WAT sections were taken at 10x magnification on a Zeiss Axioplan 2 upright fluorescent microscope.

To quantify adipocyte number and size of H&E stained WAT sections, AdipoCount software[69] was used. Briefly, this software performs thresholding & edge detection of the images and combines this information to produce an image with enhanced contrast. Resegmentation is then performed on the newly generated image using a watershed algorithm to predict where membranes may be present. The resegmented image is then checked manually against the original H&E image and any missing membranes are drawn in manually using the AdipoCount software, while any erroneous membrane predictions are removed. The resulting image (example shown in Figure 2.1a) is then subjected to cell analysis. The cell analysis process labels every cell with a number (Figure 2.1b) and measures the area of each cell which is then given a separate colour (Figure 2.1c) to enable cell-cell differentiation. Any measurements generated through analysis of non-adipocytes and blank areas are then manually deleted.

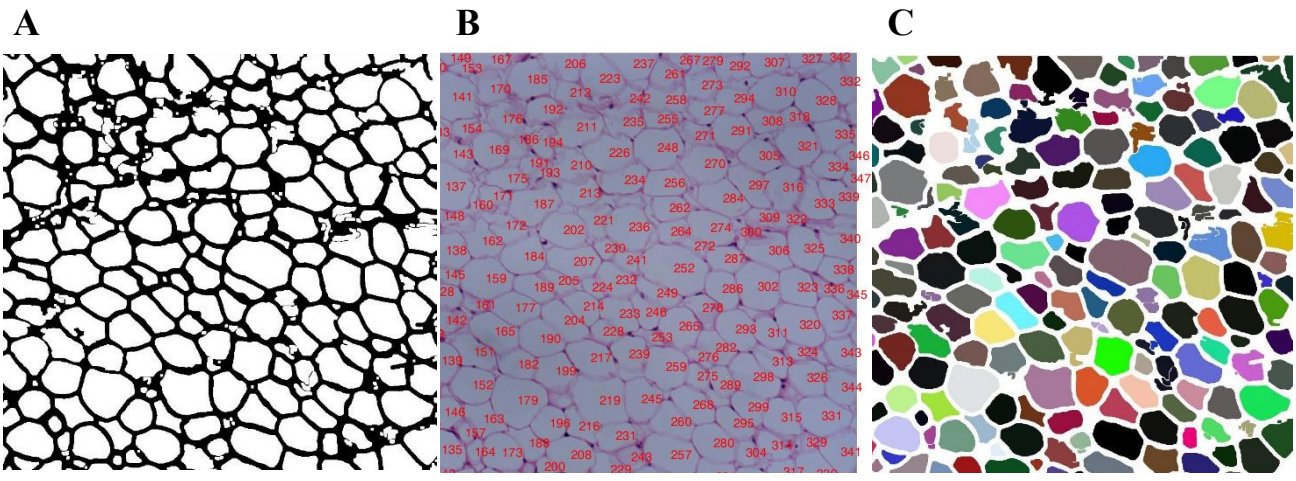


Figure 2.1. AdipoCount software processing. (A) The product of thresholding, edge detection & resegmentation (B) Cell counting and numbering (C) Cell analysis

Since the area measurements generated by the AdiopoCount software are arbritrary units these arbritrary units were converted to um^2 units. Briefly, the area of a random test adipocyte measured by AdipoCount was calibrated to the area of the same adipocyte measured by FIJI ImageJ. The scale in FIJI ImageJ was set by calibration to the scale bar in the original H&E image. (Figure 2.2)

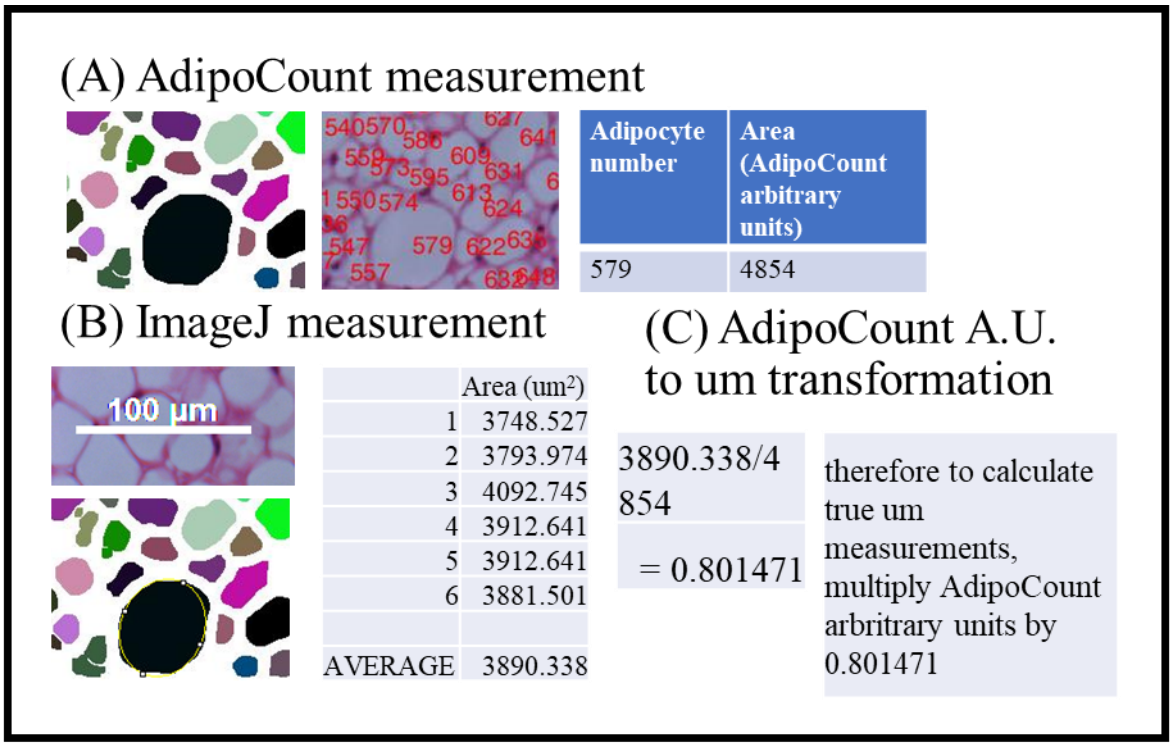


Figure 2.2. Calibration of AdipoCount software arbritrary unit values to true um values. (A) AdipoCount measurement of a random adipocyte, #579, area measurements generated in AdipoCount arbritrary units (B) Measurement of adipocyte #579 area using ImageJ, after setting the scale using the scale bar. 6 repeat area measurements were taken using ImageJ, and these were then averaged. (C) Calculation of transformation to calculate um measurements from AdipoCount arbritrary unit measurements

2.4.2 Immunofluoresence

Slides were dewaxed and rehydrated by a series of incubation steps with Xylene, ethanol and distilled water. Next, samples were permeabilised using PBS 0.5% Triton X-100 [Sigma Aldrich]. Cells were blocked with Superblock TBS blocking buffer

[Thermofisher] for 30 mins at room temperature in humid chambers. Primary antibodies diluted in Superblock were added and incubated overnight in a humid chamber. Samples were washed using PBS 0.2% Triton X-100. Secondary antibody diluted in Superblock was added and samples were incubated for 1 hour in a humid chamber. Samples were then washed again using PBS 0.5% Triton X-100. Slides were mounted in Vectashield with DAPI to visualise nuclei. Images were taken using an Olympus FV3000 confocal laser scanning microscope.

2.4.3 Antibodies used for wax embedded tissue immunofluorescence

	Target	**Manufacturer & Catalogue Number**	**Species Raised in; Monoclonal or Polyclonal**	**Dilution Used**
Primary antibody	UCP1	Abcam; ab10983	Rabbit polyclonal	1:300
Secondary antibody	DyLight® 488 Anti-Rabbit IgG	Abcam; ab96919	Donkey polyclonal	1:200

2.5 Plasmid extraction

LB agar [Sigma] plates with carbenicillin [VWR] were streaked from a bacterial stab transformed with the plasmid tPA-Dendra2. tPA-Dendra2 was a gift from Janis Lochner (Addgene plasmid # 82636). A single colony was selected from the plate after overnight culture at 37°C and used to inoculate a liquid culture. This liquid culture was incubated in a shaking incubator overnight at 37°C.

Plasmid extraction from the overnight liquid culture was carried out using the AxyPrep Plasmid Miniprep Kit [Axygen Biosciences] according to the manufacturer's instructions.

The DNA concentration of the extracted plasmid was determined using the NanoDrop™ ND-1000 Spectrophotometer.

2.6 Plasmid sequencing

Primers were synthesised by Sigma-Aldrich according to specifications of Addgene plasmid # 82636[70], namely -

5′ sequencing primer GGTGACACTATAGAATAACATCCACTTTGC

3′ sequencing primer GAGTTTGGACAAACCACAACTAGAATGCAG

Sequencing was performed by Source Bioscience. The sequences obtained were compared to published sequences for the tPA-dendra2 plasmid[70] using Clustal Omega multiple sequence alignment[71]. (Appendix 1)

2.7 Cell Culture

GLUTag cells were grown in T25 cm^2 flasks coated with 0.4% Matrigel solution. Cells were grown at 37°C with 5% CO_2. Cells were cultured in low glucose Dulbecco's modified eagles medium (DMEM) [Gibco] supplemented with 10% Fetal Bovine Serum [Sigma; lot 083M3396] and 1% Pen/Strep (V/V) [Life Technologies]. Cells were grown to 80% confluency and then split (every 4-5 days). To split, cells were washed with pre-warmed Dulbeccos PBS [Sigma], detached by addition of trypsin [Sigma] incubated for 5 mins at 37°C. The trypsin was inactivated by addition of fresh DMEM and the cells resuspended. Cells were reseeded into a fresh flask at a 1:10 ratio.

2.7.1 Cell transfection

GLUTag cells were reverse transfected with tPA-Dendra2 plasmid. Briefly, 13mm ø 1.5mm-thick glass coverslips [VWR] treated in 65% nitric acid [VWR] followed by 70%

ethanol [Sigma] were placed into 24-well plates [Corning] and coated with 0.4% Matrigel. DNA was added to Lipofectamine 2000 [Life Technologies] in a ratio of 1:3 DNA: lipofectamine and used according to the manufacturer's instructions. To each well 0.8ug of DNA, in complex with lipofectamine, was added. Cells were split, resuspended and counted using a haemocytometer. $1x10^5$ cells were added to each well onto the DNA: lipofectamine solution. This was incubated for 40-48 hours.

2.7.2 Cell fixing

Cell media was removed, and cells washed with DPBS. Then 4% PFA [Sigma] in PBS [Gibco] was added to each well for 10 mins. Cells were then washed 3x with ice-cold PBS.

2.7.3 Fixed cell immunofluorescence

Cells were permeabilised with PBS 0.25% Triton X-100 [Sigma] for 10 mins followed by 3x 5 mins PBS washing. Cells were blocked with Superblock TBS blocking buffer [Thermofisher] for 30 mins at room temperature. Primary antibodies were added and incubated overnight at +4°C in a humid chamber. The primary antibody solutions were removed, and excess unbound antibodies removed by 3x 5 min PBS washing. Secondary antibodies were then added for 1 hour at room temperature in a humid chamber in the dark. Next 3x 5mins washing with 0.05% Tween [Sigma] -PBS. Hoechst stain [Thermofisher] diluted 1:1000 was added for 10 mins in dark before 5 mins washing with PBS.

The glass coverslips were mounted upside down on a glass slide [VWR] using ProLong Gold antifade mountant [Life Technologies] and cured for 4 days at room temperature before storage at +4°C.

Imaging was performed using the Leica TCS SP8 confocal laser scanning microscope.

2.7.4 Antibodies used for fixed cell immunofluorescence

	Target	**Manufacturer & Catalogue Number**	**Species Raised in; Monoclonal or Polyclonal**	**Dilution Used**
Primary antibodies	GLP-1	Source Bioscience; LS-B9319	Rabbit monoclonal	1:100
Secondary antibodies	Anti-mouse IgG	Abcam; ab175700	Donkey polyclonal	1:1000

2.8 Live cell imaging

Cells were transfected as described above in 4 well u-slide ibidi coverslips [ThistleScientific Ltd]. Cells were then washed 2x with prewarmed DPBS and then 500ul of prewarmed Fluorobrite DMEM [Gibco] supplemented with 10% FBS and 20mM HEPES buffer [Lonza] was added to each well.

Imaging was performed using the Leica TCS SP8 **c**onfocal laser scanning microscope.

2.9 Statistical Analysis

All statistical analysis and graph generation was performed using GraphPad Prism 7.04. For comparing the means of two samples an unpaired two-tailed t-test was used (Figures 5.1-5.6). When there were more than two sample means these were compared to each other using an analysis of variance test (ANOVA) with a Tukey's multiple comparison test (Figure 4.3). All data were assumed to be normally distributed, however this should be confirmed further.

3 Results: Live Cell Imaging

3.1 Introduction: The use of tPA as a marker of GLP-1 vesicles

The incretin hormone GLP-1 is generated from post-translational cleavage of preproglucagon. Consequently it is difficult to directly label GLP-1 in cells for imaging, since any fluorescent marker encoded in transfected DNA would be cleaved off the protein. To find another means of showing GLP-1 localisation within cells, Oya and colleagues transfected GLUTag cells, a model L-cell line, with several different fluorescently-labelled peptide hormones.[72] They found that tissue-type plasminogen activator (tPA) showed high colocalization with GLP-1 and thus used fluorescently tagged tPA as a surrogate marker for GLP-1 within GLUTag cells for live cell imaging.[72]

Tissue-type plasminogen activator (tPA) is a serine protease which is named for its central role in fibrinolysis by converting plasminogen to plasmin.[73] tPA is a 69kDA glycoprotein, synthesised within cells and then released as a single chain enzyme which is subsequently cleaved into one heavy and one light tPA chain.[74] Because of its role in anticoagulation, it was originally thought that tPA was only expressed in endothelial cells as part of the fibrinolytic pathway. However tPA has since been shown to be present extensively in brain tissue[75] (including in endocrine cells of the hypothalamus)[76] and neuroendocrine tissues such as chromaffin cells of the adrenal medulla[77]. In the brain, tPA has been implicated in a range of processes including synaptic plasticity[76,78], the stress response[76], addiction[76], and neuroprotection.[75,79] tPA has also been shown to be present in other tissues apart from the brain and endothelial cells, such as macrophages[80]. Aside from fibronloysis, once secreted, tPA has been shown to play roles in cell motility[80], apoptosis[79], cancer growth[81] and extracellular matrix degradation[79].

In neurons, tPA is packaged into vesicles where its release is regulated rather than being constitutively secreted.[76] Release of tPA vesicles from a neuronal cell line, PC12, was shown to be stimulated by membrane depolarisation and abolished by Ca^{2+} channel blockers.[82] Similarly, in chromaffin cells, neuroendocrine cells of the adrenal medulla, tPA release has been shown to be controlled by a regulatory secretory pathway.[77] Using sucrose gradient fractionation and fibrin zymography, the tPA found in the chromaffin cells was shown to be contained within the noradrenaline-containing chromaffin granules. tPA and noradrenaline were also co-released in response to three different known chromaffin cell secretagogues.[77]

In this chapter I aim to visualise GLP-1 secretion from GLUTag cells so that live cell imaging of hormone secretion may be performed. GLUTag cells are neuroendocrine cells, like the chromaffin cells in which tPA has been shown to be co-stored and co-released in the secretory vesicles.[77] Membrane depolarisation of GLUTag cells causes GLP-1 secretion, similar to the release of tPA from PC12 neuronal cells following membrane depolarisation.[82] Furthermore, in our laboratory we use a combination of forskolin and IBMX to stimulate GLP-1 secretion from GLUTag cells, and forskolin has been shown to cause tPA seceretion from neural granule cells.[78] Taken together with the work of Oya *et al.*[72], who used tPA as a surrogate marker for GLP-1 in GLUTag cells, replicating this work and using tPA as an indirect indicator of GLP-1 appears to be a promising route for achieving live cell imaging of hormone secretion in GLUTag cells.

3.2 Results

To allow visualisation of tPA expressed in GLUTag cells, tPA labelled with the green-to-red photoswitchable fluorophore dendra2[83] was used. tPA-dendra2 [a gift from Janis Lochner (Addgene plasmid # 82636)] was transfected into GLUTag cells.

These cells were fixed in paraformaldyehyde and stained with the nuclear Hoechst stain to allow for high resolution confocal microscopy of the transfected GLUTag cells. Two representative images are shown in Figure 3.1, showing successful transfection of the tPA-dendra2 and its subcellular localisation to cytoplasmic vesicles.

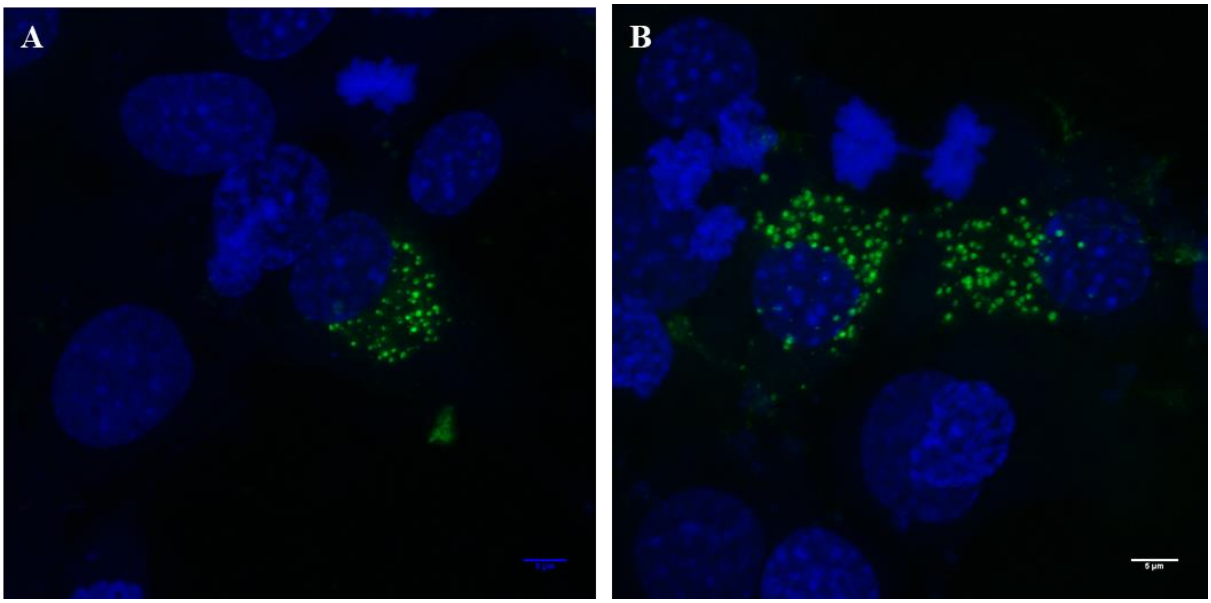


Figure 3.1. Fixed cell imaging of GLUTag cells transfected with tPA-dendra 2. (A) & (B) show two representative images. Hoechst staining & dendra2 imaging merge. Scale bar 5um.

To confirm that the tPA was co-localising with GLP-1, transfected fixed cells were immunolabelled for GLP-1. A representative photo of two immunolabelled cells is shown in Figure 3.2. A good degree of co-localisation between the tPA and GLP-1 labelling is observed, confirming tPA as an adequate surrogate indicator for GLP-1 subcellular localisation.

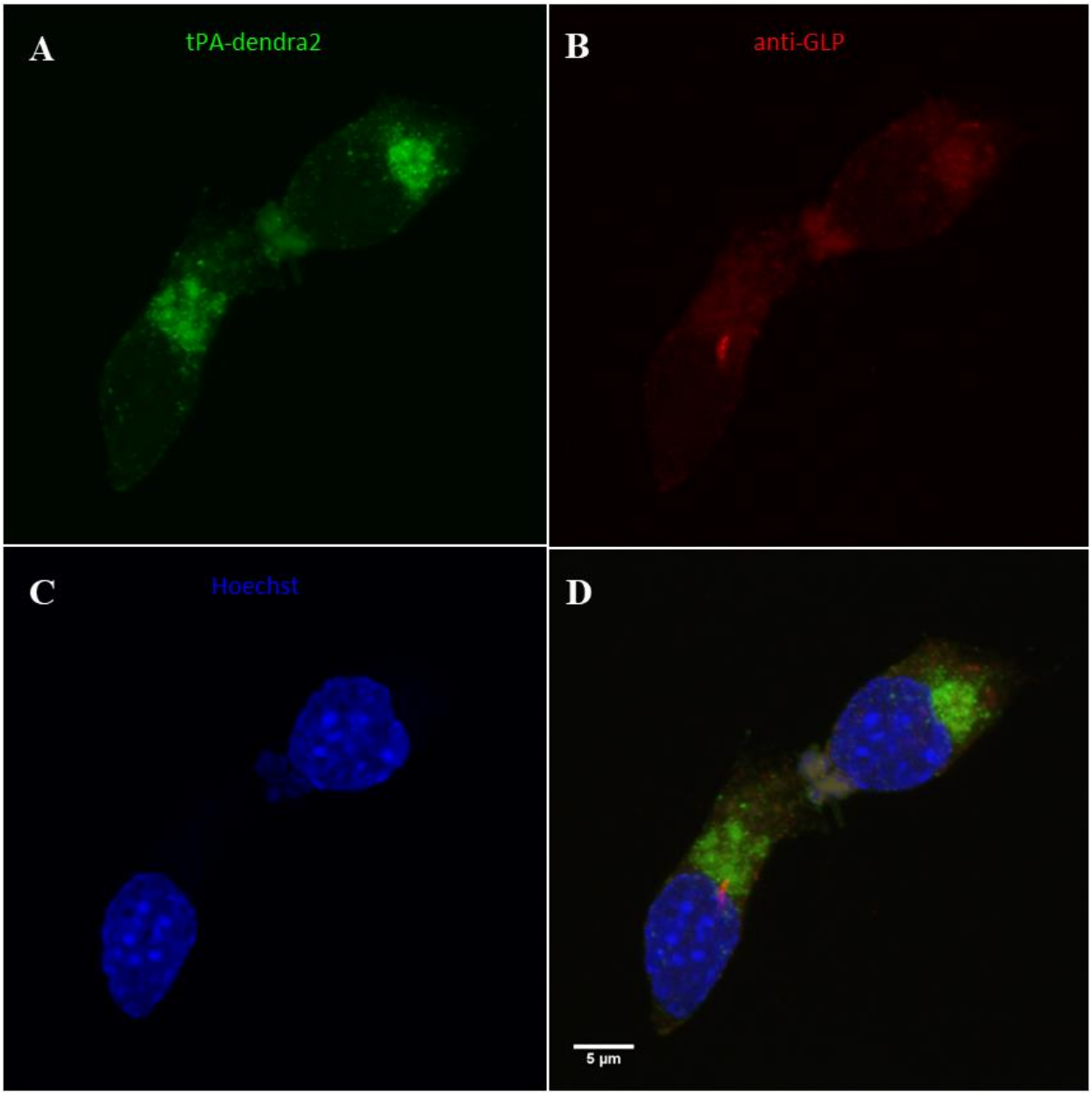


Figure 3.2. Fixed cell imaging of immunolabelled GLUTag cells transfected with tPA-dendra 2. A representative image showing two fixed and immunolabelled GLUTag cells. (A) imaging of the dendra2 fluorophore, tagged to tPA. (B) anti-GLP-1 immunolabelling (C) Hoechst nuclear stain (D) overlay. Scale bar 5um.

A preliminary trial of live cell imaging shows the ability to visualise and track GLP-1 vesicle movement indirectly via tPA-dendra2 imaging. Still images taken from two short representative videos, performed in 4.5g/L FluoroBrite DMEM media are shown in Figure 3.3.

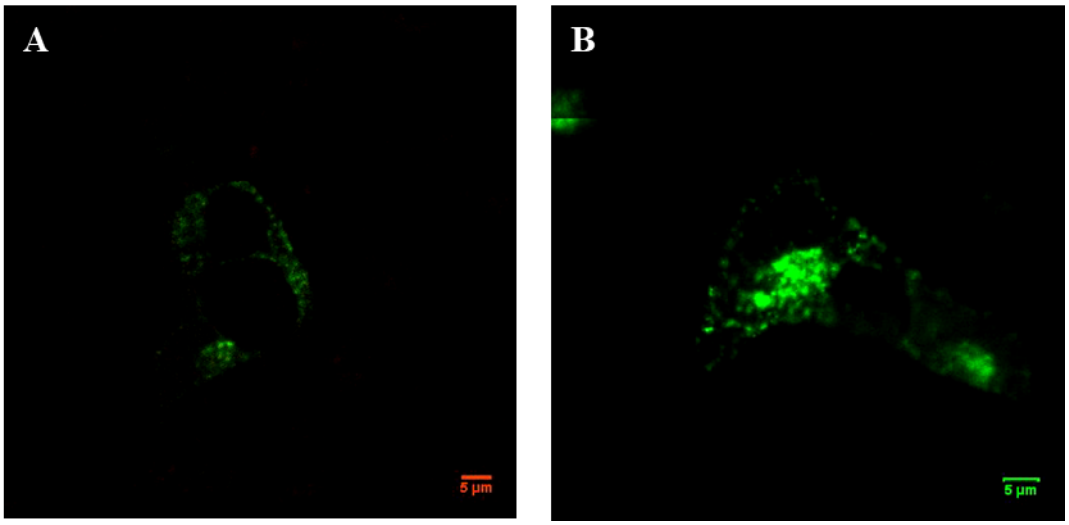


Figure 3.3. Live cell imaging snapshots. (A) & (B) Two representative snapshots from videos of tPA-dendra2 transfected GLUTag cells. Scale bar 5um.

3.3 **Discussion**

These results set up, validate, and standardise a protocol for transfection and subsequent imaging & tracking of GLP-1 vesicles in GLUTag cells via the surrogate marker tPA-dendra2. In future experiments this will enable the live indirect visualisation of GLP-1 exocytosis, which can be stimulated in GLUTag cells by the addition of forskolin and IBMX which cause increased cAMP levels, and therefore exocytosis.

However, this protocol does not come without some limitations. Firstly, it is crucial to be aware of the lack of complete colocalisation of GLP-1 and tPA-dendra2. Additionally, once secreted, tPA has been implicated in a variety of signalling processes in a large number of different cell types.[76,78,80,81] It is not inconceivable that secreted tPA might act in an autocrine or paracrine manner on GLUTag cells. This could act to change any results observed in live cell imaging that continues for long enough for multiple rounds of hormone exocytosis. It would therefore be prudent to investigate any potential role of

extracellular tPA on GLUTag cells. To study this, one could directly add recombinant tPA protein extracellularly to the media of GLUTag cells and compare any cellular changes observed in the cells to a vehicle treatment control.

The ultimate goal of the live cell imaging of GLUTag cells is to further understand the role that ABCC5 is playing in GLP-1 secretion. Once capturing videos of forskolin- and IBMX-stimulated hormone secretion has been optimised, the role of ABCC5 can be investigated using siRNA knockdown and plasmid overexpression of ABCC5 and tracking any changes to the live imaging obtained.

In conclusion, here we establish tPA-dendra2-transfected GLUTag cells as robust and reproducible model for tracking GLP-1 via live-cell imaging. The protocol established here provides a foundation on which the role of ABCC5 in GLP-1 secretion from L-cells can be investigated. This will be able to provide evidence for whether the ABCC5 mediated inhibition of GLP-1 secretion is contributed to by the movement of GLP-1 vesicles within the cell.

4 Results: Gut morphology

4.1 Intestinal villi length

Intestinal villus length, defined as the distance from the intestinal crypt to the tip of the villi, influences the rate of nutrient absorption in the gut and is therefore an area of interest in obesity research.[84] Cells in the gut have a lifespan of around 3-5 days, which therefore allows for rapid remodelling of the gut structure in response to a range of environmental cues.

It is well established that the gut structure can be changed in response to diet. Treatment of young mice with a diet high in carbohydrate but moderately deficient in protein, fat and minerals for 3 weeks resulted in decreased villus length.[85] Mice fed a high-fat diet (HFD) for 8 weeks show increased villus length[86,87] and hyperphagic db/db mice (mice lacking the leptin receptor, prone to development of T2D in later life) on a chow diet also have longer villi. Furthermore, this villus elongation caused by the elevated food intake was then shown to be reversed following 4 weeks of caloric restriction.[87]

In contrast, longer term HFD treatment (9-14 months) has been shown to cause a mild decrease in villus length.[88] Indeed data from our own laboratory supports the latter study, showing a significant decrease in murine villus length after a 4 month HFD [H. de Wet, Unpublished data]. Together this may suggest that response to diet varies over the time of persistent exposure.

After jejunoileal resection, rats showed an increase in villus length[89], a result repeated in rats following Roux-en-Y surgery.[11,90] In contrast, using a model of obesity and diabetes, the hyperphagic Zucker rat, it has been shown that duodenal-jejunal bypass surgery resulted in more broken or shortened villi when compared to sham operated Zucker rats.[91]

Taken together with the data known on changes in villi structure to diet, it seems that the changes seen after bariatric surgery are also dependent on diet before and after surgery.

GLUTag cells, a model L-cell line, treated with the GLP-1 mimetic exendin-4 show a positive feedback loop of increased GLP-1 secretion, driven by increased GLUTag cell proliferation.[92] This provides evidence that GLP-1 enhances its own secretion in an autocrine and/or paracrine positive feedback loop. Since our ABCC5 KO mice have elevated levels of circulating GLP-1, we therefore might expect to see proliferation of L-cells within the gut. In addition to GLP-1, L-cells secrete GLP-2, another product of the post-translational proteolytic cleavage of preproglucagon. GLP-2 is a 33 amino acid peptide that has been implicated in the growth and absorptive function of the intestinal epithelium, including promoting expansion of the mucosal surface area.[93] Since GLP-1 and GLP-2 are co-secreted from L-cells,[93] it is conceivable that ABCC5 KO mice may secrete higher levels of GLP-2 because of the elevated GLP-1 secretion that we have observed.

We therefore theorised that there may be a difference in gastrointestinal villi length and/or surface area in our ABCC5 KO mice compared to WT littermate controls. Preliminary data from our lab has suggested a decrease in villus length and surface area in the gut of ABCC5 KO animals (Figure 4.1) [Work completed by A. Saibudeen, de Wet Group].

Additionally, because of the lean phenotype observed in our KO animals compared to WT littermate controls, this body compositional difference could be caused by a difference in gut nutrient absorption either because of GLP-1/GLP-2 changes or via a discrete ABCC5-dependent mechanism.

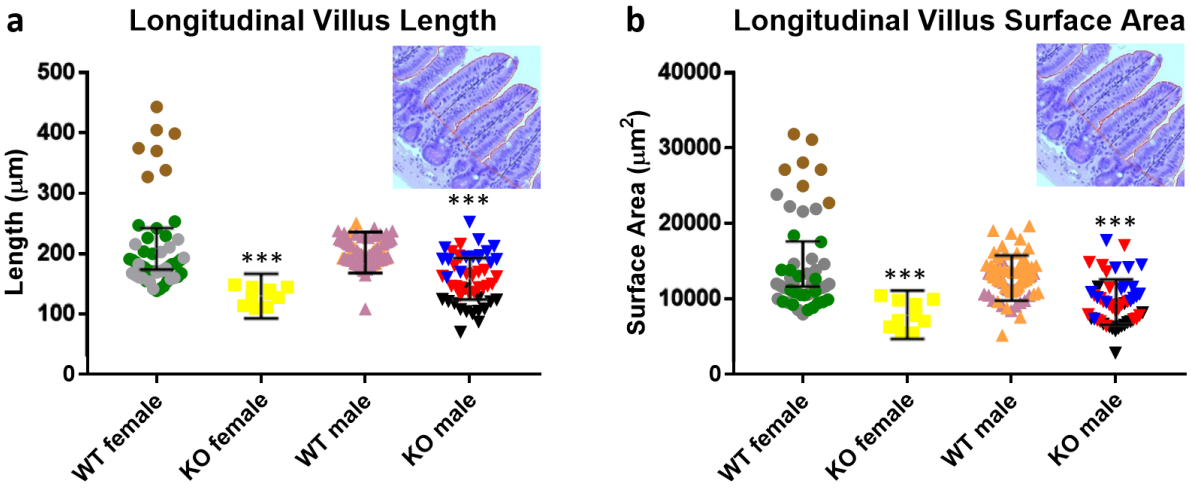


Figure 4.1. Morphometric analysis of ABCC5 KO intestinal villi in a preliminary cohort. **(a)** Longitudinal villus length **(b)** Longitudinal villus surface area. WT female (n=3), KO female (n=1), WT male (n=2) and KO male (n=3). 5-10 villi measured per animal. All data points plotted and SE of the mean shown. *P<0.05, **P<0.01, ***P<0.001 when compared with wild type (generalised linear mixed model). [Work completed by A. Saibudeen, de Wet Group.]

In this chapter I will further investigate longitudinal villi length and surface area of our ABCC5 KO mice in a subsequent animal cohort group using light microscopy of H&E stained gut sections.

4.2 **Methods**

H&E stained longitudinal gut sections from ABCC5 KO and WT mice [WT female (n=2), KO female (n=4), WT male (n=3) and KO male (n=3)] were examined using a light microscope. For each animal, a representative image of the H&E stained distal ileum was taken at 10x magnification on a Zeiss Axioplan 2 upright fluorescent microscope. FIJI ImageJ software was then used to measure the length of between n=3 and n=7 villi per animal. Measurements were generated in um after the scale in FIJI ImageJ was set by calibration to the scale bar. Villus length and villus surface area were both measured.

Villus length was defined as the distance from the intestinal crypt to the tip of the villi and this is the measurement obtained. Crypt depth also varies but this is not always in the

same way as villus length,[88] therefore crypt depth was not included in the villus length measurement.

4.3 Results

Representative photos of H&E stained longitudinal villi sections with annotated measurement lines are shown in Figure 4.2.

In contrast, to previous preliminary data from our lab, the measurements obtained from the H&E stained longitudinal villi sections show no difference in villi length or surface area between WT and ABCC5 KO mice in males or females (Figure 4.3).

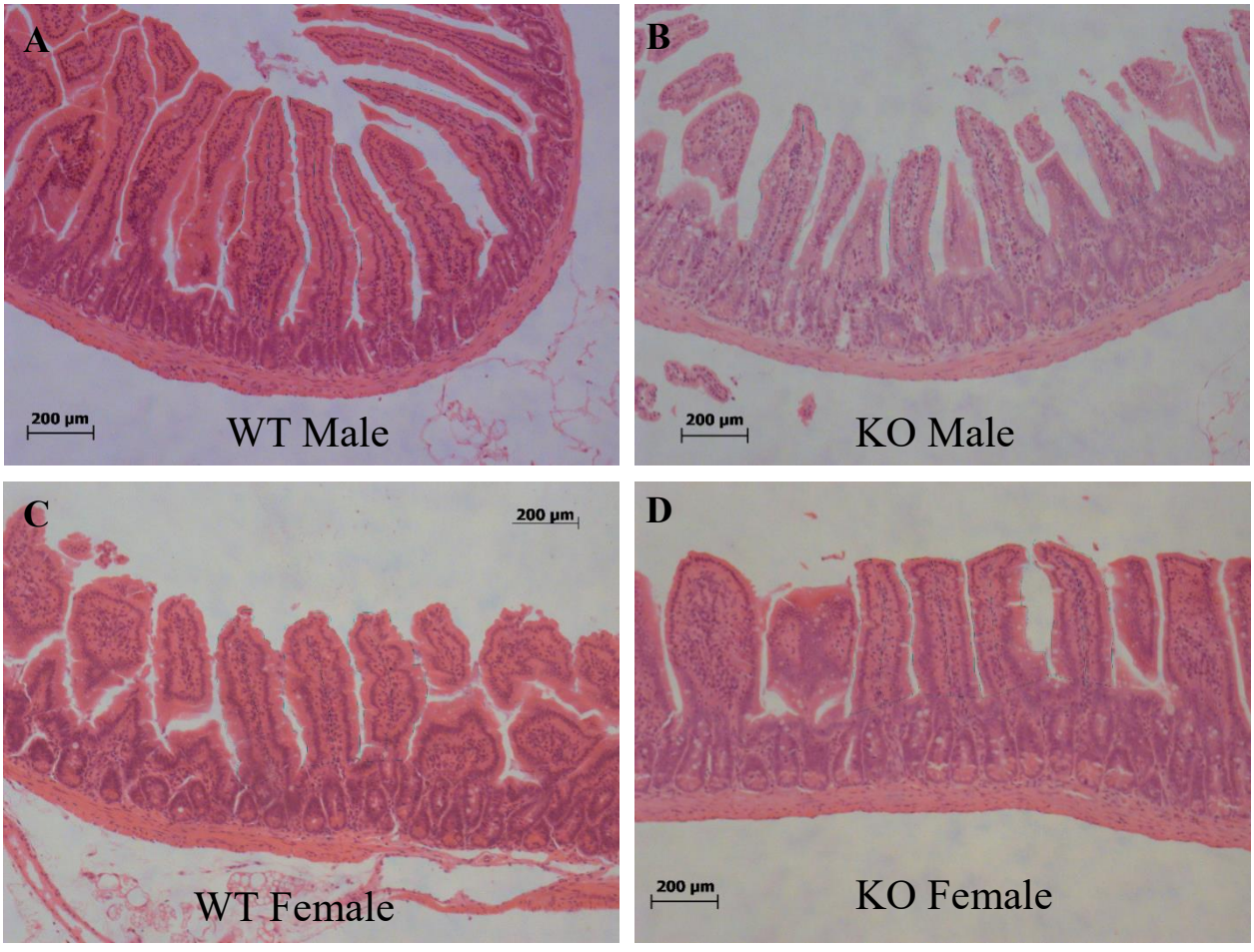


Figure 4.2. Representative images of ABCC5 KO and WT gut villi. (A) WT male, (B) KO male, (C) WT female, and (D) KO female. Measurements of gut villi length and surface area were obtained. Lines drawn for measurements shown in yellow. Scale bars 200um.

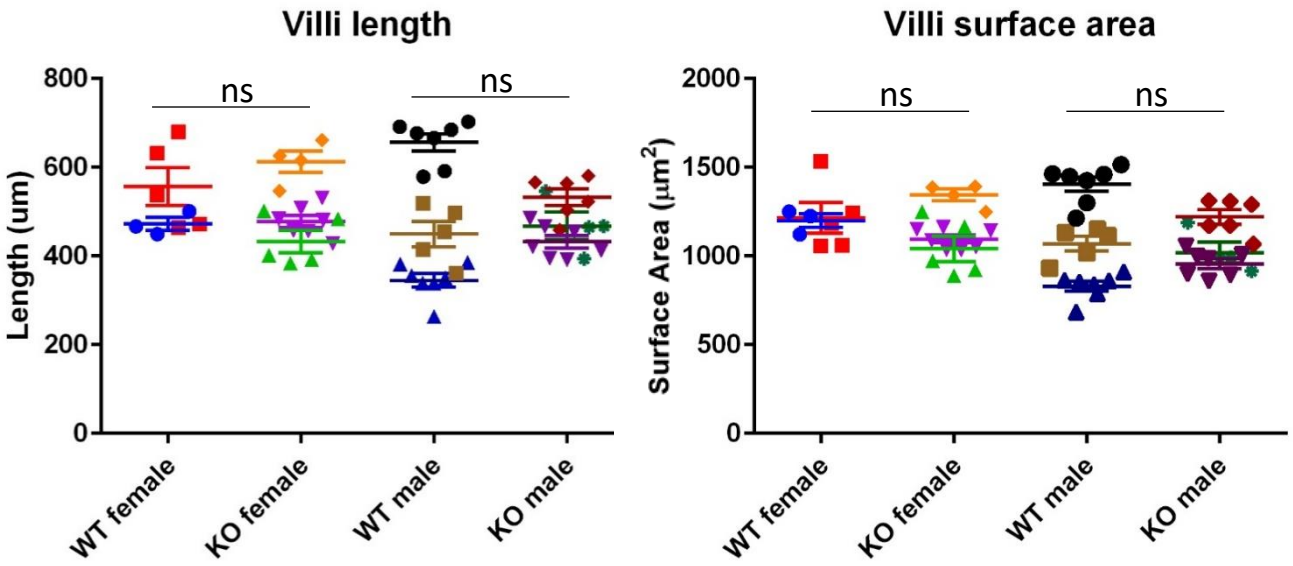


Figure 4.3. Measurements of (A) Villi length and (B) surface area. WT female (n=2), KO female (n=4), WT male (n=3) and KO male (n=3). Between n=3 and n=7 villi measurements per animal. Each animal is represented by a different colour. Error bars: mean±SEM. No significant difference between villi length and villi surface area. Statistical analysis by ANOVA with Tukey's multiple comparison test. ns (not significant).

4.4 Discussion

Preliminary data obtained in our lab on a prior cohort of ABCC5 KO mice suggested that ABCC5 KO mice have a shorter longitudinal villus length and surface area when compared to WT littermate controls. Here in a subsequent cohort of mice I have found results that do not support these preliminary findings (Figure 4.1), showing no significant difference between villus length between WT and KO animals (Figure 4.3).

The preliminary findings from our lab used a smaller number of animals, notably only n=1 female KO mice (Figure 4.1). If this individual animal was non-representative of female KOs then it possible that it may have skewed the data. However, a difference was also seen between male WT (n=2) and male KO (n=3), suggesting that there does seem to be a difference in villi length and surface area in the preliminary cohort. Furthermore, the use of a generalised linear mixed model statistical test with these preliminary data acts to adjust for the small n numbers.

Several factors may account for the different results obtained between the preliminary study and secondary cohort. One of these factors could be the age of the animals killed. The preliminary cohort were culled at 16 weeks of age while the secondary cohort were culled at 18-20 weeks. However, this small difference in age seems unlikely to be the reason for the disparity in results. More likely, the culling protocol may have contributed to the disparity in results. The preliminary cohort were fasted overnight and then given an oral dose of glucose before culling. In contrast, the secondary cohort were left on an ad libitum chow diet until culling, with no overnight fasting or oral glucose dose. Given what is known about the influence of diet on villi strucutre[85-88], it is possible that the overnight fasting may have contributed to the difference in WT and KO villi length. If this is the case, this could suggest a difference in villi plasticity response caused by the global loss of ABCC5. This may be caused by elevated GLP-1 and / or GLP-2 levels in the KO animals. However, it should be noted that the less than 24-hour time period in which the overnight fast would have occurred before culling represents a very short time for gut remodelling to be observed, even within the short 3-5 day lifespan of gut cells. Another factor that may have contributed to the difference seen between cohorts is a difference in the experimental procedures through the lifetime of the animals. For example the preliminary cohort was subjected to two sets of overnight fasts before the culling while the secondary cohort only had one.

In upcoming ABCC5 KO cohorts we will be weaning our mice onto a HFD. As it is well established that diet can modulate villi length, we would expect to see a change in length compared to the current measurements from chow-weaned cohorts. The results obtained here in chow-weaned mice will provide an important point of comparison to the future HFD data.

To further understand the gut physiology of our ABCC5 KO mice, it would be informative to study GLP-2 levels, since GLP-2 plays a role in promoting expansion of the mucosal surface area.[93] Similar to previous experiments carried out for GLP-1 measurement, GLP-2 secretion could be measured from ABCC5 KO gut primary cultures and / or circulating levels *in vivo*. Additionally, the evidence that GLP-1 is part of a positive feedback loop leading to L-cell proliferation raises the question of whether ABCC5 KO have a greater number of L-cells. The use of immunofluorescent staining of gut sections to identify and then count the number of L-cells would allow investigation of whether L-cell proliferation is elevated in ABCC5 KO animals.

In conclusion, in this secondary study of villi length and surface area of ABCC5 KO mouse gut we do not see any significant differences compared to WT littermate control animals. This contrasts with a preliminary study performed in our lab, however a variety of factors could account for this disparity. Both data sets will provide useful data to compare to future ABCC5 KO mouse cohorts that will be weaned onto a HFD.

5 Results: Adipose Tissue Physiology

5.1 Introduction

Adipose tissue metabolism is of great interest in the wake of the current obesity epidemic. Our ABCC5 KO mice show a lean phenotype when compared to WT littermate controls, having less fat mass and greater lean mass (Figure 1.5). Metabolic cage analysis has revealed that female KO mice show greater O_2 consumption, energy expenditure and locomotive activity than WT controls (Figure 1.7). Male KO mice also show greater locomotive activity compared to WT controls, but the difference in energy expenditure between KO and WT does not reach statistical significance (Figure 1.7).

Because of the discrepancy in energy expenditure and locomotive activity data in male KO mice, additional factors must be contributing to the overall energy expenditure. We have hypothesised that an additional factor modulating energy expenditure in the ABCC5 KO mice may be thermogenic activity of adipose tissue. The theory that ABCC5 KO mice show a difference in brown adipose tissue (BAT) thermogenic activity and/or white adipose tissue (WAT) browning when compared to WT littermate controls is therefore proposed. The elevated GLP-1 levels in KO mice also supports a possible change in BAT and/or WAT thermogenic activity since GLP-1 has been implicated with inducing non-shivering thermogenesis on several occasions.[36-41] Finally, our female ABCC5 KO mice have lowered circulating triglycerides compared to WT controls (Table 1.2). This could further indicate increased BAT activity via GLP-1R agonism as a previous study has showed that GLP-1R agonism accelerates triglyceride clearance from the circulation for use as a thermogenic fuel in BAT.[37]

Non-shivering thermogenesis is mediated by the protein UCP1 (uncoupling protein 1) in BAT, and in WAT that has acquired a brown-like phenotype - ‘beige’ fat. UCP1

expression is therefore the downstream target of a variety of transcriptional regulatory proteins for fat browning. PRDM16 is a transcription factor that has been shown to play an important role in brown adipocyte development, controlling the switch between skeletal muscle and BAT in My5 precursor cells.[94] However it has since been shown that PRDM16 is also expressed in subcutaneous fat depots where it plays a role in determining the thermogenic capacity and brown-like phenotype of the subcutaneous WAT, ultimately increasing UCP1 expression.[95] This PRDM16-controlled browning of WAT is unique to subcutaneous fat depots and is not seen in visceral epididymal fat depots.[95] Another protein that has been shown to play a role in regulating non-shivering thermogenesis is the endocrine fibroblast growth factor FGF21.[96] FGF21 expression in BAT is highly induced by cold exposure where it activates thermogenesis.[97,98] FGF21 has also been shown to regulate cold-induced browning of inguinal WAT, with increased FGF21 levels leading to an increase in UCP1 expression and other thermogenic markers.[99] Osmotic pump delivery of recombinant FGF21 to mice has additionally been shown to increase BAT & WAT glucose uptake and BAT thermogenic activity.[100]

In this chapter I will investigate the possibility of changes in non-shivering thermogenesis in the BAT and/or WAT of our ABCC5 KO mice compared to WT littermate controls. I will use total tissue mass, histological H&E tissue analysis and Western blot to explore changes in fat metabolism.

Both cohort 1 and 2 animals were housed at 21°C, below mouse thermoneutrality (30°C) so it would be expected to see a degree of non-shivering thermogenesis induced in all animals. However, to study the full range of thermogenic capacity, it is standard protocol to compare thermogenic physiology after a 4°C cold challenge vs 30°C thermoneutral

housing[101,102]. Due to license restrictions this was not possible in the current study but is something that should be pursued in future.

5.2 Methods

Full methods described in Chapter 2. Briefly, two cohorts of ABCC5 KO mice, housed at 21 ± 2°C were examined for effects of fat browning. iWAT was collected from the first cohort for Western blot and H&E histology analysis. iBAT and eWAT was isolated and trimmed from the second cohort and then weighed. Along with iWAT, these tissues were all processed for Western blots via snapfreezing in liquid N_2.

Protein was extracted from the snapfrozen adipose tissues in a liquid N_2-chilled pestle and mortar with fat lysis buffer. Total protein was quantified using BCA assay.

H&E histology sections were quantified by AdipoCount software[69]. Five representative images from each animal were taken and the area of each lipid droplet was then calculated and collated for each animal.

5.3 Results

5.3.1 Cohort 1

Protein extract from iWAT collected from cohort 1was probed for UCP1 (Figure 5.1a), PRDM16 and FGF21 (Figure 5.1b) by Western blot. ABCC5 KO female mice showed significantly less UCP1 expression than WT controls (Figure 5.1c). Both WT and KO female iWAT expressed very little detectable PRDM16 whereas WT males tended to express more than KO males, although this did not reach statistical significance (p=0.07) (Figure 5.1d). FGF21 was not detectable in any of the iWAT protein extracts (Figure 5.1b).

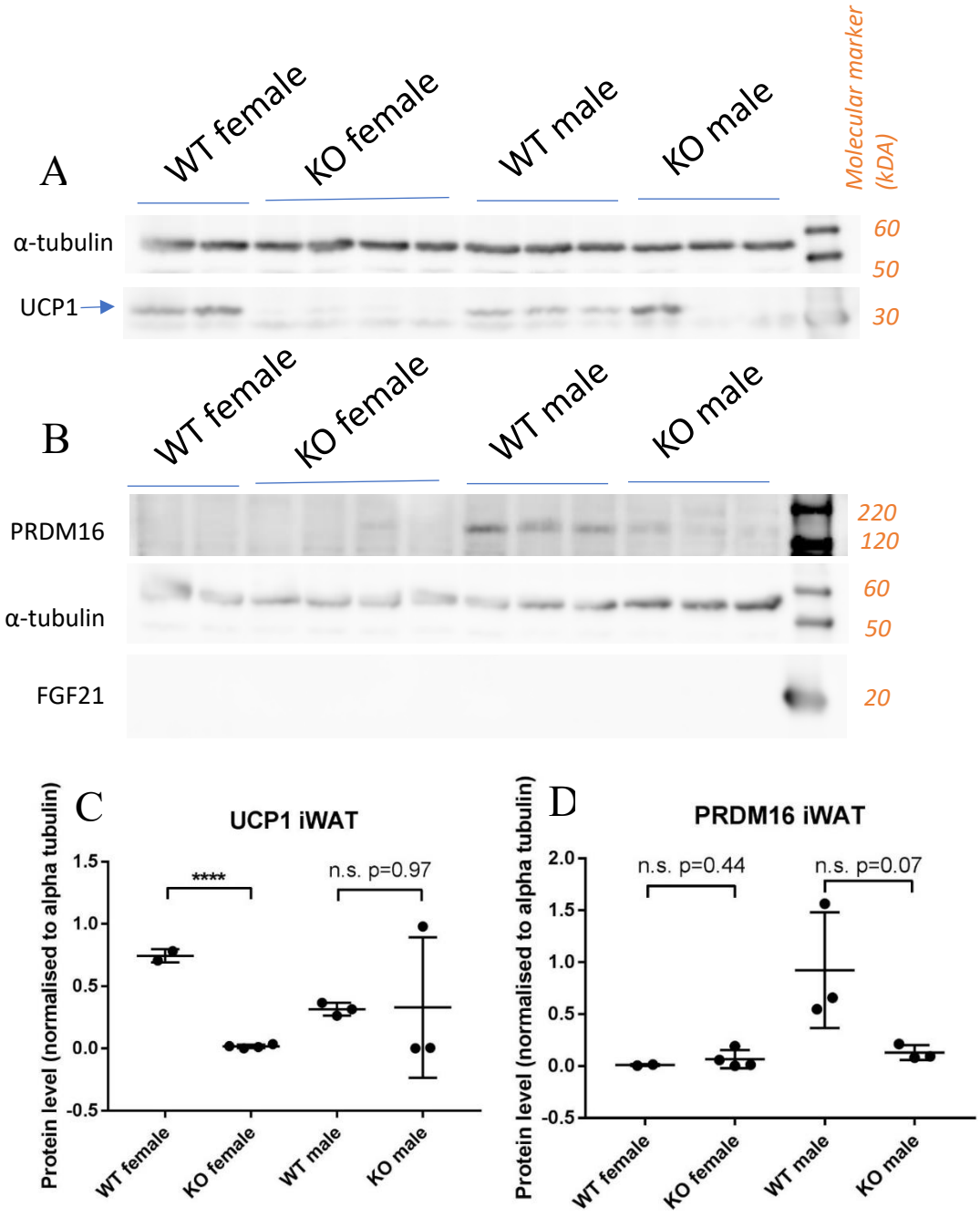


Figure 5.1. Cohort 1:Western blots of iWAT tissue lysate. (A) Western blot for UCP1 (B) Western blot for PRDM16 and FGF21 (C) Quantification of UCP1 western blot shown in (A). (D) Quantification of PRDM16 western blot shown in (B). WT female, KO female, WT male, KO male n=2,4,3 and 3 animals respectively. Error bars: mean±SD; unpaired, two-tailed *t*-test, ****P<0.0001. MW α-tubulin 50kDa; UCP1 33kDa; PRDM 140kDa; FGF21 22 kDa.

H&E stained histology sections of iWAT were examined under a light microscope (Figure 5.2a) and then analysed by AdipoCount software[69] to quantify the adipocyte area. Despite observation of greater browning of iWAT in WT than KO animals, seen as the appearance of smaller, multilocular lipid droplets (Figure 5.2a), no significant difference between adipocyte area was found by AdipoCount software analysis for males (Figure 5.2b) or females (Figure 5.2c).

5.3.2 Cohort 2

BAT and eWAT depots were dissected out of WT and KO males (Figure 5.3) and females (Figure 5.4) from cohort 2 and then immediately weighed. Representative photos of these tissues are shown in Figure 5.3a,b,e&f and Figure 5.4a,b,e&f. ABCC5 KO males had significantly less BAT (Figure 5.3c,d) and eWAT (Figure 5.3g,h) than WT littermate controls. A similar trend was observed in the ABCC5 KO females but a statistically significant difference was only reached in the eWAT depots (Figure 5.4g).

Western blot analysis of the collected adipose depots (BAT, eWAT, iWAT) for UCP1 did not show any conclusive results showing differences in expression in males (Figure 5.5) or females (Figure 5.6). This contrasts with the difference in UCP1 expression observed between KO and WT in cohort 1 (Figure 5.1a&c).

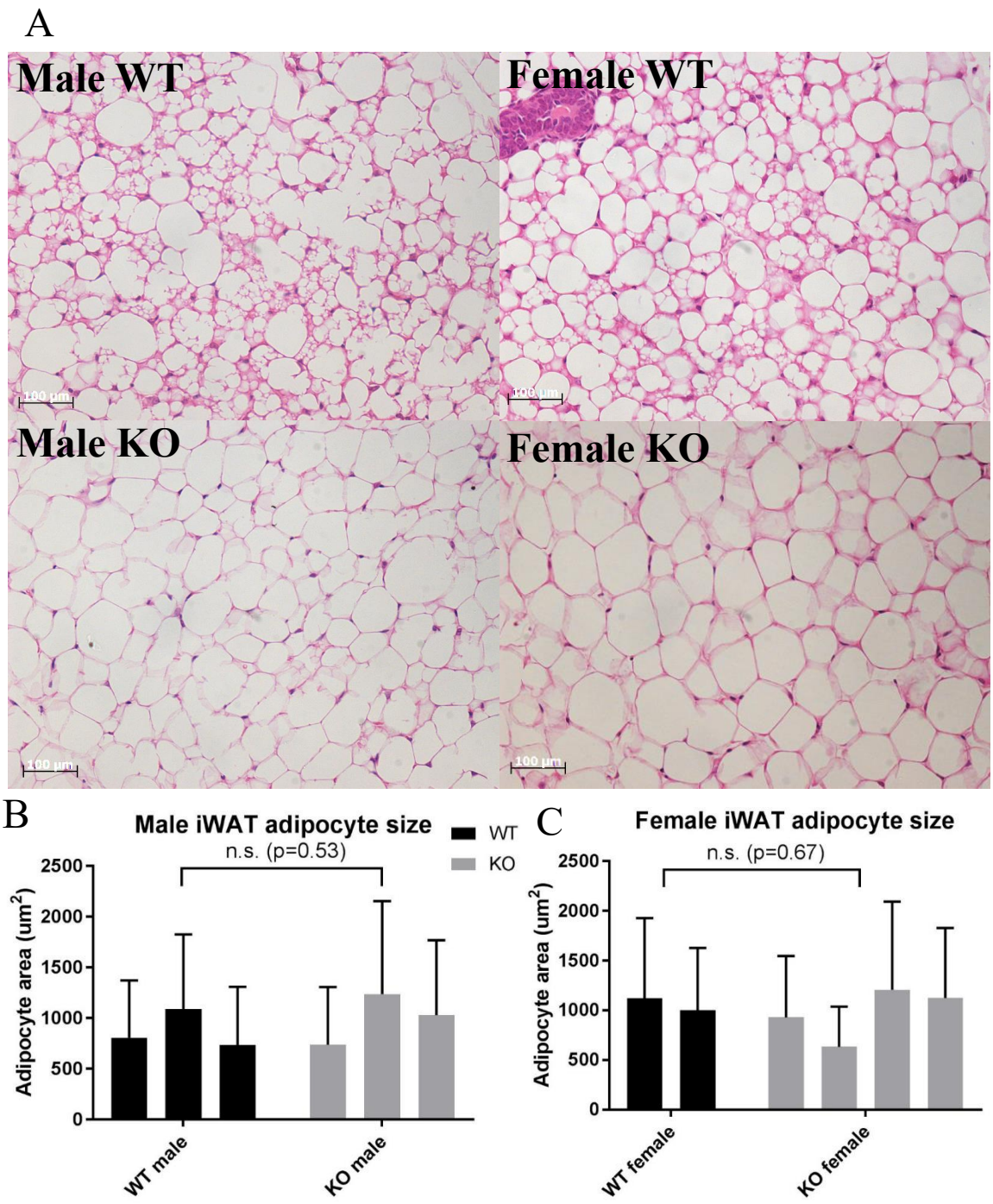


Figure 5.2. Cohort 1: H&E histology of iWAT fat depots. (A) Representative images of H&E stained iWAT sections. Scale bars 100um. (B) & (C) AdipoCount processed quantification of iWAT H&E slides. 5 representative images quantified per animal. (B) Male iWAT adipocyte area. Number of adipocytes between n=1944 and n=2721 per animal. (C) Female iWAT adipocyte area. Number of adipocytes between n=1783 and n=2713 per animal. WT female, n=2; KO female, n=4; WT male, n=3; KO male, n=3. Error bars: mean±SD; unpaired, two-tailed *t*-test comparing the mean adipocyte area of each animal.

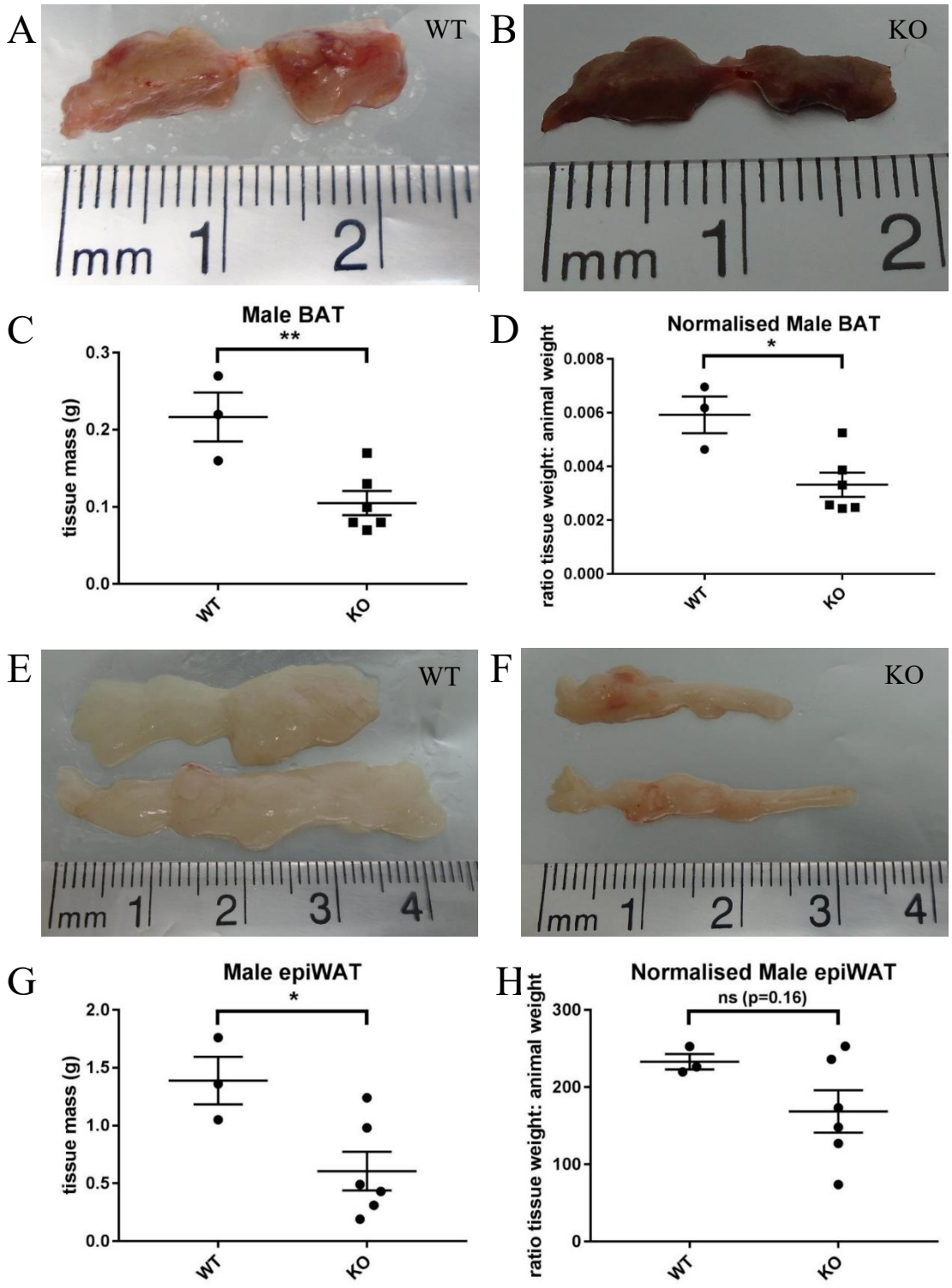


Figure 5.3. Cohort 2: Male iBAT and eWAT depots. (A) Representative image of WT iBAT (B) Representative image of KO iBAT (C) Mass of BAT tissues (D) Mass of BAT tissues normalised to total animal body weight (E) Representative image of WT eWAT (F) Representative image of KO eWAT (G) Mass of eWAT tissues (H) Mass of eWAT tissues normalised to total animal body weight. WT n=3, KO n=6 animals. Error bars: mean±SEM; unpaired, two-tailed *t*-test,*P<0.05, **P<0.01.

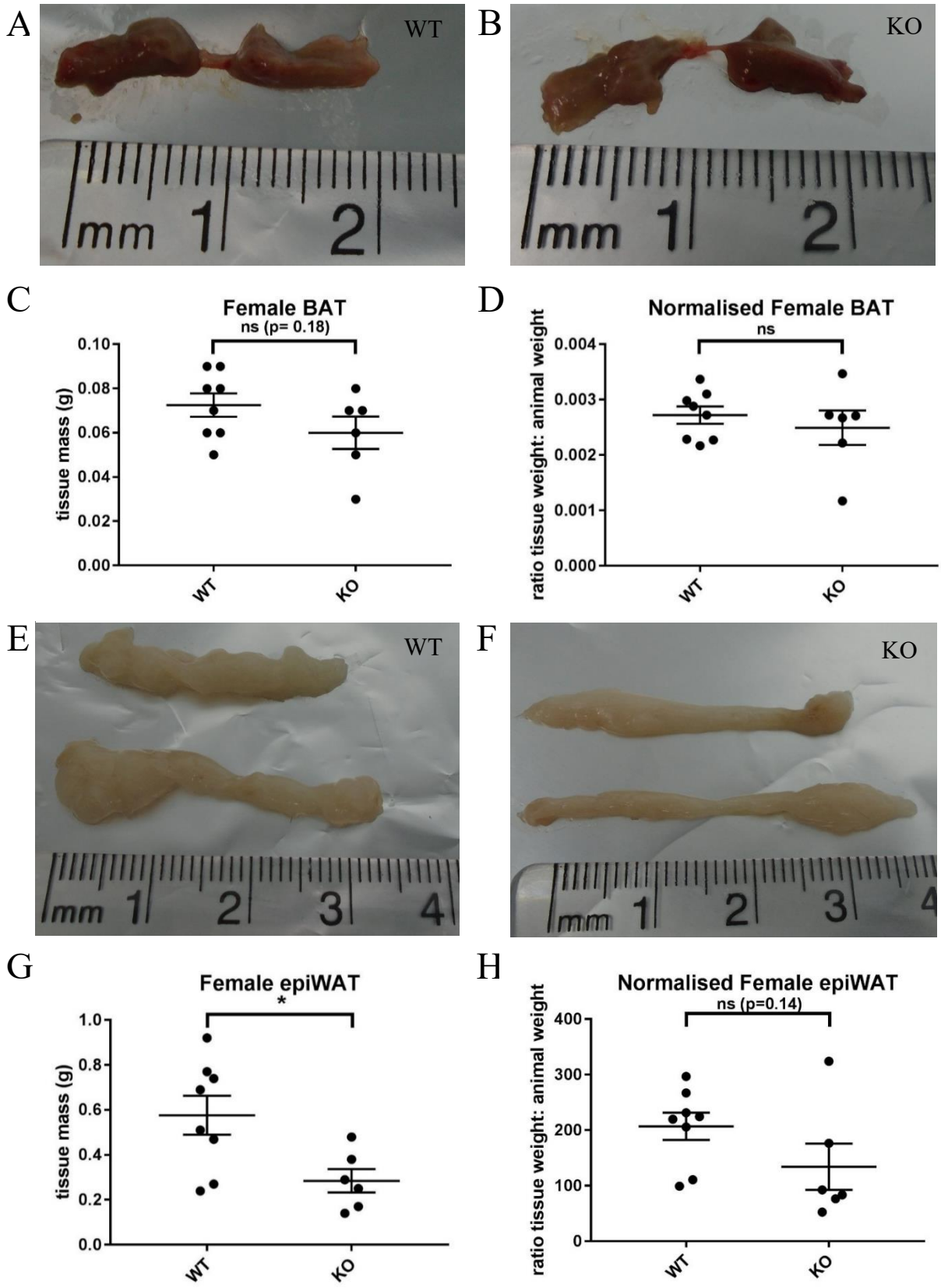


Figure 5.4. Cohort 2: Female BAT and eWAT depots. (A) Representative image of WT iBAT (B) Representative image of KO iBAT (C) Mass of BAT tissues (D) Mass of BAT tissues normalised to total animal body weight (E) Representative image of WT eWAT (F) Representative image of KO eWAT (G) Mass of eWAT tissues (H) Mass of eWAT tissues normalised to total animal body weight. WT n=8, KO n=6 animals. Error bars: mean±SEM; unpaired, two-tailed *t*-test,*P<0.05.

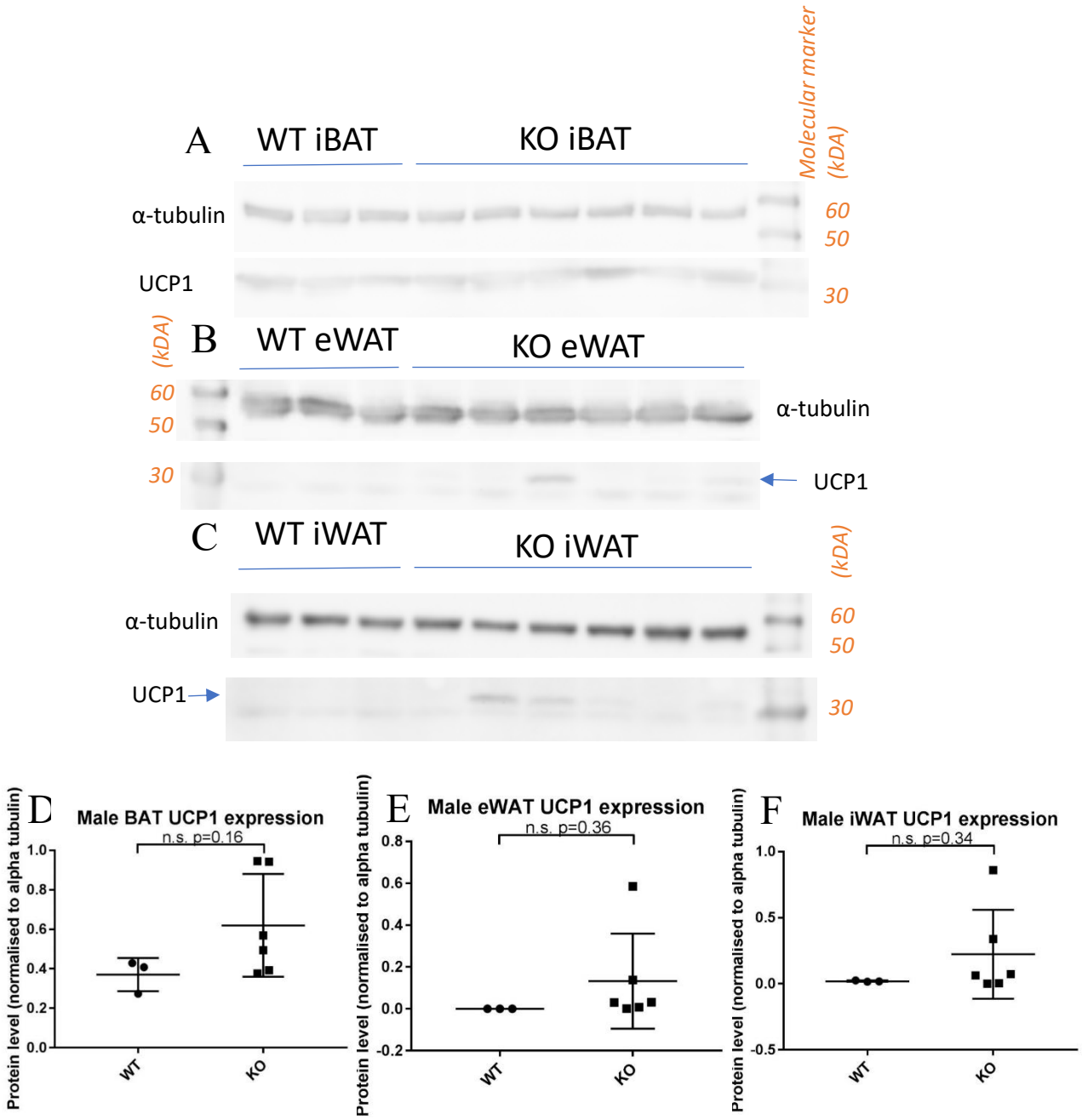


Figure 5.5. Cohort 2: Western blots of male BAT, eWAT and iWAT fat depots for UCP1 expression. (A) iBAT (B) eWAT (c) iWAT . UCP1 expression values normalised to alpha tubulin for (D) iBAT (E) eWAT and (F) iWAT. WT n=3, KO n=6 animals. Error bars: mean±SD; unpaired, two-tailed *t*-test. MW α-tubulin 50kDa; UCP1 33kDa.

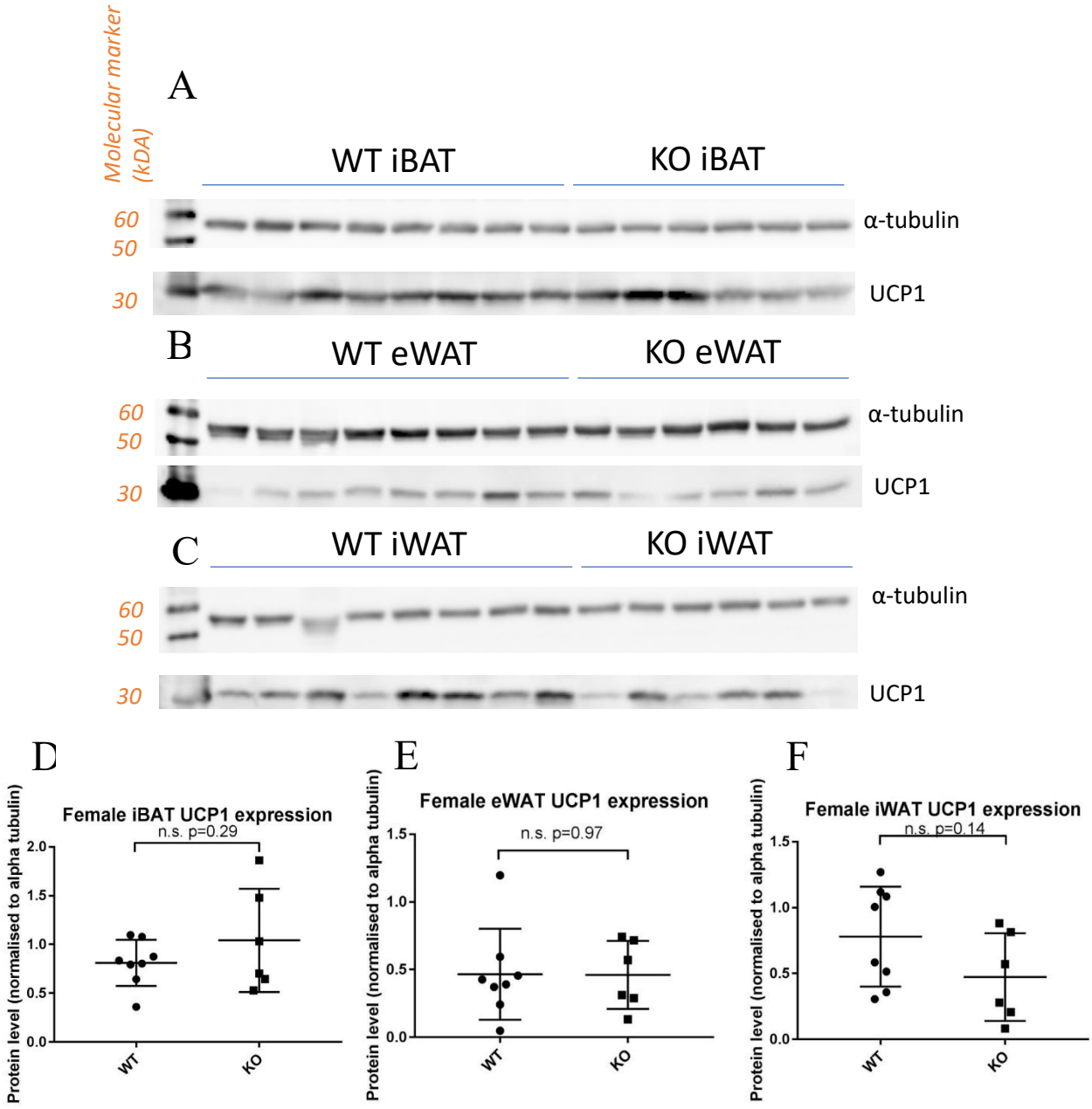


Figure 5.6. Cohort 2: Western blots of female BAT, eWAT and iWAT fat depots for UCP1 expression. (A) iBAT (B) eWAT (c) iWAT . UCP1 expression values normalised to alpha tubulin for (D) iBAT (E) eWAT and (F) iWAT. WT n=8, KO n=6 animals. Error bars: mean±SD; unpaired, two-tailed *t*-test. MW α-tubulin 50kDa; UCP1 33kDa.

5.4 Discussion

The results presented in this chapter provide some evidence of a difference in thermogenic capacity between ABCC5 KO mice and their WT littermate controls. Contrary to what might have been expected, the ABCC5 KO mice appear to have reduced thermogenic capacity compared to WT animals. However further study is required to confirm this.

Western blot analysis of iWAT from cohort 1 seemed to show a resistance to browning at the below-thermoneutral temperature of 21°C in the KO mice (Figure 5.1) due to a reduced expression of UCP1. However further studies in cohort 2 do not seem to support this (Figure 5.5 & 5.6), or at least show such a dramatic resistance to UCP1 expression in iWAT as observed in Figure 5.1.

Cohort 1 was a metabolic phenotyping cohort while cohort 2 was a behavioural phenotyping cohort. This means that the animal housing was different between cohorts: cohort 1 were housed as mixed phenotype cages; cohort 2 were housed as single phenotype cages. The phenotyping procedures performed on cohort 1 included many injections (e.g. glucose / insulin injections) inducing metabolic challenges, while the behavioural tests performed on cohort 2 were less physically stressful. Stress has been shown to induce BAT thermogenesis via sympathetic nervous system (SNS) outflow[103]. SNS also activates beige cells within WAT to promote thermogenesis (as shown in Figure 5.7). Therefore, it is possible that cohort 1 experienced more stress throughout their lifetime, which enhanced thermogenesis in iWAT. Recent behavioural studies in our lab have shown that in an open field activity test, ABCC5 KO mice do not avoid the exposed, open area of the field as WT mice do, suggesting decreased levels of stress. Therefore, it would be predicted that the KO animals would be less stressed by metabolic testing

procedures, possibly explaining the difference between WT and KO UCP1 expression detected in cohort 1 (Figure 5.1).

We have shown that KO animals have significantly less BAT and eWAT mass than WT (Figure 5.3 & 5.4). The reduced mass of the eWAT depots in KO animals is as would be expected in an animal with reduced total fat mass. In contrast, BAT mass has been negatively correlated with BMI, fat mass, and diabetes in humans.[104] Therefore in our lean and metabolically healthy KO mice it is surprising that the BAT mass is lower than WT controls, the opposite to what would be predicted. This suggests that the lean phenotype of ABCC5 KO mice is not a result of increased non-shivering thermogenesis. There are several possible causes for the reduced BAT mass observed. Firstly, it is possible that non-shivering thermogenesis is not required in the KO animals as much as in WT animals, as the increased locomotor activity of KO animals leads to more heat generation. Therefore, either because of the lack of necessity for BAT, or by an independent mechanism caused by loss of ABCC5, the BAT tissue may not be signalled to expand and develop fully.

BAT activity is regulated by the sympathetic nervous system (SNS), and BAT is highly innervated by sympathetic nerves. The level of BAT sympathetic nerve activity (SNA), noradrenaline release, and β_3-adrenergic receptor binding to brown adipocytes, determine BAT thermogenic capacity. SNA activity regulates thermogenic capacity through regulation of fuel availability via lipase activity, and by modulating UCP1 expression levels.[105] Sympathetic nerve activity is driven by BAT sympathetic premotor neurons exciting BAT sympathetic preganglionic neurons, which in turn excite sympathetic ganglion cells that directly innervate BAT (Figure 5.7).[105] The primary location of premotor neurons driving BAT thermogenesis is the rostral raphe pallidus (rRPa).[106]

Glutamatergic neurons make up a large portion of the pathway of this thermoregulatory pathway innervating BAT (Shown in blue in Figure 5.7). BAT premotor neurons in the rRPa receive a potent glutamatergic excitation; blockade of glutamate receptors in the rRPa reverses the increases in BAT SNA and BAT thermogenesis stimulated by thermogenic stimuli.[106] Since we know that ABCC5 is a glutamate conjugate transporter,

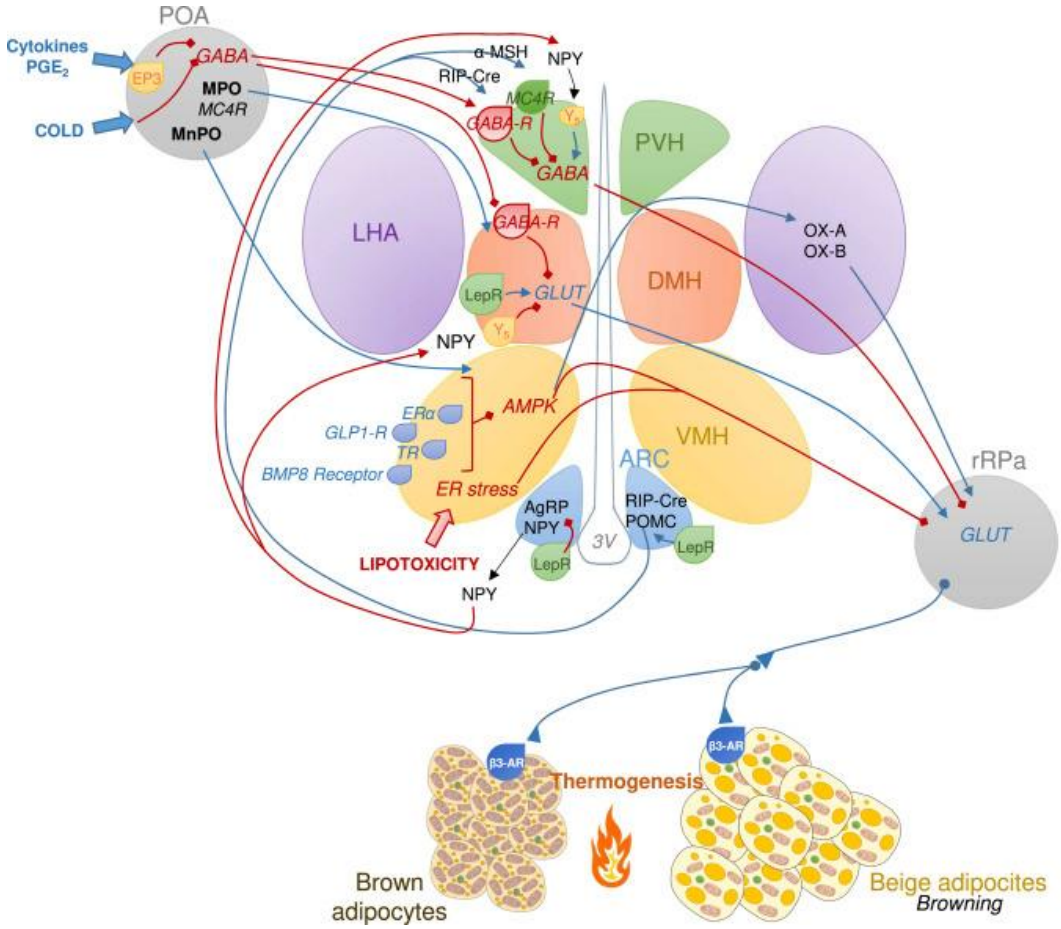


Figure 5.7. Cartoon of the neural pathways of the core thermoregulatory network innervating BAT and WAT. Taken from Contreras *et al.* Redox Biol. 2017 Aug;12:854-863.[1] doi: 10.1016/j.redox.2017.04.019.
POA, preoptic area; PGE2, prostaglandin E2; VMH, ventromedial nucleus of hypothalamus; rRPa, rostral raphe nucleus; Erα, estrogen receptor α; GLP1-R, glucagon like peptide 1 receptor; TR, thyroid hormone receptor; BMP8R, bone morphogenic protein 8 receptor; DMH, dorsomedial nucleus of the hypothalamus; ARC, arcuate nucleus of hypothalamus; AgRP, agouti-related protein; NPY, neuropeptide Y; POMC, proopiomelanocortin; PVH, paraventricular nucleus of the hypothalamus; LHA, lateral nucleus of the hypothalamus; OX, orexins; LepR, Leptin receptor; GABA-R, GABA receptor; MPO, medial POA; MnPO, median part of the POA; MC4R, melanocortin 4 receptor; β3-AR, beta 3 adrenoreceptor.

and Jansen *et al.* showed accumulation of glutamate conjugates in the brains of ABCC5 KO mice,[32] it seems possible that global loss of ABCC5 in our mice is modulating this SNS pathway of BAT activation through altered glutamatergic signalling. It would therefore be informative to measure iBAT sympathetic nerve activity in our mice. Lockie *et al.* performed this in mice by measuring the electrophysiological activity of an isolated nerve fascicle projecting to iBAT.[40]

Another consideration to explain the change in BAT mass is that while total thermogenic capacity of BAT is strongly correlated to BAT mass, the activity level of the BAT also regulates total thermogenesis.[107] Western blot analysis showed no significant difference between UCP1 expression between BAT from WT and KO animals (Figure 5.5d & 5.6d). This suggests that the activity level of the tissue may be unaffected, meaning that the reduction in mass will lead to an overall reduction in the non-shivering thermogenic capacity of BAT. BAT mass and UCP1 protein expression levels only act as indirect evidence for the thermogenic activity of BAT. Functional study of BAT temperature using a thermal imaging camera provides a powerful in vivo measurement of BAT and would be a logical next step to establish whether the difference in BAT mass results in a difference in physiological BAT temperature. The core body temperature of the animals can also be assessed with rectal thermometer measurements. Both procedures were not covered by the metabolic and behavioural work licence and could therefore not be performed.

Thyroid hormone is an activator of BAT and WAT thermogenesis,[104] acting on receptors in the VMH to stimulate SNS activity (Figure 5.7). While we see increased GLP-1 levels in our KO mice, perhaps there are other hormones that are affecting thermogenesis, such

as reduced levels of TH. Measuring TH levels from ABCC5 KO mice and WT controls might explain a potential difference in BAT mass.

All previous studies linking GLP-1R agonism with BAT and/or WAT thermogenesis were performed in male rodents[36-41], and no data have been published studying the effect of GLP-1 on fat metabolism in female rodents. Beiroa *et al.* showed that intracerebroventricular administration of the GLP-1R agonist liraglutide leads to increased mRNA and protein expression of PRDM16 and UCP1 in both BAT and eWAT of male mice.[41] Here we also found that UCP1 and PRDM16 protein expression in iWAT extract from cohort 1 was correlated in the male mice (Figure 5.1a,b) although with a decreased level of expression in the ABCC5 KO mice. Given the detection of PRDM16 in the males of chow-fed cohort 1, it will be interesting to compare these results to upcoming HFD cohorts. This is because PRDM16 has been shown to reduce HFD-induced weight gain by increasing energy expenditure.[95]

In contrast to the males, little to no PRDM16 protein was detected in either WT or KO female mice (Figure 5.1b). While no data has been reported on PRDM16 protein expression in female rodents following GLP-1R agonist, PRDM16 and UCP1 mRNA levels in female mice have been shown to increase in parallel in iWAT in a transgenic mouse that sees browning of BAT and WAT.[108] This study is typical of most published studies of non-shivering thermogenesis, where most of the data supporting browning is upregulation of mRNA levels of thermogenic genes, rather than increased protein expression. It would be desirable to see more publications showing both mRNA and protein expression data, as these do not always vary in parallel.[109,110] While we have presented protein expression data, time limitations prevented generation of mRNA expression values and this is something that should be carried out in future.

Despite UCP1 expression, no FGF21 was detectable in either WT or KO iWAT extract from cohort 1 (Figure 5.1b). While there is a lot of evidence for FGF21 causing browning of thermogenic tissues, this has always been in the context of significant cold stimuli.[96-99] In this study the animals were not subjected to a significant cold stimulus, therefore it is unsurprising that we detected no FGF21 expression.

To further understand whether the global loss of ABCC5 is modulating differentiation of thermogenic adipocytes, a primary culture protocol could be used. By deriving primary BAT and beige cells from preadipocyte cells found in the stromal-vascular fraction from isolated mouse fat depots (as described in Aune et al.[111]) and then adding plasma isolated from ABCC5 KO mice, it will be possible to study any difference in thermogenic tissue differentiation. Results from this study would tell us whether there is a circulating factor modulating the thermogenic capacity in ABCC5 KO mice, or whether central signalling may be regulating this.

Reduced mass of eWAT, as observed in our KO mice, is normally associated with WAT browning. However, Western blot analysis of these eWAT depots don't show increased expression of UCP1 (Figure 5.5 & 5.6) in KO animals. Therefore, it is unclear whether the reduction of total eWAT mass observed in KO animals is an indicator of WAT browning. eWAT is one of the major visceral fat depots in mice. Increased visceral fat in humans is strongly associated with T2D, coronary heart disease and other metabolic dysfunction.[112] Visceral fat and its resident macrophages produce more proinflammatory cytokines and less adiponectin (a hormone that regulates glucose levels and fatty acid breakdown) than subcutaneous fat.[112] Therefore the reduction in eWAT observed in our ABCC5 KO mice may be contributing to the lean, metabolically healthy phenotype observed. However because the loss of ABCC5 is global, it is difficult to ascertain the

cause of the reduced eWAT mass and whether this is a cause or an effect of the metabolic healthy phenotype. Additionally, it should be noted that correlating fat data from mice into humans has limitations; while visceral and subcutaneous fat depots exist in both humans and mice and have been shown to have similar roles, epididymal fat pads - used here, and in nearly all studies as an indicator of visceral fat – do not exist in humans.[113]

5.4.1 Technical challenges from this study

As female mice show lower total body weight than males, total BAT mass is also lower in females than males. In this study, the low weight of the female BAT, particularly the KO female BAT, caused technical difficulties because the scales used for tissue weighing were working near their lower detection limit. This means that large percentage differences in BAT mass (e.g. 0.03g to 0.04g) were less likely to be differentiated by the scales. Repetition of the female BAT mass with a more precise balance would clarify whether there is a difference between WT and KO as the data here show a trend towards (Figure 5.4c).

The AdipoCount software used here was developed with the goal of fixing several problems with previously existing adipocyte area measurement softwares such as AdipoSoft[69]. However several limitations of the AdipoCount software used here were observed during the analysis performed in Figure 5.2. Most notable was the observation that quantifying tissues that are extensively browned was poorly executed. For example, Figure 5.8 shows the product of processing of an area of H&E histology iWAT sample from cohort 1 that is highly browned, showing many small lipid droplets. Unfortunately, this large number of small lipid droplets are not detected by the AdipoCount software. There appears to be a lower threshold for lipid droplet size which the highly browned tissues containing small lipid droplets do not reach. This severely limits the accuracy of

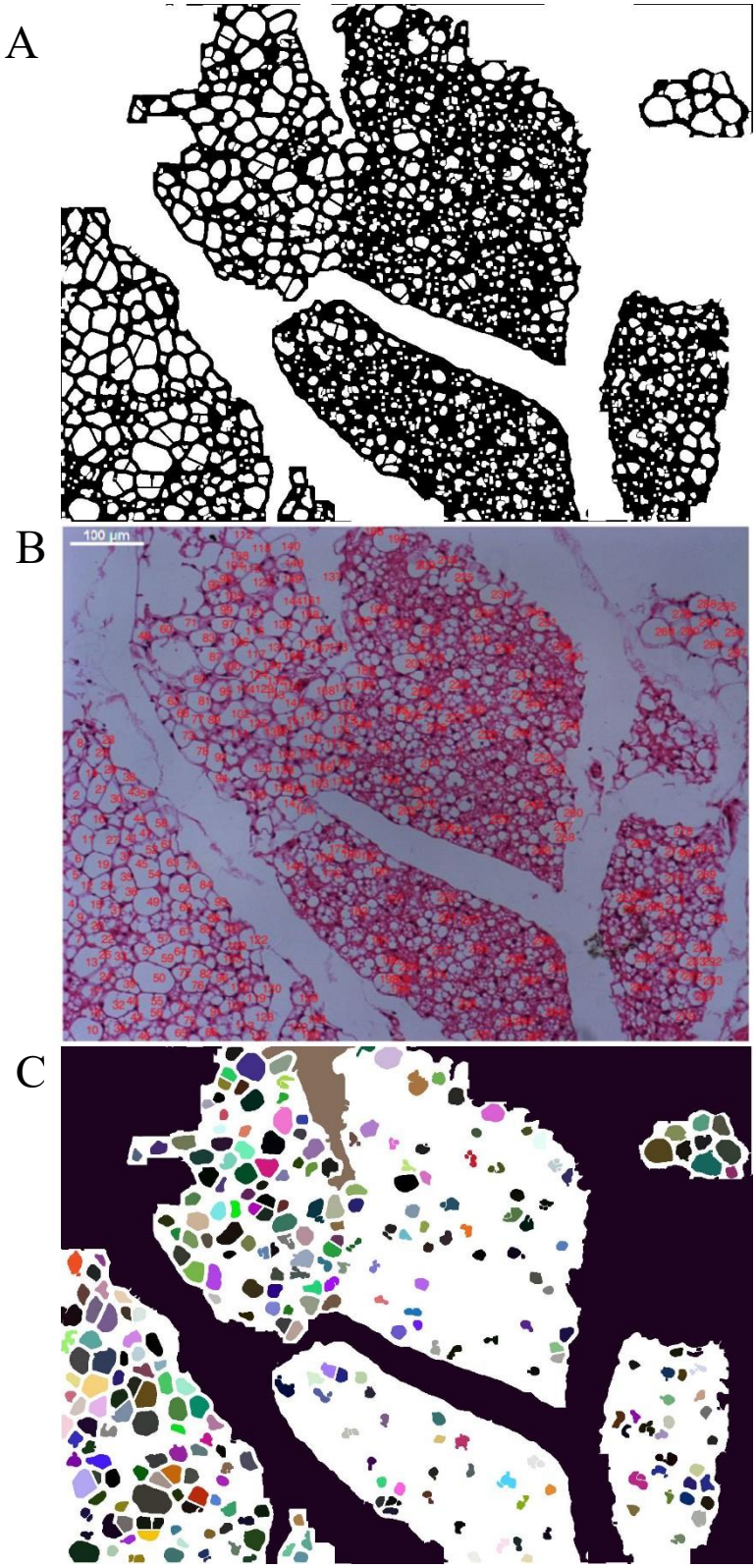


Figure 5.8. An example of an extensively browned section of iWAT (KO male) processed by AdipoCount. (A) The product of thresholding, edge detection & resegmentation (B) Cell counting and numbering (C) Final cell analysis. Scale bar 100um.

the adipocyte area calculations, since any small lipid droplets are not recognised and therefore not part of the calculation of mean adipocyte area. Therefore, it is possible that highly browned sections were not represented accurately by the AdipoCount processing. This is likely to account for, or at least contribute to, the lack of difference observed between KO and WT animals (Figure 5.3b&c), despite differences being seen by gross examination (Figure 5.3a).

In future, a variety of methods could be used to avoid the significant limitation of poor AdipoCount analysis of highly browned WAT. Firstly, by using higher magnification images it may be possible that the smaller lipid droplets may reach the threshold for recognition and measurement. Alternatively, performing anti-UCP1 immunofluorescent staining and then quantifying the UCP1 positive area is a method that has been used in several other studies[102], as well as using COX-4 as a mitochondrial marker, where the

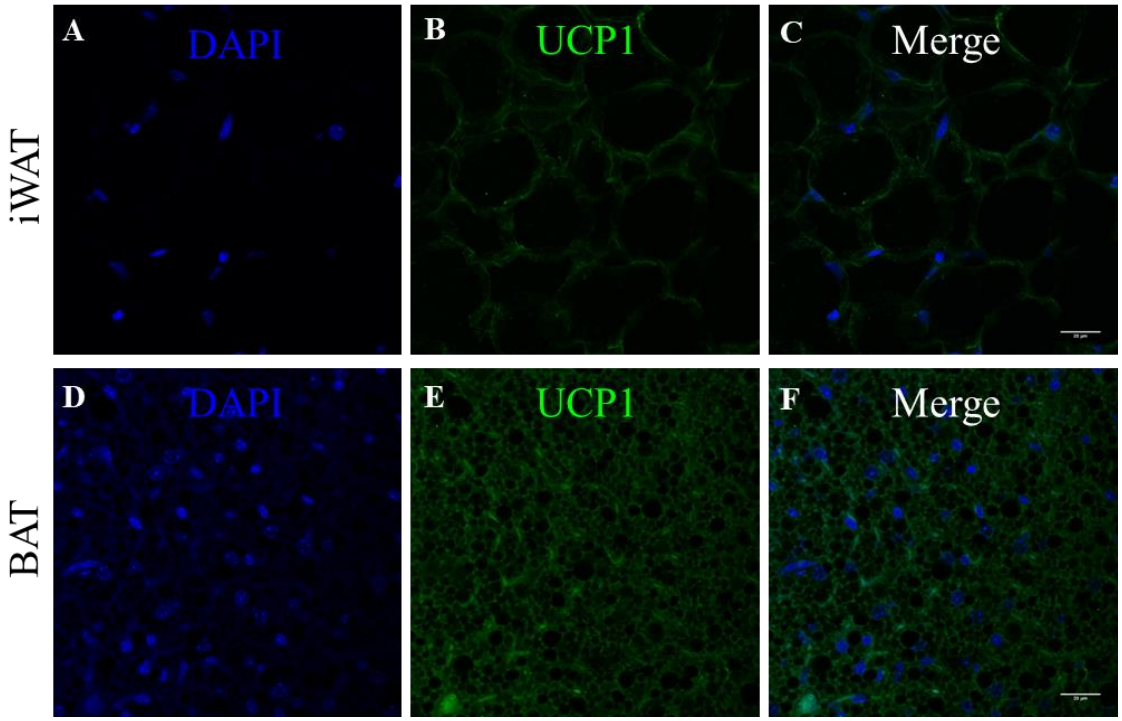


Figure 5.9. Immunofluorescent staining of iWAT (A,B,C) and BAT (D,E,F) from a WT mouse for UCP1. DAPI staining (A&D), anti-UCP1 staining (B&E) and merge (C&F). Scale bar 20um.

COX-4 positive area can again be quantified.[102] Anti-UCP1 staining was performed on both iWAT and iBAT sections from WT mice (Figure 5.9) however due to time constraints it was not possible to perform this for quantification purposes in multiple KO and WT mice.

Analysis of the current data could also be improved by looking at the distribution of adipocyte diameter or area rather than merely comparing an overall calculated mean. Zhang et al. used this method to compare the diameter of epididymal adipocytes between a KO and WT mouse model, followed by analysis by Wilcoxon signed-rank test.[114]

6 General Discussion and Conclusion

The ATP-binding cassette membrane transporter ABCC5 has been shown to transport glutamate conjugates in mammalian cells. Several of these glutamate conjugate substrates are inhibitors of glutamatergic activation. Within endocrine pancreas cells it is well documented that neuropeptides localise to separate vesicles to the large secretory insulin-containing vesicles.[115] Somewhat similarly, within GLUTag cells (a model enteroendocrine L-cell line), ABCC5 appears to be localised within vesicles that are distinct from GLP-1-containing vesicles and is not present in the cell membrane. ABCC5 KO mice generated in our lab show increased GLP-1 secretion from gut organoids, increased in vivo circulating GLP-1 levels, and increased insulin sensitivity. Our ABCC5 KO mice have a lean phenotype, with less overall fat mass than WT control animals.

The main aim of this thesis was to explore the effect of global ABCC5 loss on gut and adipose tissue physiology in mice. These results will form an important point of comparison for future ABCC5 KO mice cohorts that will be weaned onto a HFD. Despite several publications showing a link between GLP-1R agonism and WAT and BAT thermogenesis (demonstrated by upregulated UCP-1 levels), we did not find any evidence for increased BAT or WAT thermogenesis in our KO mice. Western blots for UCP1, FGF21 and PRDM16 (all proteins associated with increased thermogenesis) were inconclusive (Figures 5.1, 5.5 & 5.6), overall showing no great changes in expression despite cohort 1 exhibiting decreased UCP1 expression in iWAT (Figure 5.1). Therefore, increased thermogenesis cannot be a cause of the lean phenotype observed with ABCC5 loss. Indeed, the reduced BAT mass of cohort 2 KO animals (Figures 5.3 & 5.4) and western blots and H&E histology of cohort 1 animals (Figures 5.1 & 5.2) suggest a reduction in thermogenic capacity in ABCC5 KO mice. A likely reason for this is via

changes in glutamatergic neuronal signalling in the SNS pathway activating BAT and WAT thermogenesis. The SNS regulates non-shivering thermogenesis in multiple ways, including regulating cellular lipase activity (and therefore thermogenic fuel availability), and by modulating UCP1 expression levels.[105] While at this stage we cannot present conclusive evidence for a reduction of UCP1 expression, it is possible that thermogenic changes are being mediated by lipase activity levels in BAT and WAT.

The data presented in this thesis will form an important point of comparison for future ABCC5 KO cohorts that will be weaned onto a high-fat diet (HFD). Typically, metabolic phenotypes become more dramatic when mice are weaned onto a HFD. Therefore, it would be expected that the difference in body mass and fat mass between KO and WT animals will be greater in our future HFD cohort. HFD feeding is known to increase energy expenditure[116] and while increased BAT activity was once believed to contribute to this increase in energy expenditure, the current evidence does not support this.[117] It will therefore be of great interest to see if there are any significant changes in BAT between WT and KO mice that are fed a HFD.

There are several limitations when correlating murine fat physiology into humans. Firstly, while humans possess BAT, there is no equivalent of the interscapular BAT depot in adult humans (iBAT is present in infants). Indeed, adults were not thought to possess any BAT tissue at all until recent studies using ^{18}FDG-PET and MRI identified it in the neck and other areas.[118-120] To further complicate the story, transcriptional analysis of adult BAT depots has shown it exibits markers unique to beige WAT rather than true BAT.[121,122] This suggests that adult human BAT depots may not be best modelled by murine iBAT. Furthermore, endurance exercise which is known to stimulate WAT browning in mice, has been shown to cause no changes in WAT metabolism in obese adults.[123]

As well as a thermogenic tissue, it should not be overlooked that BAT has been shown to possess endocrine activity. A recently published study by Stanford *et al.* identified a novel batokine, 12,13-diHOME, which is released from BAT after exercise and causes skeletal muscles to increase fatty acid uptake and subsequent oxidation.[124] This was shown in both mice and humans.[124] Perhaps this batokine is playing a role in our ABCC5 KO model; increased locomotor activity of KO animals may cause increased 12,13-diHOME secretion from BAT, resulting in increased metabolic rate that causes a lean phenotype. ABCC5 loss (rather than the size of the overall BAT tissue) may be causing enhanced 12,13-diHOME secretion.

Because there are so many factors that can modulate BAT and WAT tissue mass and thermogenesis, using a global ABCC5 KO mouse model has its limitations. Furthermore, because the tissue expression pattern of ABCC5 in mice is not fully characterised, it is difficult to assess the causality of the phenotype observed. Tissue-specific KO models would give more direct insight into the role that ABCC5 is having in specific organs. The first tissue that would be logical to explore further is an enteroendocrine-specific knockdown of ABCC5. This would show the role that modulated gut hormone secretion, as a result of ABCC5 loss, is having on the whole-body metabolism of the mouse. Secondly, a brain-specific knockout would be informative for understanding any central regulation of BAT and/or WAT physiology.

Recent behavioural studies in our lab have suggested decreased levels of stress in ABCC5 KO mice [H. de Wet, Unpublished data]. Additionally, during routine handling of the mice it has been observed that the KO mice seemed less anxious and stressed. Since stress has been shown to induce BAT thermogenesis via SNS action[103,125], it seems very possible that the reduced BAT mass observed in our ABCC5 KO mice could be a result

of a reduced stress response to daily life and regular behavioural tests. Stress has also been extensively linked to metabolic disease[126], hence it is conceivable that the metabolically healthy phenotype seen in our ABCC5 KO is at least in part due to the lack of stress experienced by these animals. This would form an interesting line of future investigation.

Many future experiments have been suggested throughout this thesis. To summarise: the protocol established in Chapter 3 should be used for live cell imaging to track GLP-1 exocytosis with plasmid mediated ABCC5 overexpression and siRNA ABCC5 knockdown; the villi length and surface area measurements should be performed in future HFD cohorts and compared to the chow diet data presented in Chapter 4; and thermogenic capacity of ABCC5 KO mice should be fully investigated following the results presented in Chapter 5. Future HFD cohorts should be measured for fat pad mass and UCP1 expression. Furthermore, studying thermogenic capacity using thermal imaging and core body temperature measurements, both before and after cold challenge and thermoneutral housing will give a fuller picture of the impact of ABCC5 loss on non-shivering thermogenesis. Additionally, qPCR should be performed on BAT and WAT extract for UCP1 and other markers of browning, and AdipoCount analysis should be repeated using images of higher magnification, as well as measuring UCP1 and COX4 positive areas of immunofluorescently labelled histology sections. Thyroid hormone levels should also be measured alongside probing for possible 12,13-diHOME secretion from BAT. Moreover, primary adipocyte culture can be used to look at development of brown and beige adipocytes. Finally, because of the link between SNS activity and glutamate signalling (which ABCC5 has been implicated in), the most important experiment to perform going forward is to measure iBAT sympathetic nerve activity in our KO mice.

In conclusion, this thesis has established a protocol for live cell imaging in a model L-cell line and found no difference in villi length between WT and ABCC5 KO mice. We have also shown that ABCC5 KO mice do not have enhanced thermogenic capacity. Indeed, total BAT and eWAT mass is significantly lower than WT animals, and there is evidence of a lack of WAT and BAT browning in KO mice. This might be due to a lack of SNS activation of BAT and WAT because of ABCC5 loss-mediated changes in glutamatergic signalling. The results presented in this thesis open up future investigative possibilities to further elucidate the role of ABCC5 in metabolism.

References

1 Contreras, C., Nogueiras, R., Dieguez, C., Rahmouni, K. & Lopez, M. Traveling from the hypothalamus to the adipose tissue: The thermogenic pathway. *Redox Biol* **12**, 854-863, doi:10.1016/j.redox.2017.04.019 (2017).

2 Murphy, K. G. & Bloom, S. R. Gut hormones and the regulation of energy homeostasis. *Nature* **444**, 854-859, doi:10.1038/nature05484 (2006).

3 Leprohon, P., Legare, D. & Ouellette, M. ABC transporters involved in drug resistance in human parasites. *Essays Biochem* **50**, 121-144, doi:10.1042/bse0500121 (2011).

4 Bartelt, A. & Heeren, J. Adipose tissue browning and metabolic health. *Nat Rev Endocrinol* **10**, 24-36, doi:10.1038/nrendo.2013.204 (2014).

5 Owens, B. Cell physiology: The changing colour of fat. *Nature* **508**, S52-53, doi:10.1038/508S52a (2014).

6 *WHO factsheet: Obesity and overweight*, <http://www.who.int/mediacentre/factsheets/fs311/en/> (2018). (date accessed (21/3/2018)

7 Gonzalez-Muniesa, P. *et al.* Obesity. *Nat Rev Dis Primers* **3**, 17034, doi:10.1038/nrdp.2017.34 (2017).

8 Bray, G. A., Fruhbeck, G., Ryan, D. H. & Wilding, J. P. Management of obesity. *Lancet* **387**, 1947-1956, doi:10.1016/S0140-6736(16)00271-3 (2016).

9 Chang, S. H. *et al.* The effectiveness and risks of bariatric surgery: an updated systematic review and meta-analysis, 2003-2012. *JAMA Surg* **149**, 275-287, doi:10.1001/jamasurg.2013.3654 (2014).

10 Ionut, V., Burch, M., Youdim, A. & Bergman, R. N. Gastrointestinal hormones and bariatric surgery-induced weight loss. *Obesity (Silver Spring)* **21**, 1093-1103, doi:10.1002/oby.20364 (2013).

11 Hansen, C. F. *et al.* Hypertrophy dependent doubling of L-cells in Roux-en-Y gastric bypass operated rats. *PLoS One* **8**, e65696, doi:10.1371/journal.pone.0065696 (2013).

12 Holst, J. J. Enteroendocrine secretion of gut hormones in diabetes, obesity and after bariatric surgery. *Curr Opin Pharmacol* **13**, 983-988, doi:10.1016/j.coph.2013.09.014 (2013).

13 Lean, M. E. & Malkova, D. Altered gut and adipose tissue hormones in overweight and obese individuals: cause or consequence? *Int J Obes (Lond)* **40**, 622-632, doi:10.1038/ijo.2015.220 (2016).

14 Habib, A. M. *et al.* Overlap of endocrine hormone expression in the mouse intestine revealed by transcriptional profiling and flow cytometry. *Endocrinology* **153**, 3054-3065, doi:10.1210/en.2011-2170 (2012).

15 Nauck, M. A. & Meier, J. J. The incretin effect in healthy individuals and those with type 2 diabetes: physiology, pathophysiology, and response to therapeutic interventions. *Lancet Diabetes Endocrinol* **4**, 525-536, doi:10.1016/S2213-8587(15)00482-9 (2016).

16 Diakogiannaki, E., Gribble, F. M. & Reimann, F. Nutrient detection by incretin hormone secreting cells. *Physiol Behav* **106**, 387-393, doi:10.1016/j.physbeh.2011.12.001 (2012).

17 Pais, R., Gribble, F. M. & Reimann, F. Stimulation of incretin secreting cells. *Ther Adv Endocrinol Metab* **7**, 24-42, doi:10.1177/2042018815618177 (2016).

18 Brunton, S. GLP-1 receptor agonists vs. DPP-4 inhibitors for type 2 diabetes: is one approach more successful or preferable than the other? *Int J Clin Pract* **68**, 557-567, doi:10.1111/ijcp.12361 (2014).

19 Madsbad, S. Review of head-to-head comparisons of glucagon-like peptide-1 receptor agonists. *Diabetes Obes Metab* **18**, 317-332, doi:10.1111/dom.12596 (2016).

20 Pais, R., Rievaj, J., Larraufie, P., Gribble, F. & Reimann, F. Angiotensin II Type 1 Receptor-Dependent GLP-1 and PYY Secretion in Mice and Humans. *Endocrinology* **157**, 3821-3831, doi:10.1210/en.2016-1384 (2016).

21 Drucker, D. J., Jin, T., Asa, S. L., Young, T. A. & Brubaker, P. L. Activation of proglucagon gene transcription by protein kinase-A in a novel mouse enteroendocrine cell line. *Mol Endocrinol* **8**, 1646-1655, doi:10.1210/mend.8.12.7535893 (1994).

22 Dean, M., Rzhetsky, A. & Allikmets, R. The human ATP-binding cassette (ABC) transporter superfamily. *Genome Res* **11**, 1156-1166, doi:10.1101/gr.184901 (2001).

23 Aleksandrov, A. A., Aleksandrov, L. A. & Riordan, J. R. CFTR (ABCC7) is a hydrolyzable-ligand-gated channel. *Pflugers Arch* **453**, 693-702, doi:10.1007/s00424-006-0140-z (2007).

24 Aittoniemi, J. *et al.* Review. SUR1: a unique ATP-binding cassette protein that functions as an ion channel regulator. *Philos Trans R Soc Lond B Biol Sci* **364**, 257-267, doi:10.1098/rstb.2008.0142 (2009).

25 Lin, D. Y., Huang, S. & Chen, J. Crystal structures of a polypeptide processing and secretion transporter. *Nature* **523**, 425-430, doi:10.1038/nature14623 (2015).

26 Jedlitschky, G., Burchell, B. & Keppler, D. The multidrug resistance protein 5 functions as an ATP-dependent export pump for cyclic nucleotides. *J Biol Chem* **275**, 30069-30074, doi:10.1074/jbc.M005463200 (2000).

27 Wielinga, P. *et al.* The human multidrug resistance protein MRP5 transports folates and can mediate cellular resistance against antifolates. *Cancer Res* **65**, 4425-4430, doi:10.1158/0008-5472.CAN-04-2810 (2005).

28 Adema, A. D. *et al.* Overexpression of MRP4 (ABCC4) and MRP5 (ABCC5) confer resistance to the nucleoside analogs cytarabine and troxacitabine, but not gemcitabine. *Springerplus* **3**, 732, doi:10.1186/2193-1801-3-732 (2014).

29 Korolnek, T., Zhang, J., Beardsley, S., Scheffer, G. L. & Hamza, I. Control of metazoan heme homeostasis by a conserved multidrug resistance protein. *Cell Metab* **19**, 1008-1019, doi:10.1016/j.cmet.2014.03.030 (2014).

30 Shipp, L. E., Hill, R. Z., Moy, G. W., Gokirmak, T. & Hamdoun, A. ABCC5 is required for cAMP-mediated hindgut invagination in sea urchin embryos. *Development* **142**, 3537-3548, doi:10.1242/dev.126144 (2015).

31 Jansen, R. S. *et al.* N-lactoyl-amino acids are ubiquitous metabolites that originate from CNDP2-mediated reverse proteolysis of lactate and amino acids. *Proc Natl Acad Sci U S A* **112**, 6601-6606, doi:10.1073/pnas.1424638112 (2015).

32 Jansen, R. S., Mahakena, S., de Haas, M., Borst, P. & van de Wetering, K. ATP-binding Cassette Subfamily C Member 5 (ABCC5) Functions as an Efflux Transporter of Glutamate Conjugates and Analogs. *J Biol Chem* **290**, 30429-30440, doi:10.1074/jbc.M115.692103 (2015).

33 Direk, K., Lau, W., Small, K. S., Maniatis, N. & Andrew, T. ABCC5 transporter is a novel type 2 diabetes susceptibility gene in European and African American populations. *Ann Hum Genet* **78**, 333-344, doi:10.1111/ahg.12072 (2014).

34 Steinert, R. E., Beglinger, C. & Langhans, W. Intestinal GLP-1 and satiation: from man to rodents and back. *Int J Obes (Lond)* **40**, 198-205, doi:10.1038/ijo.2015.172 (2016).

35 Zhang, F. *et al.* Weight loss effect of glucagon-like peptide-1 mimetics on obese/overweight adults without diabetes: A systematic review and meta-analysis of randomized controlled trials. *J Diabetes* **7**, 329-339, doi:10.1111/1753-0407.12198 (2015).

36 Lee, S. J. *et al.* Loss of dorsomedial hypothalamic GLP-1 signaling reduces BAT thermogenesis and increases adiposity. *Mol Metab* **11**, 33-46, doi:10.1016/j.molmet.2018.03.008 (2018).

37 Kooijman, S. *et al.* Central GLP-1 receptor signalling accelerates plasma clearance of triacylglycerol and glucose by activating brown adipose tissue in mice. *Diabetologia* **58**, 2637-2646, doi:10.1007/s00125-015-3727-0 (2015).

38 Heppner, K. M. *et al.* Contribution of brown adipose tissue activity to the control of energy balance by GLP-1 receptor signalling in mice. *Diabetologia* **58**, 2124-2132, doi:10.1007/s00125-015-3651-3 (2015).

39 Wei, Q., Li, L., Chen, J. A., Wang, S. H. & Sun, Z. L. Exendin-4 improves thermogenic capacity by regulating fat metabolism on brown adipose tissue in mice with diet-induced obesity. *Ann Clin Lab Sci* **45**, 158-165 (2015).

40 Lockie, S. H. *et al.* Direct control of brown adipose tissue thermogenesis by central nervous system glucagon-like peptide-1 receptor signaling. *Diabetes* **61**, 2753-2762, doi:10.2337/db11-1556 (2012).

41 Beiroa, D. *et al.* GLP-1 agonism stimulates brown adipose tissue thermogenesis and browning through hypothalamic AMPK. *Diabetes* **63**, 3346-3358, doi:10.2337/db14-0302 (2014).

42 <https://www.proteinatlas.org/ENSG00000114770-ABCC5/tissue> ((date accessed (21/3/2018)

43 Nies, A. T. *et al.* Expression and immunolocalization of the multidrug resistance proteins, MRP1-MRP6 (ABCC1-ABCC6), in human brain. *Neuroscience* **129**, 349-360, doi:10.1016/j.neuroscience.2004.07.051 (2004).

44 Scheffer, G. L. *et al.* Specific detection of multidrug resistance proteins MRP1, MRP2, MRP3, MRP5, and MDR3 P-glycoprotein with a panel of monoclonal antibodies. *Cancer Res* **60**, 5269-5277 (2000).

45 Cedikova, M. *et al.* Mitochondria in White, Brown, and Beige Adipocytes. *Stem Cells Int* **2016**, 6067349, doi:10.1155/2016/6067349 (2016).

46 Thyagarajan, B. & Foster, M. T. Beiging of white adipose tissue as a therapeutic strategy for weight loss in humans. *Horm Mol Biol Clin Investig* **31**, doi:10.1515/hmbci-2017-0016 (2017).

47 Rosen, E. D. & Spiegelman, B. M. Adipocytes as regulators of energy balance and glucose homeostasis. *Nature* **444**, 847-853, doi:10.1038/nature05483 (2006).

48 Jeremic, N., Chaturvedi, P. & Tyagi, S. C. Browning of White Fat: Novel Insight Into Factors, Mechanisms, and Therapeutics. *J Cell Physiol* **232**, 61-68, doi:10.1002/jcp.25450 (2017).

49 Frikke-Schmidt, H., O'Rourke, R. W., Lumeng, C. N., Sandoval, D. A. & Seeley, R. J. Does bariatric surgery improve adipose tissue function? *Obes Rev* **17**, 795-809, doi:10.1111/obr.12429 (2016).

50 Klingenspor, M., Herzig, S. & Pfeifer, A. Brown fat develops a brite future. *Obes Facts* **5**, 890-896, doi:10.1159/000346337 (2012).

51 Wang, W. & Seale, P. Control of brown and beige fat development. *Nat Rev Mol Cell Biol* **17**, 691-702, doi:10.1038/nrm.2016.96 (2016).

52 Sanchez-Gurmaches, J. & Guertin, D. A. Adipocyte lineages: tracing back the origins of fat. *Biochim Biophys Acta* **1842**, 340-351, doi:10.1016/j.bbadis.2013.05.027 (2014).

53 Spalding, K. L. *et al.* Dynamics of fat cell turnover in humans. *Nature* **453**, 783-787, doi:10.1038/nature06902 (2008).

54 Villarroya, F., Cereijo, R., Villarroya, J. & Giralt, M. Brown adipose tissue as a secretory organ. *Nat Rev Endocrinol* **13**, 26-35, doi:10.1038/nrendo.2016.136 (2017).

55 Aldiss, P. *et al.* Exercise-induced 'browning' of adipose tissues. *Metabolism* **81**, 63-70, doi:10.1016/j.metabol.2017.11.009 (2018).

56 Stanford, K. I., Middelbeek, R. J. & Goodyear, L. J. Exercise Effects on White Adipose Tissue: Beiging and Metabolic Adaptations. *Diabetes* **64**, 2361-2368, doi:10.2337/db15-0227 (2015).

57 Neinast, M. D. *et al.* Activation of natriuretic peptides and the sympathetic nervous system following Roux-en-Y gastric bypass is associated with gonadal adipose tissues browning. *Mol Metab* **4**, 427-436, doi:10.1016/j.molmet.2015.02.006 (2015).

58 Poher, A. L., Altirriba, J., Veyrat-Durebex, C. & Rohner-Jeanrenaud, F. Brown adipose tissue activity as a target for the treatment of obesity/insulin resistance. *Front Physiol* **6**, 4, doi:10.3389/fphys.2015.00004 (2015).

59 Hui, X. *et al.* Adiponectin Enhances Cold-Induced Browning of Subcutaneous Adipose Tissue via Promoting M2 Macrophage Proliferation. *Cell Metab* **22**, 279-290, doi:10.1016/j.cmet.2015.06.004 (2015).

60 Hoffmann, J. M. *et al.* BMP4 Gene Therapy in Mature Mice Reduces BAT Activation but Protects from Obesity by Browning Subcutaneous Adipose Tissue. *Cell Rep* **20**, 1038-1049, doi:10.1016/j.celrep.2017.07.020 (2017).

61 Townsend, K. L. & Tseng, Y. H. Brown fat fuel utilization and thermogenesis. *Trends Endocrinol Metab* **25**, 168-177, doi:10.1016/j.tem.2013.12.004 (2014).

62 Morrison, S. F., Madden, C. J. & Tupone, D. Central neural regulation of brown adipose tissue thermogenesis and energy expenditure. *Cell Metab* **19**, 741-756, doi:10.1016/j.cmet.2014.02.007 (2014).

63 Morrison, S. F., Madden, C. J. & Tupone, D. Central control of brown adipose tissue thermogenesis. *Front Endocrinol (Lausanne)* **3**, doi:10.3389/fendo.2012.00005 (2012).

64 Liu, C. *et al.* PPARgamma in vagal neurons regulates high-fat diet induced thermogenesis. *Cell Metab* **19**, 722-730, doi:10.1016/j.cmet.2014.01.021 (2014).

65 Ruan, H. B. *et al.* O-GlcNAc transferase enables AgRP neurons to suppress browning of white fat. *Cell* **159**, 306-317, doi:10.1016/j.cell.2014.09.010 (2014).

66 Dodd, G. T. *et al.* Leptin and insulin act on POMC neurons to promote the browning of white fat. *Cell* **160**, 88-104, doi:10.1016/j.cell.2014.12.022 (2015).

67 McGlashon, J. M. *et al.* Central serotonergic neurons activate and recruit thermogenic brown and beige fat and regulate glucose and lipid homeostasis. *Cell Metab* **21**, 692-705, doi:10.1016/j.cmet.2015.04.008 (2015).

68 McDonough, A. A., Veiras, L. C., Minas, J. N. & Ralph, D. L. Considerations when quantitating protein abundance by immunoblot. *Am J Physiol Cell Physiol* **308**, C426-433, doi:10.1152/ajpcell.00400.2014 (2015).

69 Zhi, X. *et al.* AdipoCount: A New Software for Automatic Adipocyte Counting. *Front Physiol* **9**, 85, doi:10.3389/fphys.2018.00085 (2018).

70 *Addgene Plasmid #82636*, <https://www.addgene.org/82636/> ((date accessed (21/3/2018)

71 *Clustal Omega multiple sequence alignment*, <https://www.ebi.ac.uk/Tools/msa/clustalo/> (

72 Oya, M. *et al.* The G protein-coupled receptor family C group 6 subtype A (GPRC6A) receptor is involved in amino acid-induced glucagon-like peptide-1 secretion from GLUTag cells. *J Biol Chem* **288**, 4513-4521, doi:10.1074/jbc.M112.402677 (2013).

73 Collen, D. & Lijnen, H. R. Basic and clinical aspects of fibrinolysis and thrombolysis. *Blood* **78**, 3114-3124 (1991).

74 Lin, L. & Hu, K. Tissue Plasminogen Activator: Side Effects and Signaling. *J Drug Des Res* **1** (2014).

75 Yepes, M. Tissue-type plasminogen activator is a neuroprotectant in the central nervous system. *Front Cell Neurosci* **9**, 304, doi:10.3389/fncel.2015.00304 (2015).

76 Melchor, J. P. & Strickland, S. Tissue plasminogen activator in central nervous system physiology and pathology. *Thromb Haemost* **93**, 655-660, doi:10.1160/TH04-12-0838 (2005).

77 Parmer, R. J. *et al.* Tissue plasminogen activator (t-PA) is targeted to the regulated secretory pathway. Catecholamine storage vesicles as a reservoir for the rapid release of t-PA. *J Biol Chem* **272**, 1976-1982 (1997).

78 Baranes, D. *et al.* Tissue plasminogen activator contributes to the late phase of LTP and to synaptic growth in the hippocampal mossy fiber pathway. *Neuron* **21**, 813-825 (1998).

79 Grummisch, J. A., Jadavji, N. M. & Smith, P. D. The pleiotropic effects of tissue plasminogen activator in the brain: implications for stroke recovery. *Neural Regen Res* **11**, 1401-1402, doi:10.4103/1673-5374.191204 (2016).

80 Lin, L., Jin, Y., Mars, W. M., Reeves, W. B. & Hu, K. Myeloid-derived tissue-type plasminogen activator promotes macrophage motility through FAK, Rac1, and NF-

kappaB pathways. *Am J Pathol* **184**, 2757-2767, doi:10.1016/j.ajpath.2014.06.013 (2014).

81 Hurtado, M. *et al.* Activation of the epidermal growth factor signalling pathway by tissue plasminogen activator in pancreas cancer cells. *Gut* **56**, 1266-1274, doi:10.1136/gut.2006.097188 (2007).

82 Gualandris, A., Jones, T. E., Strickland, S. & Tsirka, S. E. Membrane depolarization induces calcium-dependent secretion of tissue plasminogen activator. *J Neurosci* **16**, 2220-2225 (1996).

83 Baker, S. M., Buckheit, R. W., 3rd & Falk, M. M. Green-to-red photoconvertible fluorescent proteins: tracking cell and protein dynamics on standard wide-field mercury arc-based microscopes. *BMC Cell Biol* **11**, 15, doi:10.1186/1471-2121-11-15 (2010).

84 Dailey, M. J. Nutrient-induced intestinal adaption and its effect in obesity. *Physiol Behav* **136**, 74-78, doi:10.1016/j.physbeh.2014.03.026 (2014).

85 Ueno, P. M. *et al.* Alanyl-glutamine promotes intestinal epithelial cell homeostasis in vitro and in a murine model of weanling undernutrition. *Am J Physiol Gastrointest Liver Physiol* **301**, G612-622, doi:10.1152/ajpgi.00531.2010 (2011).

86 de Wit, N. J. *et al.* The role of the small intestine in the development of dietary fat-induced obesity and insulin resistance in C57BL/6J mice. *BMC Med Genomics* **1**, 14, doi:10.1186/1755-8794-1-14 (2008).

87 Mao, J. *et al.* Overnutrition stimulates intestinal epithelium proliferation through beta-catenin signaling in obese mice. *Diabetes* **62**, 3736-3746, doi:10.2337/db13-0035 (2013).

88 Beyaz, S. *et al.* High-fat diet enhances stemness and tumorigenicity of intestinal progenitors. *Nature* **531**, 53-58, doi:10.1038/nature17173 (2016).

89 Iqbal, C. W., Qandeel, H. G., Zheng, Y., Duenes, J. A. & Sarr, M. G. Mechanisms of ileal adaptation for glucose absorption after proximal-based small bowel resection. *J*

Gastrointest Surg **12**, 1854-1864; discussion 1864-1855, doi:10.1007/s11605-008-0666-9 (2008).

90 Taqi, E. *et al.* The influence of nutrients, biliary-pancreatic secretions, and systemic trophic hormones on intestinal adaptation in a Roux-en-Y bypass model. *J Pediatr Surg* **45**, 987-995, doi:10.1016/j.jpedsurg.2010.02.036 (2010).

91 Li, B., Lu, Y., Srikant, C. B., Gao, Z. H. & Liu, J. L. Intestinal adaptation and Reg gene expression induced by antidiabetic duodenal-jejunal bypass surgery in Zucker fatty rats. *Am J Physiol Gastrointest Liver Physiol* **304**, G635-645, doi:10.1152/ajpgi.00275.2012 (2013).

92 Kappe, C., Zhang, Q., Holst, J. J., Nystrom, T. & Sjoholm, A. Evidence for paracrine/autocrine regulation of GLP-1-producing cells. *Am J Physiol Cell Physiol* **305**, C1041-1049, doi:10.1152/ajpcell.00227.2013 (2013).

93 *Glucagon-like peptide-2*, <https://www.sciencedirect.com/topics/biochemistry-genetics-and-molecular-biology/glucagon-like-peptide-2> ((date accessed (21/3/2018)

94 Seale, P. *et al.* PRDM16 controls a brown fat/skeletal muscle switch. *Nature* **454**, 961-967, doi:10.1038/nature07182 (2008).

95 Seale, P. *et al.* Prdm16 determines the thermogenic program of subcutaneous white adipose tissue in mice. *J Clin Invest* **121**, 96-105, doi:10.1172/JCI44271 (2011).

96 Fisher, F. M. & Maratos-Flier, E. Understanding the Physiology of FGF21. *Annu Rev Physiol* **78**, 223-241, doi:10.1146/annurev-physiol-021115-105339 (2016).

97 Chartoumpekis, D. V. *et al.* Brown adipose tissue responds to cold and adrenergic stimulation by induction of FGF21. *Mol Med* **17**, 736-740, doi:10.2119/molmed.2011.00075 (2011).

98 Hondares, E. *et al.* Thermogenic activation induces FGF21 expression and release in brown adipose tissue. *J Biol Chem* **286**, 12983-12990, doi:10.1074/jbc.M110.215889 (2011).

99 Fisher, F. M. *et al.* FGF21 regulates PGC-1alpha and browning of white adipose tissues in adaptive thermogenesis. *Genes Dev* **26**, 271-281, doi:10.1101/gad.177857.111 (2012).

100 Emanuelli, B. *et al.* Interplay between FGF21 and insulin action in the liver regulates metabolism. *J Clin Invest* **124**, 515-527, doi:10.1172/JCI67353 (2014).

101 de Jong, J. M., Larsson, O., Cannon, B. & Nedergaard, J. A stringent validation of mouse adipose tissue identity markers. *Am J Physiol Endocrinol Metab* **308**, E1085-1105, doi:10.1152/ajpendo.00023.2015 (2015).

102 Fischer, C. *et al.* A miR-327-FGF10-FGFR2-mediated autocrine signaling mechanism controls white fat browning. *Nat Commun* **8**, 2079, doi:10.1038/s41467-017-02158-z (2017).

103 Zhang, W. & Bi, S. Hypothalamic Regulation of Brown Adipose Tissue Thermogenesis and Energy Homeostasis. *Front Endocrinol (Lausanne)* **6**, 136, doi:10.3389/fendo.2015.00136 (2015).

104 Lee, Y. H., Jung, Y. S. & Choi, D. Recent advance in brown adipose physiology and its therapeutic potential. *Exp Mol Med* **46**, e78, doi:10.1038/emm.2013.163 (2014).

105 Morrison, S. F. Central neural control of thermoregulation and brown adipose tissue. *Auton Neurosci* **196**, 14-24, doi:10.1016/j.autneu.2016.02.010 (2016).

106 Tan, C. L. & Knight, Z. A. Regulation of Body Temperature by the Nervous System. *Neuron* **98**, 31-48, doi:10.1016/j.neuron.2018.02.022 (2018).

107 Pan, D. *et al.* MicroRNA-378 controls classical brown fat expansion to counteract obesity. *Nat Commun* **5**, 4725, doi:10.1038/ncomms5725 (2014).

108 Shibata, M. *et al.* AgRP Neuron-Specific Deletion of Glucocorticoid Receptor Leads to Increased Energy Expenditure and Decreased Body Weight in Female Mice on a High-Fat Diet. *Endocrinology* **157**, 1457-1466, doi:10.1210/en.2015-1430 (2016).

109 Greenbaum, D., Colangelo, C., Williams, K. & Gerstein, M. Comparing protein abundance and mRNA expression levels on a genomic scale. *Genome Biol* **4**, 117, doi:10.1186/gb-2003-4-9-117 (2003).

110 Nedergaard, J. & Cannon, B. UCP1 mRNA does not produce heat. *Biochim Biophys Acta* **1831**, 943-949, doi:10.1016/j.bbalip.2013.01.009 (2013).

111 Aune, U. L., Ruiz, L. & Kajimura, S. Isolation and differentiation of stromal vascular cells to beige/brite cells. *J Vis Exp*, doi:10.3791/50191 (2013).

112 Hamdy, O., Porramatikul, S. & Al-Ozairi, E. Metabolic obesity: the paradox between visceral and subcutaneous fat. *Curr Diabetes Rev* **2**, 367-373 (2006).

113 Rosen, E. D. & Spiegelman, B. M. What we talk about when we talk about fat. *Cell* **156**, 20-44, doi:10.1016/j.cell.2013.12.012 (2014).

114 Zhang, R., Maratos-Flier, E. & Flier, J. S. Reduced adiposity and high-fat diet-induced adipose inflammation in mice deficient for phosphodiesterase 4B. *Endocrinology* **150**, 3076-3082, doi:10.1210/en.2009-0108 (2009).

115 Scotuzzi, M. *et al.* Multi-color electron microscopy by element-guided identification of cells, organelles and molecules. *Sci Rep* **7**, 45970, doi:10.1038/srep45970 (2017).

116 Westerterp, K. R. Diet induced thermogenesis. *Nutr Metab (Lond)* **1**, 5, doi:10.1186/1743-7075-1-5 (2004).

117 Kozak, L. P. Brown fat and the myth of diet-induced thermogenesis. *Cell Metab* **11**, 263-267, doi:10.1016/j.cmet.2010.03.009 (2010).

118 Cypess, A. M. *et al.* Identification and importance of brown adipose tissue in adult humans. *N Engl J Med* **360**, 1509-1517, doi:10.1056/NEJMoa0810780 (2009).

119 Yeung, H. W., Grewal, R. K., Gonen, M., Schoder, H. & Larson, S. M. Patterns of (18)F-FDG uptake in adipose tissue and muscle: a potential source of false-positives for PET. *J Nucl Med* **44**, 1789-1796 (2003).

120 Cohade, C., Osman, M., Pannu, H. K. & Wahl, R. L. Uptake in supraclavicular area fat ("USA-Fat"): description on 18F-FDG PET/CT. *J Nucl Med* **44**, 170-176 (2003).

121 Sharp, L. Z. *et al.* Human BAT possesses molecular signatures that resemble beige/brite cells. *PLoS One* **7**, e49452, doi:10.1371/journal.pone.0049452 (2012).

122 Jespersen, N. Z. *et al.* A classical brown adipose tissue mRNA signature partly overlaps with brite in the supraclavicular region of adult humans. *Cell Metab* **17**, 798-805, doi:10.1016/j.cmet.2013.04.011 (2013).

123 Tsiloulis, T. *et al.* No evidence of white adipocyte browning after endurance exercise training in obese men. *Int J Obes (Lond)* **42**, 721-727, doi:10.1038/ijo.2017.295 (2018).

124 Stanford, K. I. *et al.* 12,13-diHOME: An Exercise-Induced Lipokine that Increases Skeletal Muscle Fatty Acid Uptake. *Cell Metab* **27**, 1111-1120 e1113, doi:10.1016/j.cmet.2018.03.020 (2018).

125 Kataoka, N., Hioki, H., Kaneko, T. & Nakamura, K. Psychological stress activates a dorsomedial hypothalamus-medullary raphe circuit driving brown adipose tissue thermogenesis and hyperthermia. *Cell Metab* **20**, 346-358, doi:10.1016/j.cmet.2014.05.018 (2014).

126 Tamashiro, K. L., Sakai, R. R., Shively, C. A., Karatsoreos, I. N. & Reagan, L. P. Chronic stress, metabolism, and metabolic syndrome. *Stress* **14**, 468-474, doi:10.3109/10253890.2011.606341 (2011).

Appendix

```
CLUSTAL O(1.2.4) multiple sequence alignment

EMBOSS_001      ------------------------------------------------------------    0
EMBOSS_002      TTCCtCCTCCTTGCTTCaTGTTGTCTTGGATCCAGTTCAGGTAATTAGTGACCTTTGTGT    60

EMBOSS_001      ------------------------------------------------------------    0
EMBOSS_002      ATATCCCTGGCACGTCCTTCTGCCCACAGCCGAGGCCCCAGCTGATGATGCCCAGTAAAG    120

EMBOSS_001      ------------------------------------------------------------    0
EMBOSS_002      TCATCCGCTTATCGATCATGCACACCAGAGGGCCTCCTGAGTCACCCTGGCACGCGTCAT    180

EMBOSS_001      ------------------------------------------------------------    0
EMBOSS_002      GGACGTCTTGGTTGCCCCCAGTTCGGGTGTCTCCTGCACACAGCATGTTGCTCGTGATGG    240

EMBOSS_001      ------------------------------------------------------------    0
EMBOSS_002      TTTTGTTAAACAGATGCTGTGAGGTACAGCGGCTGGACGGATACAGTCTGACGTGAGCCT    300

EMBOSS_001      ------------------------------------------------------------    0
EMBOSS_002      CCTTCAGCCGGTCAGAGAAGAAAGGAGAGGATGCCTCATGCTTGCCGTAGCCAGAAAGCT    360

EMBOSS_001      ------------------------------------------------------------    0
EMBOSS_002      CACACTCTGTCCAGTCAGGAAGCTGTACGTCGGGGTCAGGGAGGCAGGCAGTGCCGACAG    420

EMBOSS_001      ------------------------------------------------------------    0
EMBOSS_002      AACTGCTCTCCTGGGCACACTGACTGGAATCTGACCTCAGCTGCAGTAATGCGATGTCAT    480

EMBOSS_001      ------------------------------------------------------------    0
EMBOSS_002      TGTCATAAGTGTCGTCATCAAATTCCTTATGGACTATGTACTTTTCGATCTCGAATGTCT    540

EMBOSS_001      ------------------------------------------------------------    0
EMBOSS_002      GCTCCTCCTTTCCAGGGACCACTCTGTATGTTCTGCCCAAGACCACTTTAAGATGATGGG    600

EMBOSS_001      ------------------------------------------------------------    0
EMBOSS_002      GTGGAAACCTCTCTACAAAGCAGTGGGCGGCAGATAGCACCCAGCAGGAACTGATCAGCA    660

EMBOSS_001      ------------------------------------------------------------    0
EMBOSS_002      CCCCTCCACACAGGAATCTCTCTCCTGGAGACCTCTTGTTCTTGACAAAGATGGCGGCCT    720

EMBOSS_001      ------------------------------------------------------------    0
EMBOSS_002      GCCAAGGGTGTGAGGTGATGTCTGTGAAGAGTCCTCCTTTAATTCGAAACTGAGGCTGTT    780

EMBOSS_001      ------------------------------------------------------------    0
EMBOSS_002      TGTATTGCCTCAGGCCGCAGGTGGAGCATGGGGACATGTCGCAATATTCCCATGTCAGCT    840

EMBOSS_001      -----------------NNNNANNNNNNNNNNNNNNNNNNNTCGATNNNNNCCANNNN    43
EMBOSS_002      TTCGGTCCTTCATCACGTGGCACCAAGGTTTGGCATCCCCATCTGGGTTCCGGCAATAAT    900
                                 *                     * * *    * *

EMBOSS_001      NN---------------NNNNNNNNNNNNNNNNNCNTCCNGCNNCTTTNNNGNNNNGNNT    88
EMBOSS_002      TGTGTCTGCCCAGGCCAAGTGCCTGGGAGTTGGCCCTCCACGCTGTGT------AAGTCT    954
                                          * ***      * *        *  *

EMBOSS_001      TCACNNNNNNNNACCAGGGANTACACAGGNNGTTCAGANNNNGNNCNTCGGGTCCTACAG    148
EMBOSS_002      TGCC-TATCAGGATCATGGAATTCCATGGGAGGCAGGAGG-----CCTTGGATGTGGTAA    1008
                *  *        * ** *** * *   **  *    **       * * ** *     *

EMBOSS_001      AGCCGACCCTGCCAGNANAATGAAANNAGAACCTNCAGNAACAAACCTTTANNCNNAACN    208
EMBOSS_002      AGCTGTGGGTGCCACGGTAAGTCACACc---tctatataagcagagctcgtttaGTGAAC    1065
                *** *    *****    **   *        **  *  * ** * **         *

EMBOSS_001      AGCCAATTCNNNGTTCNNNNNNNCCTNANCNNTTNCCNNATNNGNCNTNNANN----NNN    264
EMBOSS_002      CGTCAGATCGCCTGGAGACGCCATCCACGCTGTTTTGACCTCCATAGAAGACACCGGGAC    1125
                 * **  **              *    *  **      *         *

EMBOSS_001      GGNNAANNTCTNGGGGNTNNGGGAAANTNNNNNNGGNCCNNGGNNGNCNNANNNNNNG--    322
EMBOSS_002      CGATCCAGCCTCCGCGGCCGG-GAACGGTGCATTGGAACGCGGATTCCCCGTGCCAAGAG    1184
                 *       **  * *    * ***         **  *  **    *         *
```

```
EMBOSS_001      ---C---NNNGGNNCCTNNNGGCNNNCNANGTGTGNCCCNNCNNTNTCGGGNNGGC----    372
EMBOSS_002      TGACGTAAGTACCGCCTATAGAGTCTATAGGCCCACCCCCTTGGCTTCGTTAGAACGCGG    1244
                   *          ***   *       * *     ***       ***      *

EMBOSS_001      --CCCCNNNNCCCCNAAAANNTTTGTNNNNNTGGAAANCCCNAAAAANTGGNNTTTNCAAN    430
EMBOSS_002      CTACAATTAATACATAACCTTATGTAT-CATACACATACGATTTAGGTGACACTATAGAA    1303
                   *        *  **   * ***     *  * *  *     *  **    *    *

EMBOSS_001      TGGGGGGGGGGTNNNCCGNNNTCNNNCCNNGGGNCCCCNGNNNNNNNNNNNNNNNNNAA    490
EMBOSS_002      TAAC-ATCCACTTTGCCTTTCTCTCCACAGGTGTCCACTCCCAGGTCCAACTGCACCTCG    1362
                *          *   **    **    *  * * ** *

EMBOSS_001      NTTTNN---------NNNNNNNNNNNNGNGGNNCCNNNNNNNNNGGAANTTTTTTTTTTG    541
EMBOSS_002      GTTCTATCGATTGCCACCATGAAGGGAGAGCTGTTGTGCGTCCTGCTGCTTTGTGGAGTG    1422
                 **                        * *               *    *** *    **

EMBOSS_001      GGGNNAAAAANNNNNNNNGGGGNANNNNNNNNNNNNNNNNNNNNANNNANNCCCCNNNN    601
EMBOSS_002      GCGTTCACGTTGCCTGACCAGGGAATACACAGGAGG----TTCAGAAG-AG-----GAGC    1472
                * *   *              ** *                    *   *

EMBOSS_001      NNTTTTTTNNNNNNNGNCNNNNNNGNNNNNNNNN---NNNNNNNNNNNNNNGGGGNCCN    658
EMBOSS_002      TCGGTCCTACAGAGCGACCTGCAGAGATGAACAGACTCAGACAACTTACCAACAGCATCA    1532
                    *  *       * *       *                            *   *

EMBOSS_001      NNTNGGGGNNNNCCCCCNNCNCCNNNAAAAAAAAGGGGGGGGNNNTN-------------    705
EMBOSS_002      GTCATGGCTACGTCCCATGCTC--AGAGGCAATCGGGTGGAATACTGCCGGTGCAACAGC    1590
                     **      ***   * *    *   **  *** **     *

EMBOSS_001      ------NAAAAANNNNNNN-----CNNNCCCCNNGGGGNAAAAAANNNNNNNNNNNNNNC    754
EMBOSS_002      GGCCTGGCACAGTGCCACTCGGTGCCCGTCCGAAGTTGCAGTGAACCGAGATGC---TTC    1647
                       * *             *    **   *  * *   **            *

EMBOSS_001      NNNNNNNNNNNCNNAAAAAAACNCNNNNNNNNNNTN---------------------NN    793
EMBOSS_002      AATGGGGGTACGTGTCAGCAGGCCCTGTATTTCTCTGACTTCGTCTGCCAGTGCCCTGAC    1707
                             *  *   *          *

EMBOSS_001      NNNNNNNNNNGNGGGNNCNNNNAAAANNNTNNNNNNNNNNNNNNNNNGGGGGNNNNNNN    853
EMBOSS_002      GGATTTGTTGGGAAACGCTGTGATATAGATACCAGAGCAACCTGCTTCGAGGGCCAGGGC    1767
                      *      *    * *    *                  * ***

EMBOSS_001      NNNGNNAAANNCNNNNNNNTTTTTTTTNNNNNNNNANANNNNCCCCCCNNNNNNNCNNNN    913
EMBOSS_002      ------ATCACCTACAGAGGCACATGGAGCACAGCAGAAAATGGGGCTGAATGCA-TCAA    1820
                      *    *          *          * *       *

EMBOSS_001      NNNNNNNNNNNNNNCCCCCCCCCNNNGGGNNNNNN-----NNNNNTNNTTNTTTNNNNAG    968
EMBOSS_002      CTGGAATAGCAGTGCCCTGTCCCAGAAGCCCTACAGTGCAAGGAGGCCAAATGCCATCAA    1880
                             ***   ***    *                       *      *

EMBOSS_001      GNNGGNNNNNNNNNNNNNNNNNTNNNNNCTNNNCNNCNNNCNNGNNNTNNNNNNTTTNN    1028
EMBOSS_002      GCTGGGCCTTGGGA-ACCACAATTACTGCAGAAACCCAGACCGAGACGTGAAGCCCTGGT    1939
                *  **                *          *      *  *   *       *
EMBOSS_001      NTNNNNNNNNNCNNNCNNNNNNNNNNNNNTNTNNTNNNNNNNNNNNNNNNNNNGAATTT    1088
EMBOSS_002      GCTATGTCTTtaAGGCAGGGAAGTATACCA--CGGAGTTCTGCAGCACGCCGGCTTGCCC    1997
                             *

EMBOSS_001      GNGATGCTATTGCTTTATTTGTAACCATTATAAGCTGCAATAAACAAGTTGGGCCATGGC    1148
EMBOSS_002      TAAGGGACCAACTGAGGACTGCTATGTttATaAGCTGCAaTaAACaAGTTGGGCCATGGC    2057
                     *             **  *   **********************************

EMBOSS_001      GGCCAAGCTTCTGCAGGTCGACTCTAGATCAACCACACCTGGCTGGGCAGGGGGCTGTAG    1208
EMBOSS_002      GGCCAAGCTTCTGCAGGTCGACTCTAGATCAACCACACCTGGCTGGGCAGGGGGCTGTAG    2117
                ************************************************************

EMBOSS_001      CGGGCCACGGCGTGCTCGTACAGCTTCACCTTGTTGTAGTCGCTGTCGTTGCCCAGGATC    1268
EMBOSS_002      CGGGCCACGGCGTGCTCGTACAGCTTCACCTTGTTGTAGTCGCTGTCGTTGCCCAGGATC    2177
                ************************************************************

EMBOSS_001      TCGATGCGGTGGTCCACGAAGTGGGCGTCGGGCAGCTGCACCACCTTCTTGGCCTTGTAG    1328
EMBOSS_002      TCGATGCGGTGGTCCACGAAGTGGGCGTCGGGCAGCTGCACCACCTTCTTGGCCTTGTAG    2237
                ************************************************************

EMBOSS_001      GTGGTCTTGAAGTCGCACAGGTAGTGGCCGCCGCCCTCCAGCAGCAGGGCCATGTTGATG    1388
EMBOSS_002      GTGGTCTTGAAGTCGCACAGGTAGTGGCCGCCGCCCTCCAGCAGCAGGGCCATGTTGATG    2297
                ************************************************************

EMBOSS_001      TTGCCCACCAGCAGGCCGTCGCGCACGTGCAGCTTCTCGGTGCTGGGCTCCCACTTCAGG    1448
EMBOSS_002      TTGCCCACCAGCAGGCCGTCGCGCACGTGCAGCTTCTCGGTGCTGGGCTCCCACTTCAGG    2357
                ************************************************************
```

```
EMBOSS_001      GTCTTCTTCTGCATCACGGGGCCGTTGGGGGGGAAGTTCNNNTCCTGNNANCNTNNATNN    1508
EMBOSS_002      GTCTTCTTCTGCATCACGGGGCCGTTGGGGGGGAAGTTGGTGCCCTTGAAGCGCACGTTC    2417
                ************************************     ***   * *     *

EMBOSS_001      NNNNNNNTNNNCNNNNNNGGCNNNNNNNNANNNNTTNTNNNNCNNNNTNNTNTCTNTCCN    1568
EMBOSS_002      TGGAAGAAGCAGTCGCCCTCCAGGCTGATGTCGCTGCGG-------ATGGTGCAGATGCC    2470
                                *             *            *  *     * *

EMBOSS_001      NTTNNGANTNNANNNNN---NTNNNTCCANNNNNNANCNANNNTNNNNNNNNNNCC----    1621
EMBOSS_002      CTTGTCCTCGAAGGTCATGGTGCGCTCCCAGCTGTAGCCCTCGGGGAAGCTCTGCTTGAA    2530
                 **        *             ***       * *                 *

EMBOSS_001      ----------T---CNNTNNNNNNTNNNNNATCANNNCNNTTCTNNANNCNATCNTNNC    1667
EMBOSS_002      GTAGTCGGGGATGTCCTCGGGGTACTTGGTGAACACCCGGTTGCCGTAGTGCACGGCGGT    2590
                          *   *         *     * **      * *   *    *

EMBOSS_001      NNANTNNTTATNTT-NCNNNNNNNNATNNNNNCNTANN----NNNNNNCNNNNNNNNNNT    1722
EMBOSS_002      GGTCAGGATGTCGTAGCTGAAGGGCAGGGGGGCGCCCTCCTTCACGGTCAGGTTGGCGGT    2650
                       * *  *  *        *      *                *        *

EMBOSS_001      ANGNNNNNANNNNNNNNNN------NNANNNNNNNNNNNNNNNNNN-NNNNNNNTACTN    1775
EMBOSS_002      CTGGGTGCCCTCGTAGGGCTTGCCCTTGCCCTCGCCCTCGATCACGAAGGCGTGGCCGTT    2710
                  *                                                     *

EMBOSS_001      TNNNNNNNNNNNNNTNNNTNNATNNACNNNNATNATNNNNNNNTNNNACCTTANNNNCNA    1835
EMBOSS_002      CACGTTGCCCTCCATGTGCACCTTCACGCGCATGTCCTCCTTGATCAGGTTACCCCGGGA    2770
                             *       *  **    **                 *       *

EMBOSS_001      TCNTNCCNN-----------CNTNCNNNTTNTT--------------------------    1857
EMBOSS_002      TCCTCCTCCACTTCCTCCTCCTTGCTTCATGTTGTCTTGGATCCAGTTCAGGTAATTAGT    2830
                ** * *              * * *    * **

EMBOSS_001      ------------------------------------------------------------    1857
EMBOSS_002      GACCTTTGTGTATATCCCTGGCACGTCCTTCTGCCCACAGCCGAgGCCCCAGCTGATGAT    2890

EMBOSS_001      ------------------------------------------------------------    1857
EMBOSS_002      GCCCAGTAAAGTCATCCGCTTATCGATCATGCACACCAgAgGGCCTCCTGAgTCACCCTG    2950

EMBOSS_001      ------------------------------------------------------------    1857
EMBOSS_002      GCACGCGTCATGGACGTCTTGGTTGCCCCCAgTTCGGGTGTCTCCTGCACACAgCATGTT    3010

EMBOSS_001      ------------------------------------------------------------    1857
EMBOSS_002      GCTCGTGATGGTATGAAGGGAGAGCTGTTGTGCGTCCTGCTGCTTTGTGGAGTGGCGTTC    3070

EMBOSS_001      ------------------------------------------------------------    1857
EMBOSS_002      ACGTTGCCTGACCAGGGAATACACAGGAGGTTCAGAAGAGGAGCTCGGTCCTACAGAGCG    3130

EMBOSS_001      ------------------------------------------------------------    1857
EMBOSS_002      ACCTGCAGAGATGAACAGACTCAGACAACTTACCAACAGCATCAGTCATGGCTACGTCCC    3190

EMBOSS_001      ------------------------------------------------------------    1857
EMBOSS_002      ATGCTCAGAGGCAATCGGGTGGAATACTGCCGGTGCAACAGCGGCCTGGCACAGTGCCAC    3250

EMBOSS_001      ------------------------------------------------------------    1857
EMBOSS_002      TCGGTGCCCGTCCGAAGTTGCAGTGAACCGAGATGCTTCAATGGGGGTACGTGTCAGCAG    3310

EMBOSS_001      ------------------------------------------------------------    1857
EMBOSS_002      GCCCTGTATTTCTCTGACTTCGTCTGCCAGTGCCCTGACGGATTTGTTGGGAAACGCTGT    3370

EMBOSS_001      ------------------------------------------------------------    1857
EMBOSS_002      GATATAGATACCAGAGCAACCTGCTTCGAGGGCCAGGGCATCACCTACAGAGGCACATGG    3430

EMBOSS_001      ------------------------------------------------------------    1857
EMBOSS_002      AGCACAGCAGAAAATGGGGCTGAATGCATCAACTGGAATAGCAGTGCCCTGTCCCAGAAG    3490
```

```
EMBOSS_001      ------------------------------------------------------------  1857
EMBOSS_002      CCCTACAGTGCAAGGAGGCCAAATGCCATCAAGCTGGGCCTTGGGAACCACAATTACTGC  3550

EMBOSS_001      ------------------------------------------------------------  1857
EMBOSS_002      AGAAACCCAGACCGAGACGTGAAGCCCTGGTGCTATGTCTTTAAGGCAGGGAAGTATACC  3610

EMBOSS_001      ------------------------------------------------------------  1857
EMBOSS_002      ACGGAGTTCTGCAGCACGCCGGCTTGCCCTAAGGGACCAACTGAGGACTGCTATGTTGGA  3670

EMBOSS_001      ------------------------------------------------------------  1857
EMBOSS_002      AAAGGTGTGACTTACCGTGGCACCCACAGCTTTACCACATCCAAGGCCTCCTGCCTCCCA  3730

EMBOSS_001      ------------------------------------------------------------  1857
EMBOSS_002      TGGAATTCCATGATCCTGATAGGCAAGACTTACACAGCGTGGAGGGCCAACTCCCAGGCA  3790

EMBOSS_001      ------------------------------------------------------------  1857
EMBOSS_002      CTTGGCCTGGGCAGACACAATTATTGCCGGAACCCAGATGGGGATGCCAAACCTTGGTGC  3850

EMBOSS_001      ------------------------------------------------------------  1857
EMBOSS_002      CACGTGATGAAGGACCGAAAGCTGACATGGGAATATTGCGACATGTCCCCATGCTCCACC  3910

EMBOSS_001      ------------------------------------------------------------  1857
EMBOSS_002      TGCGGCCTGAGGCAATACAAACAGCCTCAGTTTCGAATTAAAGGAGGACTCTTCACAGAC  3970

EMBOSS_001      ------------------------------------------------------------  1857
EMBOSS_002      ATCACCTCACACCCTTGGCAGGCCGCCATCTTTGTCAAGAACAAGAGGTCTCCAGGAGAG  4030

EMBOSS_001      ------------------------------------------------------------  1857
EMBOSS_002      AGATTCCTGTGTGGAGGGGTGCTGATCAGTTCCTGCTGGGTGCTATCTGCCGCCCACTGC  4090

EMBOSS_001      ------------------------------------------------------------  1857
EMBOSS_002      TTTGTAGAGAGGTTTCCACCCCATCATCTTAAAGTGGTCTTGGGCAGAACATACAGAGTG  4150

EMBOSS_001      ------------------------------------------------------------  1857
EMBOSS_002      GTCCCTGGAAAGGAGGAGCAGACATTCGAGATCGAAAAGTACATAGTCCATAAGGAATTT  4210

EMBOSS_001      ------------------------------------------------------------  1857
EMBOSS_002      GATGACGACACTTATGACAATGACATCGCATTACTGCAGCTGAGGTCAGATTCCAGTCAG  4270

EMBOSS_001      ------------------------------------------------------------  1857
EMBOSS_002      TGTGCCCAGGAGAGCAGTTCTGTCGGCACTGCCTGCCTCCCTGACCCCGACGTACAGCTT  4330

EMBOSS_001      ------------------------------------------------------------  1857
EMBOSS_002      CCTGACTGGACAGAGTGTGAGCTTTCTGGCTACGGCAAGCATGAGGCATCCTCTCCTTTC  4390

EMBOSS_001      ------------------------------------------------------------  1857
EMBOSS_002      TTCTCTGACCGGCTGAAGGAGGCTCACGTCAGACTGTATCCGTCCAGCCGCTGTACCTCA  4450

EMBOSS_001      ------------------------------------------------------------  1857
EMBOSS_002      CAGCATCTGTTTAACAAAACCATCACGAGCAACATGCTGTGTGCAGGAGACACCCGAACT  4510

EMBOSS_001      ------------------------------------------------------------  1857
EMBOSS_002      GGGGGCAACCAAGACGTCCATGACGCGTGCCAGGGTGACTCAGGAGGCCCTCTGGTGTGC  4570

EMBOSS_001      ------------------------------------------------------------  1857
EMBOSS_002      ATGATCGATAAGCGGATGACTTTACTGGGCATCATCAGCTGGGGCCTCGGCTGTGGGCAG  4630

EMBOSS_001      ------------------------------------------------------------  1857
EMBOSS_002      AAGGACGTGCCAGGGATATACACAAAGGTCACTAATTACCTGAACTGGATCCAAGACAAC  4690
```

```
EMBOSS_001      ------------------------------------------------------------    1857
EMBOSS_002      ATGAAGCAAGGAGGAGGAAGTGGAGGAGGATCCCGGGGTAACCTGATCAAGGAGGACATG    4750

EMBOSS_001      ------------------------------------------------------------    1857
EMBOSS_002      CGCGTGAAGGTGCACATGGAGGGCAACGTGAACGGCCACGCCTTCGTGATCGAGGGCGAG    4810

EMBOSS_001      ------------------------------------------------------------    1857
EMBOSS_002      GGCAAGGGCAAGCCCTACGAGGGCACCCAGACCGCCAACCTGACCGTGAAGGAGGGCGCC    4870

EMBOSS_001      ------------------------------------------------------------    1857
EMBOSS_002      CCCCTGCCCTTCAGCTACGACATCCTGACCACCGCCGTGCACTACGGCAACCGGGTGTTC    4930

EMBOSS_001      ------------------------------------------------------------    1857
EMBOSS_002      ACCAAGTACCCCGAGGACATCCCCGACTACTTCAAGCAGAGCTTCCCCGAGGGCTACAGC    4990

EMBOSS_001      ------------------------------------------------------------    1857
EMBOSS_002      TGGGAGCGCACCATGACCTTCGAGGACAAGGGCATCTGCACCATCCGCAGCGACATCAGC    5050

EMBOSS_001      ------------------------------------------------------------    1857
EMBOSS_002      CTGGAGGGCGACTGCTTCTTCCAGAACGTGCGCTTCAAGGGCACCAACTTCCCCCCCAAC    5110

EMBOSS_001      ------------------------------------------------------------    1857
EMBOSS_002      GGCCCCGTGATGCAGAAGAAGACCCTGAAGTGGGAGCCCAGCACCGAGAAGCTGCACGTG    5170

EMBOSS_001      ------------------------------------------------------------    1857
EMBOSS_002      CGCGACGGCCTGCTGGTGGGCAACATCAACATGGCCCTGCTGCTGGAGGGCGGCGGCCAC    5230

EMBOSS_001      ------------------------------------------------------------    1857
EMBOSS_002      TACCTGTGCGACTTCAAGACCACCTACAAGGCCAAGAAGGTGGTGCAGCTGCCCGACGCC    5290

EMBOSS_001      ------------------------------------------------------------    1857
EMBOSS_002      CACTTCGTGGACCACCGCATCGAGATCCTGGGCAACGACAGCGACTACAACAAGGTGAAG    5350

EMBOSS_001      ----------------------------------------------------    1857
EMBOSS_002      CTGTACGAGCACGCCGTGGCCCGCTACAGCCCCCTGCCCAGCCAGGTGTGGT    5402
```